The Pennsylvania State University

The Graduate School

Department of Physics

SUPERFLOW IN QUANTUM SOLIDS

A Thesis in

Physics

by

Anthony C. Clark

Submitted in Partial Fulfillment
of the Requirements
for the Degree of

Doctor of Philosophy

August 2007

The thesis of Anthony C. Clark was reviewed and approved* by the following:

Moses H. W. Chan
Evan Pugh Professor of Physics
Thesis Advisor
Chair of Committee

Milton W. Cole
Distinguished Professor of Physics & Materials Science and Engineering

Jainendra K. Jain
Erwin W. Mueller Professor of Physics

Thomas E. Mallouk
DuPont Professor of Materials Chemistry and Physics
Director of Penn State MRSEC, The Center for Nanoscale Science

Julian D. Maynard
Distinguished Professor of Physics

Jayanth R. Banavar
Distinguished Professor of Physics
George A. and Margaret M. Downbrough Department Head of Physics

*Signatures are on file in the Graduate School

ABSTRACT

The understanding of the apparent superfluid nature of solid ^{4}He is incomplete. There are many theoretical models proposing defect-based mechanisms for the non-classical rotational inertia (NCRI) that is observed in torsional oscillator measurements. It is clear that further experimental work is necessary to determine if any of the present models are applicable to solid ^{4}He.

These issues have been addressed in two parts. First, the behavior of solid hydrogen under rotation was investigated in order to determine if the possible supersolid phase is unique to ^{4}He. Although there are clear indications of quantum mechanical motion of residual ortho-hydrogen impurities within the solid, NCRI is not observed in any solid H_2 samples.

Second, modifications to the traditional experimental apparatus were employed in order to make it possible to grow solid ^{4}He at a fixed point on the solid-liquid coexistence curve within a torsional oscillator for the first time. A vast improvement in the overall reproducibility of the data is consistent with the formation of single crystals within the sample cell. The onset of NCRI is consistently found to be 79mK in helium crystals containing only ~1ppb of isotopic impurities. These results demonstrate that the supersolid-like behavior of solid ^{4}He is not associated with superfluid liquid flowing along grain boundaries.

Further results suggest that vortices exist in the solid, and that the onset of NCRI corresponds to the temperature at which their motion is suppressed. Below ~35mK the vortices are strongly pinned.

TABLE OF CONTENTS

LIST OF FIGURES

LIST OF TABLES

ACKNOWLEDGEMENTS

I first want to thank my advisor, Moses Chan, who has been ridiculously generous to me over these past six years. I cannot imagine what graduate school would have been like without him. These years will not be forgotten.

I am honored to have four esteemed members of the scientific community on my committee (and keeping me on my toes): Milton Cole, Jainendra Jain, Tom Mallouk, and Jay Maynard. I am grateful for the assistance of many past and current members of the Physics Department: Jayanth B., Tim B., Jean B., Barry D., John H., Ryan J., Randi N., John P., Denise P., Rick R., and Anne S. I owe a great deal to Mitsunori Hieda and James Kurtz for providing guidance early on. I am also indebted to Horst Meyer for all of his advice during my later years. There are two students who repeatedly assisted me in various aspects of the experiments (after I became one of those lazy, senior graduate students), so I am compelled to give special thanks to Xi Lin and Mike Bowne. I also cannot forget those whom, armed with beverages, kept me sane during this time: Ben Ueland and Josh West.

I want to thank my family and friends for supporting me in countless ways. I have neither the space on this page, nor the words, to truly express how appreciative I am.

Lastly, there is my closest friend who in no way assisted me with this project. Rather, I am grateful for her efforts to distract me from my work. She is beautiful and unique, and will hopefully always be treated as such. Without having ever met her, I am utterly afraid to think of the man I would have become. For that, she forever holds a place in my heart.

Chapter 1

Introduction

1.1 Overview of Thesis

This thesis addresses two questions relevant to supersolidity. The first: is the supersolid phase unique to helium? To answer this question I investigated the rotational properties of solid hydrogen [**Clark 2006b**], which is the next most likely material to exhibit superfluidity. No supporting evidence was found, but in the process I observed interesting effects related to the motion of residual ortho-hydrogen impurities within the solid. The second question: what kinds of defects, if any, are vital to the existence of the supersolid phase? To address to this issue, I have studied the superfluid properties of helium crystals grown under a variety of conditions [**Clark 2007**]. I have found that large crystals of helium still exhibit non-classical rotational inertia (NCRI) [**Leggett 1970**]. For single crystals, the onset of NCRI is abrupt and its temperature dependence in this region is entirely reproducible, suggesting the presence of a true phase transition.

My results are presented in the following order. In this chapter, I provide a very brief history of, and introduction to, superfluidity. This is followed by a few words on the present status of superfluidity in solid ^{4}He. In Chapter 2, I discuss some relevant properties of solid hydrogen and helium. In particular, I intend for the review of helium crystal growth to serve as a useful resource for graduate students (and others) in the future. The third chapter delves into the experimental details of both studies carried out.

Chapter 4 is devoted to the two excruciating years I spent on solid hydrogen, while Chapter 5 is dedicated to solid helium. Both the experimental results and detailed discussions are included in these chapters. The main conclusions are summarized in chapter 6.

1.2 Superfluidity

Just two years after his pioneering success of liquefying ^{4}He, Kamerlingh Onnes found that upon cooling the liquid below 2.2K, it began to expand rather than continuing to contract [**Onnes 1911**]. However, the trait usually associated with superfluidity, vanishing viscosity, was not clearly demonstrated until 1938 [**Kapitza 1938**]. At this point liquid ^{4}He became the first substance proven to exhibit superflow. About 35 years later came the discovery of superfluid liquid ^{3}He, which undergoes a transition three decades lower in temperature [**Osheroff 1972**]. Another 35 years passed before superfluid properties were manifested in the gaseous phase of matter, i.e. in dilute atomic gases [**Matthews 1999**]. Now, in the opening decade of the 21st century, those in our field have the joy of arguing over what is possibly the latest addition to this list, superfluid solid ^{4}He [**Kim 2004a**].

Superfluidity occurs in systems obeying Bose-Einstein statistics, and is usually associated with Bose-Einstein condensation (BEC). The BEC temperature (T_{BEC}) corresponds to the point where the thermal de Broglie wavelength becomes less than the critical interparticle separation at which quantum coherence is achievable. For a non-interacting gas the following equation applies.

$$T_{BEC} = \frac{h^2}{2\pi k_B m}\left(\frac{n}{2.612}\right)^{2/3} = (113.68)\left(W_M\right)^{-1}\left(V_M\right)^{-2/3} \qquad \text{Eq. 1.1}$$

For convenience, the molecular weight (W_M) is in g/mol and the molar volume (V_M) is in cc/mol. The transition temperature is higher for the lighter and denser (number density) elements in the periodic table.

From Eq. **1.1**, T_{BEC} = 3.1K for liquid ^{4}He and T_{BEC} = 7.1K for liquid H_2. The problem with the latter is that freezing occurs under saturated vapor pressure at the triple point of 13.8K. In the effort to observe superfluidity in H_2, there have been many attempts to supercool the liquid below the triple point. At present, the superfluid state of the bulk liquid phase continues to elude scientists.

1.2.1 Quantum Statistics

The relationship between superfluid ^{4}He and BEC is not straightforward. For example, consider that there are two types of bosons. The first is a composite of an even number of fermions (^{4}He atoms, cooper paired ^{3}He atoms, etc.), while the second is a collective mode of particles (spin waves, phonons, rotons, etc.). It has been argued that both systems can form a BEC, but with very different consequences [**Kohn 1970**]. It appears that only BEC of the first kind can lead to off-diagonal long range order (ODLRO). Since superfluidity requires that the reduced density matrices for a system in coordinate space possess ODLRO [**Yang 1962**], it may be that only the first type of bosonic system can support superfluidity. This concept may need to be re-examined in the future by both theorists and experimentalists.

Another example where the connection between BEC and superfluidity is slightly complicated is in two dimensions (2D). Theoretically, finite temperatures produce enough fluctuations to destroy long range order [**Hohenberg 1967**]. However, a local "condensate" wave function can be defined in small regions of the system [**Kosterlitz 1977**]. The difference in the phase of the wave function from one region to the next is minimal since the lowest energy excitations are bound vortex pairs of opposite vorticity. As a result quasi-long range coherence, and thus superflow, can endure up to a critical velocity and/or temperature at which vortex pairs unbind.

The relationship between BEC and superfluidity is different for liquid ^{4}He, liquid ^{3}He, and dilute gases. However, the lack of viscosity in each case is the result of coherent motion, and is just one aspect of a system described by a single macroscopic wave function.

1.2.2 Macroscopic Behavior

What is important in the above examples is that the entire superfluid component can be well described by a coherent wave function (WF), whose amplitude and phase are allowed to vary in space and time. The WF is necessarily normalized so that the modulus (ψ_0) squared is equal to the superfluid density. Hence, the solution to the Schrödinger equation determines the superfluid density and phase (S) throughout the system.

$$\psi(\mathbf{r},t) = \psi_0(\mathbf{r},t)\exp[iS(\mathbf{r},t)] \qquad \text{Eq. 1.2}$$

Following the usual quantum mechanical treatment [**Tilley 1990**], the momentum operator can be applied to Eq. **1.2** to obtain the following relation between the superfluid velocity (v_S) and phase.

$$\boldsymbol{v}_s = \frac{\hbar}{m}\nabla S \qquad \text{Eq. 1.3}$$

Consider the flow pattern of helium in some region. The circulation around some closed loop in a multiply connected region, such as an annulus, can be calculated.

$$\kappa = \oint \boldsymbol{v}_s \cdot d\boldsymbol{l} = \frac{\hbar}{m}\oint \nabla S \cdot d\boldsymbol{l} = \frac{\hbar}{m}\Delta S = n\frac{h}{m} \qquad \text{Eq. 1.4}$$

for $n = 1, 2, 3\ldots$

Since the superfluid WF is single-valued, the phase change must be an integral number of 2π. The non-zero, quantized circulation is the reason persistent currents can be generated.

In a simply connected region (such as a cylinder), the integral is zero. Exceptions to this occur when vortices enter into the superfluid. Since the wave function has zero amplitude at the core of a vortex line, the topology is effectively changed. In the "rotating bucket" experiment the number of generated vortices, and thus the circulation, are entirely determined by the angular velocity when cooling through the superfluid onset temperature. When it is less than a critical value, the helium will come to rest and be in the true ground state [**Hess 1967**]. At larger speeds, a triangular array of $\kappa = (1)(h/m)$ vortices will be created [**Packard 1972**]. Since these vortices are quantized in circulation, they are considered to be direct evidence of superfluidity.

1.3 Supersolidity

London made the connection between BEC and superfluidity in liquid ^{4}He [**London 1938**]. Soon after a similar proposal was put forth for solid ^{4}He [**Wolfke 1939**]. A general consensus of the solid system has not been reached since this time even though there are now more than 100 theory papers on the subject. One firm conclusion from experiments is that "disorder" in solid ^{4}He can enhance the observed NCRI fraction (NCRIF), i.e. the fraction of the solid that appears to be superfluid. What remains to be seen is whether or not disorder itself is directly responsible for the phenomenon.

1.3.1 Theoretical Background

A comprehensive theoretical discussion of supersolids is beyond the scope of this thesis, not to mention my intellect. The reader is referred to the original review of theoretical and experimental prospects of supersolidity [**Meisel 1992**], as well as an article that discusses more recent works [**Prokof'ev 2007**]. However, for those with time on their hands, I definitely advise skimming through all of the individual papers. Although I list almost all of the theory publications from the 21st century that I am aware of, only those having the most direct relevance to the present experiments are discussed in any detail. In the very least I hope this section serves as a convenient index of the literature. I begin with a very simple picture of supersolidity, i.e., delocalization due to zero point motion. I then briefly discuss the ground state of solid ^{4}He and some of the techniques that have been used to investigate it. The last few sections on theory (annotated with experimental facts) summarize the conclusions of numerous publications,

sorted according to the microscopic mechanisms that they have addressed.

1.3.1.1 Simplest Notion of Supersolidity

The flow of particles between any two points, or around any closed loop, necessarily involves some degree of particle delocalization within a solid. The primary candidates to exhibit supersolidity are then solids possessing the least localized of constituents to begin with. The combination of the large zero-point energy of individual atoms, and weak attractive interaction between them, make helium the most quantum mechanical solid of all the elements. In fact, in low density hcp crystals (V_M = 21cc/mol) the rms deviation of any ^{4}He atom from its lattice site is 0.96Å along the c-axis [**Burns 1997**]. This corresponds to 16% of the atomic spacing in that direction, and 26% of the nearest neighbor separation in the basal plane. This motion is entirely due to quantum mechanical zero-point motion. In contrast, at much higher densities (V_M = 11cc/mol) the deviation is only 11% of the nearest neighbor distance and stems from thermal vibrations [**Arms 2003**]. As a comparison, the fraction of molecular motion in zero pressure solid H_2 (V_M = 22.65cc/mol) at 5.4K is 18% of the nearest neighbor distance, and is attributed to zero point motion [**Nielsen 1973**]. In most materials, the Lindemann ratios that correspond to the above values (multiply by $\sqrt{3}$) would be indicative of melting. These results are consistent with what is considered a standard measure of the quantum nature of a substance, the de Boer parameter [**de Boer 1948**].

$$\Lambda = \frac{h}{\sigma\sqrt{m\varepsilon}} \qquad \text{Eq. 1.5}$$

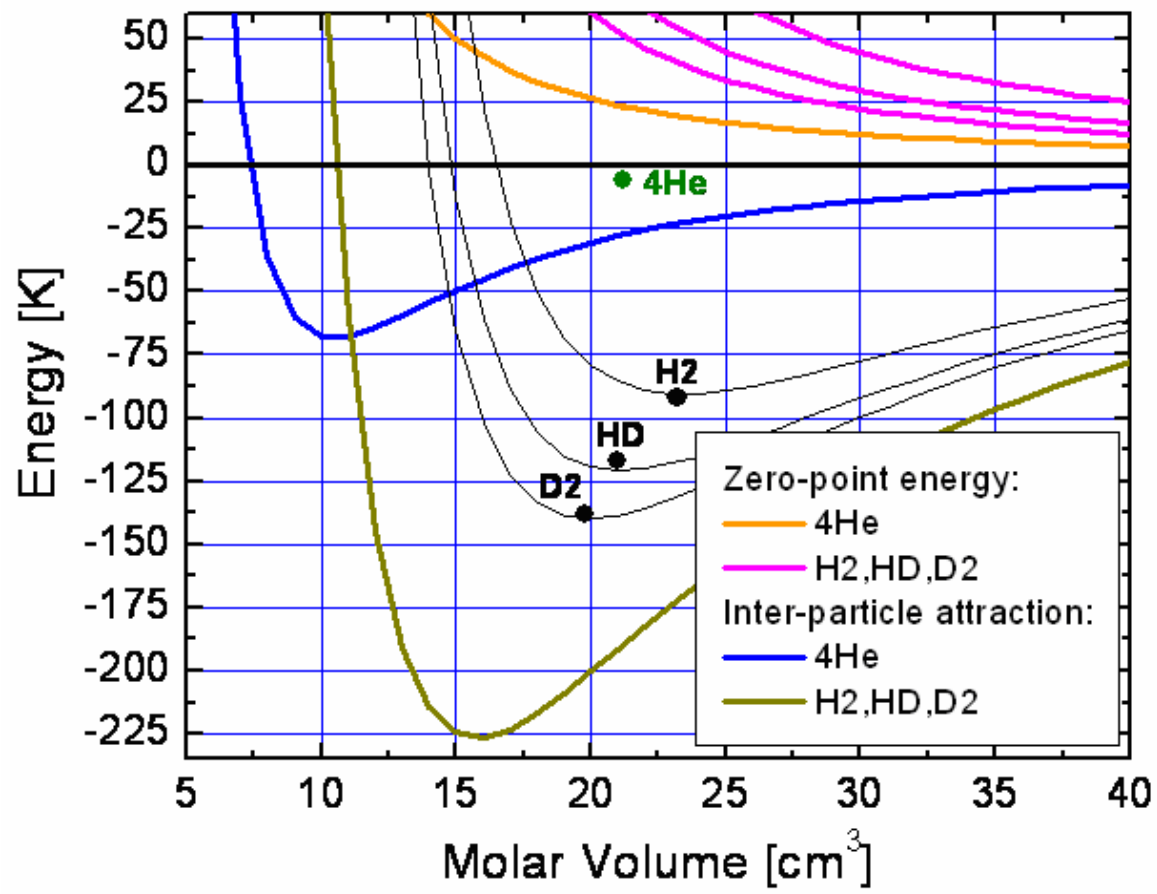

Fig. **1-1**: Comparison of the potential and kinetic energies of ^{4}He and the hydrogen isotopes. The lines depict (old) calculated curves. See Ref. [**London 1954**] for details. The points correspond to measurements.

The parameters σ and ε are unique to each material and describe the interparticle potential energy. Only helium and hydrogen isotopes have Λ greater than unity (Λ_{3He} = 3.0, Λ_{4He} = 2.6, Λ_{H2} = 1.7, Λ_{HD} = 1.4, Λ_{D2} = 1.2).

Eq. **1.5** is similar to the expression for the thermal de Broglie wavelength that was used to estimate T_{BEC} in Eq. **1.1**. The critical separation (σ) is determined by the interparticle potential. For both ^{4}He and H_2 the value of σ is on the order of 3Å. Instead of quantum mechanics competing against thermal energy, here the well depth of the

potential is important. Although H_2 has half the mass of ^{4}He the well depth is much greater, ~35K versus ~7K, and thus helium is more quantum mechanical. This is portrayed in Fig. **1-1**, in which are plotted some approximate values [**London 1954**] of the potential and kinetic energies of ^{4}He and the hydrogen isotopes. The potential energy at each molar volume was obtained by summing over all (one mole) of the atoms/molecules arranged in an hcp lattice. London crudely estimated (his words, not mine) the zero point kinetic energy by interpolating between reasonable upper and lower limits. The resultant total energy appears consistent with experiments. However, since the interparticle potential London used is outdated this is partly due to chance. For example, the potential energy shown in Fig. **1-1** for H_2 at the triple point (V_M = 23.16cc/mol) is between 10% and 20% too small (it should be between -200 and -240K) [**Silvera 1980**]. Similarly, the potential and kinetic energies between V_M = 18 and 21cc/mol for ^{4}He in Fig. **1-1** are only within ± 10% of modern calculations [**Whitlock 1979**], [**McFarland 1994**],[**Vitiello 1999**].

Still, one can see that the total energy of a ^{4}He atom at the lowest solid state density (V_M ~ 21cc/mol) is roughly ten times less negative than that of a H_2 molecule (V_M ~ 23cc/mol). It is therefore natural to expect higher exchange rates between weakly bound ^{4}He atoms (~100kHz [**Ceperley 1995**]) in a solid lattice, in comparison to H_2 molecules (~1kHz [**Meyer 1987**]).

1.3.1.2 The Ground State: Theory, Simulation, and a Confused Experimentalist

The problem of supersolidity has been "attacked" by many people, and from many different directions. Several early treatments investigated various trial wave functions, presumably with the hope to properly describe the ground state of a quantum solid such as ^{4}He. While Reatto showed that a Jastrow wave function (JWF) commonly used for liquid ^{4}He has ODLRO [**Reatto 1969**], Chester pointed out that such a JWF could also describe a crystal [**Chester 1970**]. Thus, it was determined that some systems can simultaneously possess both types of long range order. Clark and Ceperley [**Clark 2006a**] have pointed out that a JWF, which is of the form

$$\psi_J \propto \exp\left[-\sum_{i<j} u(r_{ij})\right] \qquad \text{Eq. 1.6}$$

where $u(r_{ij})$ is fixed by a variational approach to minimizing the ground state energy, cannot accurately describe many physical properties of solid ^{4}He near melting. They go on to describe various other trial wave functions that are more suitable to solid ^{4}He, some of which have, and some of which do not have BEC. One WF includes the Jastrow term of Eq. **1.6**, multiplied by a Wannier function that is localized about lattice sites. The resulting function does not have BEC in the absence of defects [**Shi 2005**]. Another trial wave function [**Zhai 2005**], which Clark and Ceperley call "metallic," has both BEC and NCRI. However, the theory of Zhai and Wu does not address the issue of gapless vacancies [**Prokof'ev 2007**], in regard to a commensurate supersolid. That is, Prokof'ev and Svistunov [**Prokof'ev 2005**] have apparently proven that superflow within a commensurate crystal (# atoms = # sites) is only achievable if vacancies and (their corresponding) interstitial atoms are present. The ground state of the system becomes

incommensurate when the number of vacancies and interstitials differ, which is expected [**Prokof'ev 2005**] due to their lack of symmetry (i.e., vacancies have a lower activation energy).

The presence/absence of BEC in each function mentioned above was determined analytically. However, powerful numerical tools have also been used to study solid ^{4}He, most of which involve some type of Monte Carlo simulation. In many cases the starting point is still a trial wave function. Galli and Reatto, for example, have employed a shadow wave function (SWF) that results in accurate physical description of the solid upon optimization of the wave function parameters [**Galli 2006**]. (The SWF is a variationally optimized projection into imaginary time of the JWF.) In fact, at present the best variational representation of solid ^{4}He is given by a SWF, which turns out to have BEC. For the commensurate state the calculated BEC fraction is small, 5×10^{-6} at 26bar, and has been associated with vacancy-interstitial pairs [**Galli 2005**] (this may be questionable, i.e., as I mentioned above at least some SWF's cannot describe commensurate states). Regardless, this number is enhanced when a net fraction of vacancies are present (meaning that there are more vacancies than interstitials), $\sim 10^{-3}$ at 54bar [**Galli 2006**].

Recent numerical studies of commensurate ^{4}He that do not propose a specific trial wave function are those of Ceperley and collaborators [**Ceperley 2004**],[**Clark 2006a**], which instead involve path integral Monte Carlo (PIMC) calculations. Although this technique requires less assumptions than those using trial wave functions (only the He-He interaction is needed), finite size effects are common since it is difficult to simulate large systems (eg., greater than several hundred atoms). Superfluidity in PIMC is represented

by a finite winding number, which means that many exchanges of atoms take place on the order of the sample size. Ceperley *et al.* have found no indication of BEC in defect-free ^{4}He crystals [**Clark 2006a**]. In addition, using a sophisticated model they found that the calculated exchange frequencies [**Ceperley 1995**] in the solid are too low to support to NCRI [**Ceperley 2004**].

Other, slightly (or vastly) different PIMC simulations are those of Prokof'ev, Svistunov, and collaborators. With the aid of a "worm" algorithm, efficient sampling of configurational space allowed them to calculate the superfluid density of relatively large systems (several thousand atoms). With this technique, a commensurate crystal was found to be insulating [**Boninsegni 2006b**]. Calculations of the same kind have also been applied to a quenched superglass phase [**Boninsegni 2006b**], as well as superfluid grain boundaries between ^{4}He crystals [**Pollet 2007**].

Since the commensurate solid is suggested to be insulating [**Prokof'ev 2005**],[**Clark 2006a**],[**Boninsegni 2006b**] (or to at least have a smaller BEC fraction [**Galli 2005**] than if vacancies are present [**Galli 2006**]) an extremely important question is the following. Which scenario best describes the ground state of solid ^{4}He, commensurate or incommensurate?

1.3.1.3 Vacancies

The condensation of vacancies and/or other point defects was the first microscopic mechanism proposed in the early theoretical exploration of possible supersolidity of ^{4}He [**Andreev 1969**]. One can place an upper limit of $x_V \sim 0.1\%$ for the

vacancy concentration in single crystals of ^{4}He, based on the temperature dependence of the lattice constant measured by x-ray diffraction [**Fraass 1989**]. This number is comparable to the originally observed NCRIF ~1% [**Kim 2004a**], but is much less than the value of 20% that was recently reported in rapidly quenched samples [**Rittner 2007**]. While the number of vacancies would presumably scale in some way with NCRIF, no information on x_V exists for disordered ^{4}He solids. Recent computations have suggested that the observed onset temperature of T_O = 200mK can be explained by x_V = 0.23% [**Galli 2006**]. However, no explanation was offered for the large range of NCRI fractions associated with this single onset temperature. In a different numerical study of higher vacancy concentrations [**Boninsegni 2006a**], it was found that ~1 < x_V < 6% is unstable, in that vacancies are attracted to one another and therefore phase-separate from the bulk crystal. In a theoretical approach [**Mahan 2006**], the interaction between static vacancies was also found to be attractive. Thus, the existence and potential role of vacancies remains undetermined.

1.3.1.4 Grain Boundaries, Glasses, and Dislocations

Other defects that have been studied in detail are grain boundaries [**Burovski 2005**],[**Dash 2005**],[**Sasaki 2006**],[**Pollet 2007**]. It has been proposed that liquid ^{4}He wets the surfaces between crystalline grains, and that the observed NCRI is actually the result of liquid superflow. If so, Kosterlitz-Thouless theory [**Kosterlitz 1977**] may be applicable to these thin superfluid films [**Ambegaokar 1978**]. For T_O = 200mK, the effective thickness of the superfluid film should be about 0.06nm, i.e., two tenths of a

monolayer. Surprisingly, Pollet *et al.* find that a superfluid grain boundary with T_O ~500mK has a thickness of ~1nm, which is roughly seven times larger than expected from Ref. [**Ambegaokar 1978**]. This may be a finite size effect of the very small system that was simulated in Ref. [**Pollet 2007**]. In either case (Pollet *et al.* given in parentheses), enormous surface areas are necessary to constitute even just 1%, let alone 20%, of the entire sample volume. For example, a 1cc sample must contain ~150m^2 (3m^2) of area for NCRIF = 1%. This would correspond to an average crystallite size of 20nm (1μm), which is ~5,000 (~100) times smaller than the smallest, experimentally quantified value that I am aware of [see Chapter 2]. It therefore has been suggested that grain boundaries connect larger, micron-sized pockets of liquid, although none have yet been detected [**Balibar 2007**]. In fact, the coexistence of liquid and solid in the temperature range of interest has only been recorded on the 25bar melting boundary, while NCRI persists up to at least 137bar (20% greater in density) [**Kim 2006**].

Despite these shortcomings, the grain boundary model has continued to receive a great deal of attention. There is one twist on this in which the high density, liquid regions are considered to be somewhat glassy. This hypothetical glass phase of ^{4}He reportedly possesses superfluid properties [**Boninsegni 2006b**]. A dislocation-induced glass has also been proposed [**Balatsky 2007**],[**Manousakis 2007**]. One of these works [**Balatsky 2007**], however, involves an unfortunate mistreatment of heat capacity data that I obtained [**Clark 2005**]. In any case, all of the above proposals suggest that the solid samples grown in the laboratory contain these sorts of disordered regions. The existence of NCRI then depends on whether or not the defect-rich, superfluid portions of the solid percolate throughout the sample.

1.3.1.5 Indifference to Defects

Among the theoretical and numerical studies of perfect crystals, some have found that NCRI is possible [**Galli 2005**],[**Zhai 2005**],[**Cazorla 2006**],[**Saslow 2006**], and others that it is impossible [**Ceperley 2004**],[**Prokof'ev 2005**],[**Shi 2005**]. These papers remind us of the uncertainty in the role of defects. Regardless, it is conceded in most of these works that crystalline defects will enhance the effect. Phenomenological approaches have the advantage of looking beyond these sources of confusion. As a result, some recent works [**Son 2005**] have led to interesting predictions that can, and hopefully will, be experimentally tested.

The last theory paper that I want to mention advocates a free vortex liquid model [**Anderson 2007**]. Anderson describes solid ^{4}He as a three-dimensional (3D) density wave, through which some fraction of ^{4}He can flow. The true transition temperature is assumed to be less than 20mK, while the behavior observed in experiments is that of the vortex liquid existing above T_O. Thermally activated vortices move in response to superfluid velocity fields so as to reduce the circulating supercurrents. The number of vortices, and the rate at which they can move into or out of the sample, both increase with temperature. Thus, the supercurrents are most effectively eliminated at high temperature. NCRIF is large at low temperature since there are very few vortices, all with low mobility. Also, vortex motion is slowed by the presence of ^{3}He impurities, which are dragged along with them. When the finite response time of vortices is longer than the measurement period in torsional oscillator experiments, NCRIF and T_O should be enhanced.

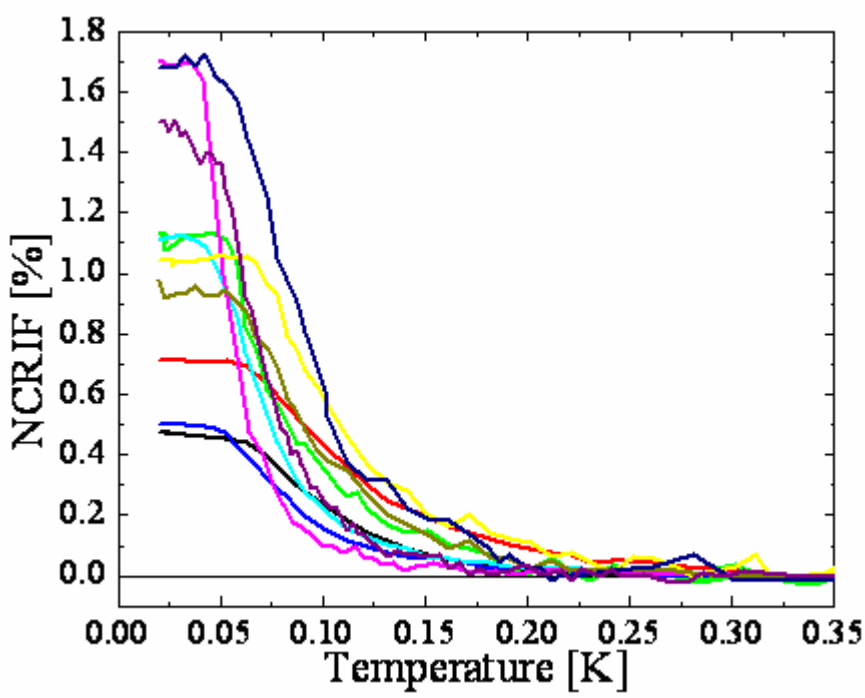

Fig. **1-2**: NCRIF vs. *T* for several samples from Ref. [**Kim 2004a**]. Solid pressures range from 25 to 65bar. The qualitative behavior is the same for all samples, but the T_O and the low temperature NCRIF widely vary.

1.3.2 Experimental Work

One serious problem that the experimental community is facing is the lack of "success" in using techniques other than the torsional oscillator (TO). Still much can be learned from the TO experiments to date, which are described in the first section below. The following section then addresses two "21st century" dc flow studies. Lastly, I mention a variety of other interesting experimental results. Just as the previous discussion on theory, I hope the following serves as a useful collection of references.

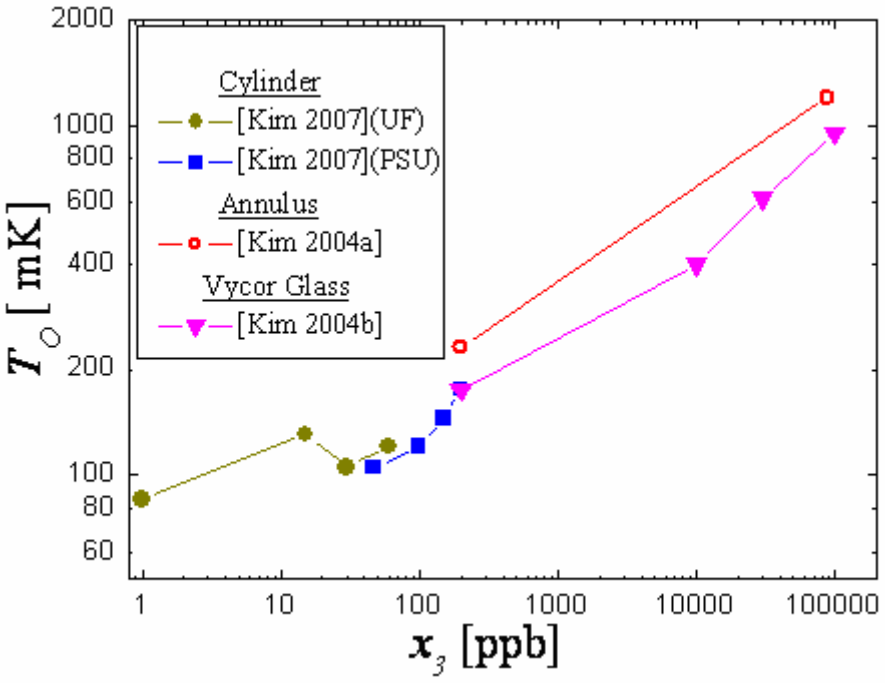

Fig. **1-3**: ^{3}He dependence of the onset temperature. Solid helium samples confined in different geometries all show similar behavior.

1.3.2.1 Previous Torsional Oscillator Experiments

Since Dr. E. Kim's original experiments, the finding of NCRI in solid ^{4}He has been replicated in four other laboratories [**Rittner 2006**],[**Kondo 2007**],[**Penzev 2007**],[**Aoki 2007**]. The temperature dependence of NCRI is qualitatively reproducible [see Fig. **1-2**], and is characterized by saturation in the low temperature limit and a gradual decay to zero at higher temperature. However, the onset temperature, where NCRI becomes resolvable from the noise, varies between ~200 and ~400mK in all of the studies of commercially pure helium (~300 ppb of ^{3}He). It is obvious from Fig. **1-2** that these variations even occur from sample to sample grown within the same cell. Using

more careful growth methods, the scatter in the NCRIF from Ref. [**Kim 2004c**] was partially reduced to reveal a non-monotonic pressure dependence of unknown origin [**Kim 2006**].

The temperature dependence can also be modified by the addition of ^{3}He impurities [**Kim 2004a**],[**Kim 2004b**],[**Kim 2007**],[**Clark 2007**]. The impurity atoms broaden the transition and, on average, result in a higher T_O [see Fig. **1-3**]. Lastly, recent measurements on the same cylindrical sample at two different frequencies found that the onset of NCRI was noticeably to higher temperature at higher frequency [**Aoki 2007**].

Another important result is that of annealing. In one study the observed NCRIF ~0.5% was reduced to <0.05% following heat treatments [**Rittner 2006**]. While the reverse effect has also been observed upon annealing [**Penzev 2007**], it is clear that crystal quality must have some relevance. Otherwise, it is extremely difficult to explain the vast range of NCRI fractions measured in different cells, which varies from as little as 0.03% up to 20% [**Rittner 2007**],[**Kim 2007**].

However, complications arise when attempts are made to apply a simple picture (such as vacancy or grain boundary models) to solid helium. For example, the solid samples grown in porous Vycor glass (pores ~7nm) [**Kim 2004b**] and porous gold (pores ~490nm) [**Kim 2005**] are undoubtedly the lowest in quality of any found in the literature. The small confining dimensions hinder the formation of large crystals. In addition the large surface to volume ratio in porous media results in high densities of strained and defect-rich regions. And yet, the NCRIF in these porous hosts is only on the order of a percent, suggesting that crystalline defects are not vital to NCRI. In what appears to be a complete contradiction, the NCRIF in quench condensed samples grown in a “thin”

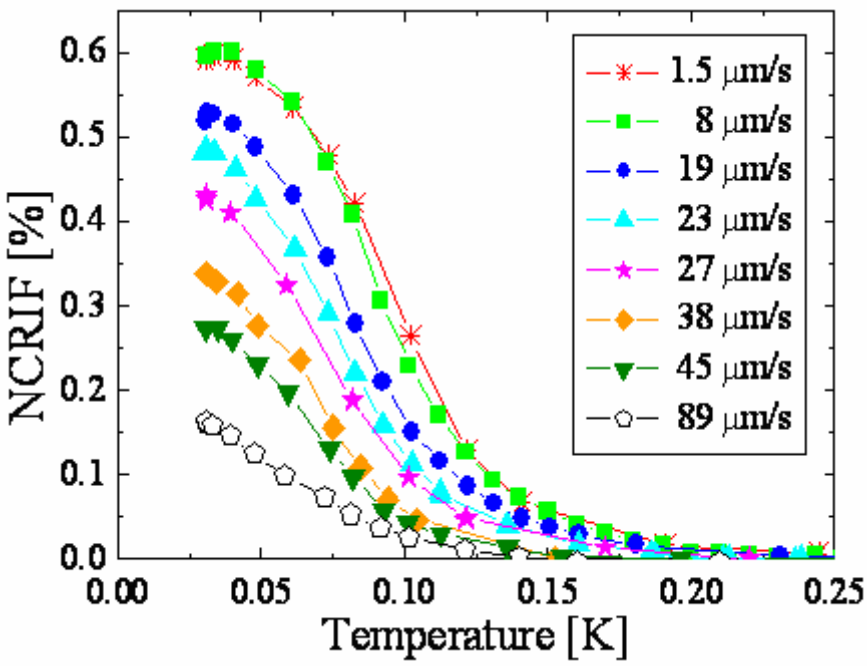

Fig. **1-4**: The effect on NCRIF due to different TO oscillation speeds. The pressure of the sample from Ref. [**Kim 2006**] is 137bar.

annulus (width of 0.15mm) are found to be as large as 20% [**Rittner 2007**], while those in thicker annuli (0.3 and 0.6mm) are limited to a few percent.

The differences between the experiments carried out in the bulk and in porous media might in some way be related to disparities in the hydrodynamics and/or topology of the systems. It is known that the measured NCRIF is influenced over the entire temperature range by the oscillation speed of the TO [see Fig. **1-4**]. Plotting the low temperature value of NCRIF as a function of the velocity reveals that NCRIF is only attenuated above a certain value [see Fig. **1-5**]. It therefore may be suitable to define a critical velocity of ~10μm/s [**Kim 2006**]. For the dimensions of the annulus this velocity corresponds to approximately one quantum of circulation (using Eq. **1.4**, $n \sim 3$).

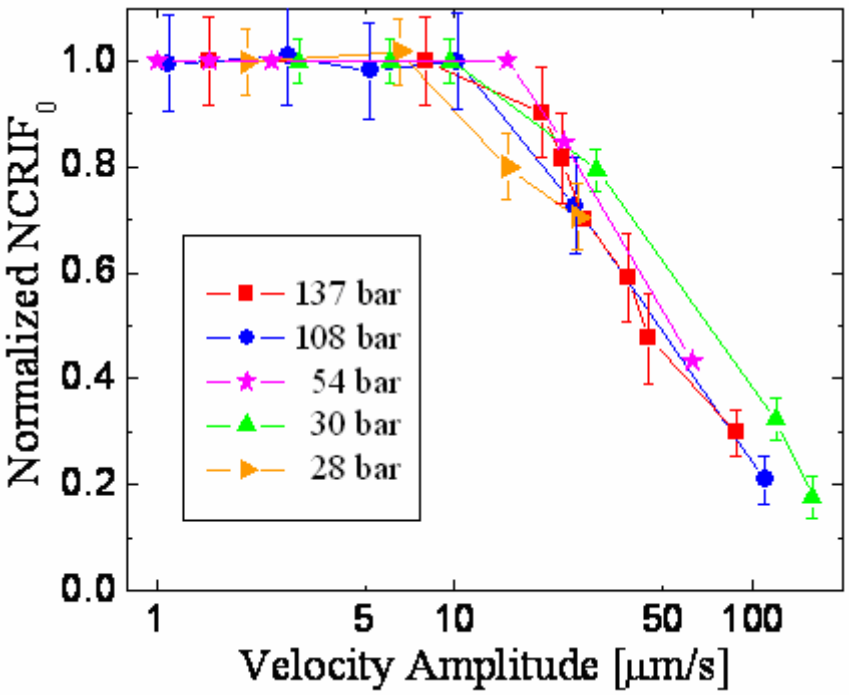

Fig. **1-5**: Velocity dependence of NCRIF [**Kim 2006**]. The fraction has been normalized by the low temperature limiting value. The curve appears to be universal for all samples grown in the same annulus.

The sinusoidal motion of the TO is such that the attenuated NCRIF could also be the result of a critical displacement or acceleration. However, the recent frequency study [**Aoki 2007**] supports the interpretation of Ref. [**Kim 2006**]. The attenuation of NCRIF upon increasing velocity was found to be identical at both measurement frequencies. In contrast, plots similar to Fig. **1-5**, but with displacement or acceleration as the abscissa, were found not to coincide at the two frequencies.

Additional observations from Ref. [**Aoki 2007**] include reversible and irreversible changes of NCRIF upon changes in the oscillation speed above and below ~40mK, respectively. These results are likely related to some of the behavior that I have observed in ^{4}He crystals, which is presented in Chapter 5.

1.3.2.2 DC Flow Experiments

There are two main dc flow experiments that have been carried out since NCRI was observed in bulk ^{4}He. The first was an attempt to squeeze the solid through an array of glass capillaries, each of which were 25μm in diameter [**Day 2006**]. Plastic flow in samples was observed just below the melting point where the solid is soft. However no anomalous dc or very low frequency (0.01 to 0.1Hz) ac flow was seen between 35mK and 1K.

The other experiment investigated dc flow in ^{4}He samples of solid-liquid coexistence [**Sasaki 2006**]. They observed flow of liquid ^{4}He through the solid phase, concluding that superfluid liquid could permeate along grain boundaries. This occurred in three of thirteen samples. Due to experimental difficulties, the temperature dependence of this phenomenon could not be investigated thoroughly. However, while the flow in two samples was studied at 50mK (no precise T_O was reported), the third sample exhibited the same behavior at 1.13K, indicating that it is due to relatively thick superfluid films flowing along grain boundaries or cracks in the solid.

1.3.2.3 Miscellaneous Experiments

There are a number of neutron scattering measurements that have recently been carried out, but all with marginal sensitivity and at temperatures above the point of saturation in NCRI [**Adams 2007**].

An inspection of the mechanical response of solid ^{4}He to low amplitude vibrations of a diaphragm has revealed several low frequency, non-linear resonances that are

highly sample-dependent [**Mukharsky 2006**]. The resonant modes have not yet been explained and their relation to the TO experiments is uncertain.

The pressure of the solid phase and of solid-liquid mixtures has been re-examined recently. In the former, evidence of a glassy phase (quadratic temperature dependence in excess to the phonon contribution) was reported in unannealed solid samples [**Grigor'ev 2007**]. Annealing removed, or at least diminished, the glassy component. The melting curve measurements observed no deviations from the solid and liquid phonon contributions to within ~2μbar (although they quote a value of 0.5μbar) down to 10mK [**Todoshchenko 2006**]. These two experiments can be compared with a recent specific heat study from our own laboratory [**Lin 2007**]. Due to extremely long growth periods, between 4 and 24hr, our samples were presumably of the "annealed" type in Ref. [**Grigor'ev 2007**]. The wider temperature range and greater accuracy of our measurement allowed us to definitively rule out the existence of a glassy phase in our samples. The most interesting detail of our study is that we observed a very small and broad heat capacity peak in the temperature range of interest, i.e. centered near 75mK. Surprisingly, the peak is unaffected by the addition of up to at least 30ppm of ^{3}He impurities. The ^{3}He only results in a constant background term, much like that of an ideal gas. The peak is also potentially present on the melting boundary, although experimental complications make the data less "clean." Through integration, we find that the peak we observe is marginally within the sensitivity of Ref. [**Todoshchenko 2006**]. Unfortunately, their pressure gauge exhibited anomalous behavior precisely in this temperature regime, so it is difficult to say if the two experiments are contradictory.

Chapter 2

The Solid Phase: Meet and Greet

There are a few important attributes of the two condensed gases discussed in this thesis. In order to make jargon in the upcoming chapters common place, I am providing this review.

For a broad and extremely informative examination of the solid hydrogens, see Ref. [**Silvera 1980**]. For a shorter, more specific discussion on the quantum mechanical "hopping" in solid H_2 that is discussed in this thesis, see the reviews by Dr. H. Meyer [**Meyer 1987**],[**Meyer 1998**], and references therein.

I intend for the section below on helium to serve as a useful review of the early attempts in the growth of helium crystals, since I have not come across any general survey that covers the full range of growth techniques. As in every part of this thesis, I encourage the reader to investigate all of the individual papers listed in the bibliography.

2.1 Ortho-to-Para Conversion in Hydrogen

The two lowest rotational energy levels of a H_2 molecule are the para- and ortho-states, having angular momentum $J = 0$ and $J = 1$, respectively. The energy gap between the ground state and $J = 1$ is $\Delta E = 170.5$K, which seems large but is in fact much less than that for $J > 1$. For this reason only the two lowest states are thermally populated for temperatures below ~20K.

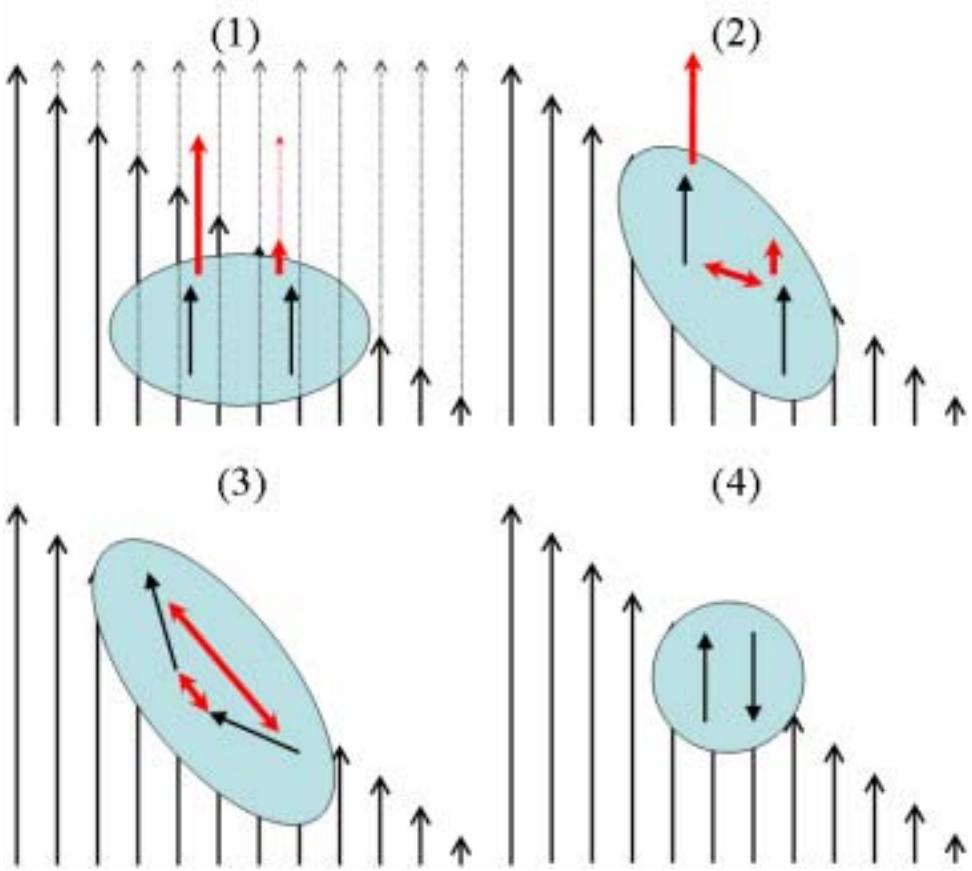

Fig. **2-1**: Cartoon of the magnetic forces on individual spins within an ortho-H_2 molecule. The thin arrows in the first frame show how a homogeneous magnetic field results in translation of the ortho-H_2 molecule. An inhomogeneous field is necessary to promote the conversion to para-H_2. Thus, ortho-H_2 molecules will only convert if they are in the vicinity of another of their kind, or other magnetic impurities.

Below 4K the equilibrium concentration of ortho-H_2 (x) is essentially zero. However, the conversion rate from ortho-H_2 to para-H_2 in the solid is very slow for 0.5K < T < 13.8K. The slow rate is a consequence of the reaction constant of only k = 1.9% per hour, and the dependence on the square of the concentration (note, not the initial concentration!).

$$\frac{dx}{dt} = -kx^2 \qquad \text{Eq. 2.1}$$

For example, about three weeks of conversion are required for x to drop from 0.01 to 0.009.

The conversion rate increases at lower temperature for reasons that will be discussed momentarily. However, the most effective way to promote conversion is by keeping H_2 in the liquid phase (T > 13.8K) in the presence of a high surface area, magnetic material. The appropriate catalyst contains isolated magnetic impurities that produce highly inhomogeneous magnetic fields locally, which is the exact requirement to induce a spin flip within a H_2 molecule [see Fig. **2-1**]. Conversion is most efficient in the liquid phase because the molecules are very mobile and therefore more likely to come into contact with magnetic impurities. In this way x can be reduced to as low as 10^{-4}, although 10^{-3} to 10^{-2} are more typical experimental values. Since ortho-to-para (OP) conversion within the solid phase is irreversible ($x > x_{eq}$, always) the average ortho-concentration of each sample only decreases with time.

OP conversion is an exothermic process that can be quite taxing on a ^{3}He-^{4}He dilution refrigerator, which usually has a cooling power of ~100μW at 100mK. Starting from some initial concentration (x_0), the heat release at a later time is given by

$$\dot{Q} = U \frac{k x_0^{\,2}}{(1 + x_0 k t)^2} \qquad \text{Eq. } \mathbf{2.2}$$

where the heat of conversion (U) is 1.06kJ/mol. If room temperature H_2 gas is rapidly condensed and frozen into the solid phase then it is possible to have x ~0.75. For the sample size in the present study (0.4cc of solid equals 35mmol) the amount of power generated during the initial stages of conversion in this case would be ~85μW!

2.2 Low Temperature Behavior of Ortho-H_2 Impurities

As mentioned above, the mobility of molecules is obviously much higher in the liquid than in the solid. The hopping time for thermally activated diffusion in the solid phase goes as $(\sim 10^{-13}\text{s})(e^{200/T})$, such that times are <1s above 7K and extremely long below 4K. The distribution of ortho-H_2 throughout the sample can therefore only be considered random above several Kelvin. In agreement with this, statistical distributions of ortho-H_2 molecules, characterized by pressure measurements ($dP/dT \propto$ free energy), have been shown to be frozen in below ~3K [**Jarvis 1968**].

Long equilibration time constants (tens of hours) are typical in studies of ortho-H_2 diffusion in solid para-H_2 [**Meyer 1987**],[**Meyer 1998**]. However, in the dilute limit (x <0.1) it has been found that isolated ortho-H_2 molecules (singles) can propagate ballistically at T <100mK [**Amstutz 1968**]. The impurities effectively travel throughout the lattice via the transferal of J from molecule to molecule rather than by particle exchange [see Fig. **2-2**]. This process is called resonant OP conversion [**Oyarzun 1971**]. The mechanism behind this is not perfectly understood, but some of the proposed ideas [**Meyerovich 1994**] are at least qualitatively consistent with experiments [**Meyer 1987**],[**Meyer 1998**].

The “equilibrium” state of the solid thus involves a temperature-dependent distribution of singles, pairs (two neighboring ortho-H_2 molecules), and larger clusters of ortho-H_2 [**Meyer 1969**]. At several Kelvin, all of the ortho-H_2 molecules are randomly distributed as singles. As the temperature is lowered the number of isolated singles decreases in favor of the formation of pairs and larger clusters. In local regions the ortho-

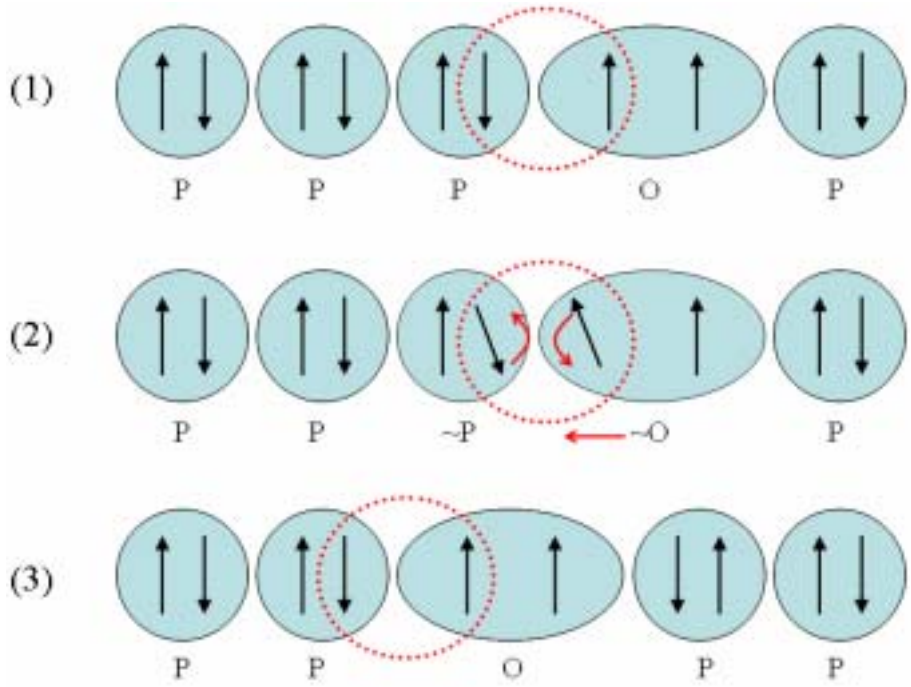

Fig. **2-2**: Cartoon of resonant OP conversion.

H_2 concentration is enhanced, resulting in faster OP conversion rates [**Schweizer 1979a**].

Clustering was first observed by monitoring the time evolution of the nuclear magnetic resonance (NMR) absorption spectra for ortho-H_2 singles and pairs after rapid warming or cooling of solid H_2 crystals [**Amstutz 1968**]. The singles decay rate exhibits a non-monotonic temperature dependence, decreasing dramatically between 300 and 100mK. Well below 100mK the decay of singles is on a time scale of minutes rather than hours. The pair spectrum also shows an increased decay rate at low temperature but time constants are at least one order of magnitude longer, e.g., on the order of 10h at 25mK [**Washburn 1980**]. Since it is difficult to resolve the NMR spectra of triples or larger clusters [**Harris 1968**], NMR studies cannot quantify the degree of mobility of larger ortho-H_2 clusters that form at low temperature. Their presence, however, has been

detected for solid H_2 crystals held at 25mK for only 24h [**Schweizer 1979b**].

Thermodynamic investigations, which examine the system in its entirety (singles, pairs, triples, etc.), have also been carried out. Specific references can be found in the aforementioned reviews [**Meyer 1987**],[**Meyer 1998**]. One experiment that stands out involved simultaneous NMR and thermal conductivity measurements [**Li 1990**]. The time evolution of the thermal conductivity was found to depend strongly on temperature. For T >300mK the time dependence could be described by a simple exponential. However, contrary to the singles decay rate, a sum of two exponentials best fit the conductivity data below 300mK. This difference may be related to the presence of ortho-H_2 clusters at lower temperature. Further discussion is deferred to Chapter 4.

2.3 Growth, Morphology, and Quality of Helium Crystals

The first time ^{4}He was ever solidified was in 1926 [**Keesom 1942**], three days before my grandmother was born. Since that time several growth procedures have been perfected, by which I mean that they result in the reliable formation of high quality single crystals. However, the last eighty years of research has still somehow led to an uncertainty in the morphology and quality of the ^{4}He solid samples in recent torsional oscillator studies [**Kim 2004a**],[**Rittner 2007**],[**Rittner 2006**],[**Kondo 2006**],[**Penzev 2007**],[**Aoki 2007**], which are grown by the blocked capillary (BC) method. Since the BC method is not used very often in careful studies of extremely high quality crystals, many of our conclusions on the BC sample morphology must be drawn from “vintage” publications.

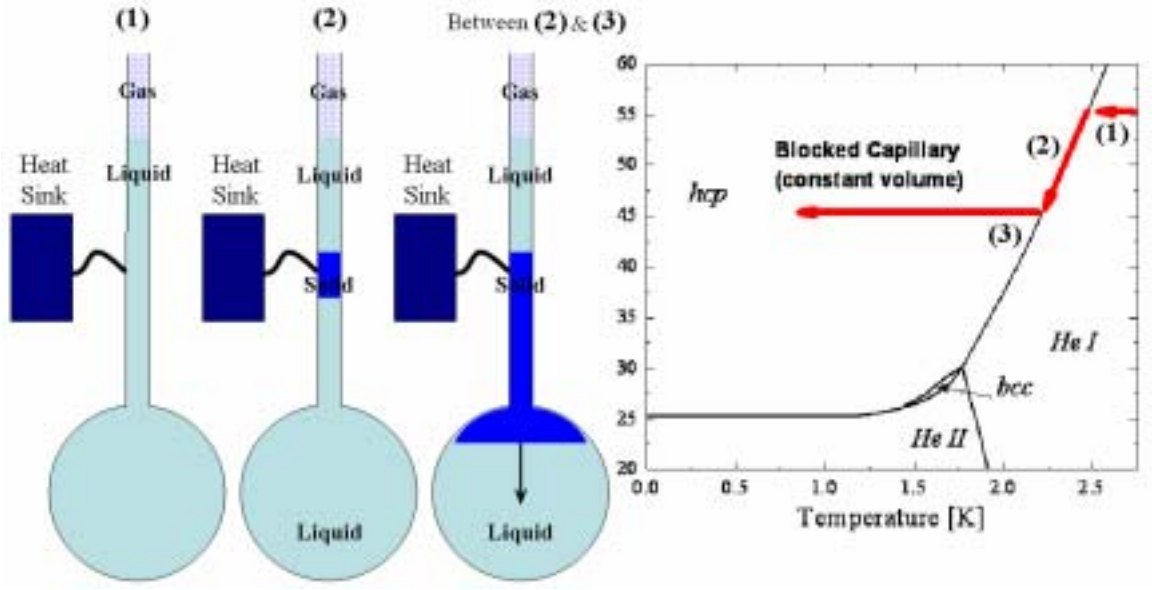

Fig. **2-3**: Cartoon and thermodynamic path of the BC method used to grow solid helium samples.

The BC method involves filling a sample cell with high pressure liquid ^{4}He, freezing a section of ^{4}He in the filling line (the block), and then cooling the constant volume below the block along the solid-liquid coexistence boundary [see Fig. **2-3**].

Two growth techniques that are superior to the BC method [**Vos 1967**] are carried out at a fixed point anywhere on the solid-liquid coexistence curve [see Fig. **2-4**]. This can only be done if no block forms in the capillary to the cell. The first of the two techniques is constant pressure (CP) growth, and is achieved by slowly cooling the cell while a specific freezing pressure (P_F) is maintained. The second, constant temperature (CT) growth, takes place at a single freezing temperature (T_F) for minimal overpressures above P_F. The latter technique is most often empolyed, as it is in this study, when growing low pressure solids from the superfluid phase [**Vos 1967**],[**Heybey 1967**].

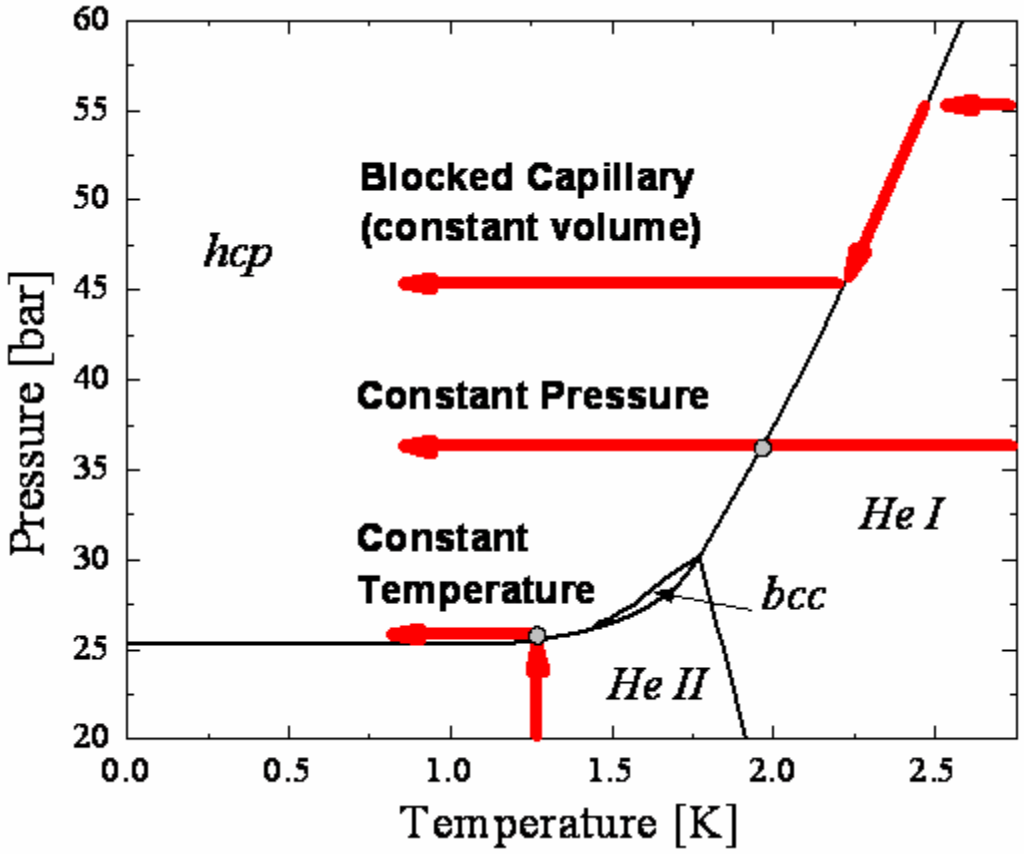

Fig. 2-4: Comparison of the thermodynamic paths of BC, CP, and CT growth. The latter two actually take place on a single point (anywhere) on the solid-liquid coexistence curve.

Below I review many of the works leading up to the well established CP and CT growth methods of today. There is a lot of information, so the reader is encouraged to take it slow and remember to read the brief summary at the end.

2.3.1 Early Years

One problem with some of the pioneering papers on solid ^{4}He is that the scientists had little knowledge to go on and were therefore using a collage of irregular growth

methods. Therefore, some of the conclusions from these experiments are questionably applicable to present day studies. The purpose of this section is to sort out some of these details.

2.3.1.1 Scattering

The crystalline structure of ^{4}He was determined from x-ray diffraction in 1938 [**Keesom 1938**]. There are no specific details about the exact growth procedure, although it is implied that the pressure in the cell was simply raised up to 38bar to cause solidification while some "low enough temperature" (<1.7K) was maintained. Since careful CP and CT methods were not yet developed it might be expected that polycrystalline samples would form. In fact, Keesom and Taconis originally anticipated powder patterns (rings) on the exposed film. Having found none, nor any diffraction spots, the original cryostat was modified so that it could be rotated by 45° during the exposure time. The result was to bring several points of the 3D diffraction pattern into focus on the screen for a long enough duration so as to produce diffraction spots. It worked, and the patterns observed were traced back to the hcp structure. Among their samples, a single crystal was grown once, while every other time two crystals were formed in the cell (2mm diameter aluminum tube).

The next x-ray experiment in the literature studied BC samples [**Schuch 1962**]. They were unable to produce powder samples, but instead grew several large crystals within the cell. This was true for both the hcp and bcc phases. Similarly, no powder

patterns were obtained with neutron scattering for samples grown by BC [**Minkiewicz 1968**] or by abrupt freezing of samples from the superfluid phase using very large pressure steps (~10bar) [**Henshaw 1958**].

Almost all of the x-ray and neutron scattering measurements since the above were completed have been carried out on single crystals grown at CP. I mention a few of these studies in the upcoming sections.

2.3.1.2 Optics

The first successful visualization [**Shaln'kov 1962**] of ^{4}He crystal growth was reported in 1962. Samples were grown at a large CP, where P_F ~100bar. Difficulties in achieving large crystals were due to the large latent heat and slow recrystallization rates at high pressure.

A few years later came a more thorough study [**Vos 1967**] of crystals grown using the BC, CT, and CP techniques. The optical birefringence was measured, allowing for the determination of crystal sizes and orientations. They found the freezing surface of BC samples would gradually move across the cell. In addition, several nuclei formed on the glass walls of the cell, which would then grow with hexagonal-dendritic shapes. This is due to the higher thermal conductivity in the liquid. Samples consisted of a “fine” polycrystalline structure upon complete solidification, which, if kept near the freezing temperature, would continually coarsen over a time period of 3 to 30min. Samples that were grown into the bcc phase at CT never exhibited dendritic growth. However, with the slight aid of annealing, the best single crystals were obtained with CP growth.

In the same year, optical birefringence measurements were carried out [**Heybey 1967**] on hcp crystals grown at CT with T_F ~1.2K. At least 40% of the time it was found that large crystals (~2cc) were grown in <5min. In other cases, the samples were either crystals oriented with the c-axis along the optical axis, or made of many small crystallites. The former seems likely, since it would be odd to achieve single crystals half of the time and powder samples (which were absent in Ref.'s [**Keesom 1938**], [**Schuch 1962**], [**Minkiewicz 1968**],[**Henshaw 1958**]) the other half of the time.

In the late 1970s and throughout the 1980s many optical measurements on solid ^{4}He were carried out and experimentation was fine-tuned. For a review, see Ref. [**Balibar 2005**].

2.3.1.3 Thermal Conductivity

In the ballistic limit at low temperature the mean free path (λ_{ph}) for phonon scattering is limited by the size of individual crystallites, or in the case of large crystals, by the smallest cell dimension. Early thermal conductivity measurements were on BC samples, and found λ_{ph} ~0.1mm, which increased upon annealing [**Webb 1953**]. A similar annealing effect was observed in a later experiment in which individual grains within the sample, again ~0.1mm, were actually found to be of extremely high quality [**Armstrong 1979**].

Since the work of Ref. [**Webb 1953**] most studies have been carried out on samples grown at CP or CT. In the earliest works [**Mezhov-Deglin 1965**],[**Ackerman 1966**], the success rate for growing single crystals from the normal fluid at CP is at least

25%. A later study employing CP growth improved this fraction to more than two-thirds [**Hogan 1969**], while CT growth from the superfluid using overpressures of a few tenths of a bar above P_F was found to be extremely reliable [**Fox 1972**]. In many of these studies, BC samples were prepared for comparison. However, some of the inferences that were made could not be verified until later [keep reading to learn the whole story].

2.3.1.4 Sound

The first longitudinal [**Vignos 1966**] and transverse [**Lipschultz 1965**] sound velocity measurements in the hcp phase were conducted in the mid-1960s, on samples grown at CT. The sound speeds varied drastically from sample to sample, indicating that large crystals were being formed each time, but with a different orientation. In contrast, sound velocities measured in the isotropic bcc phase were consistent from sample to sample [**Lipschultz 1965**].

2.3.2 Crystal Quality

In the early 1970s several experiments involving *in situ* characterization of samples clarified the connection of thermal conductivity and sound measurements with sample morphology and crystal orientation.

2.3.2.1 Understanding Thermal Conductivity

Thermal conductivity has been measured in samples characterized by x-ray diffraction [**Fain 1970a**] and/or optical birefringence [**Berman 1973**]. The x-ray study was carried out at much higher pressure (290bar) than other works discussed in this chapter. One of six samples was a single crystal while the others were made up of multiple, usually three, large crystals. Although crystals were large in each sample, the overall quality was considered poor in all but the single crystal sample. They did find, interestingly, that the quality of samples grown rapidly could be vastly improved upon annealing. In contrast, slowly grown samples did not improve, so that is was concluded that small amounts of grown-in strain were stable.

The optical study was carried out on lower pressure (~39bar) samples grown at a CP. As did some earlier investigators, they also grew BC samples for comparison. The thermal conductivity was verified to be highly anisotropic in single crystals. However, in BC samples they found that it is uncommon to produce many randomly oriented crystallites, i.e. the type of sample that would lead to a powder diffraction pattern.

2.3.2.2 Understanding Sound Velocity

The sound velocity has also been measured in samples characterized by x-ray diffraction [**Greywall 1971**] and/or optical birefringence [**Crepeau 1971**],[**Wanner 1970**]. The x-ray study investigated CP samples at several pressures above ~30bar and mapped out the azimuthal angular dependence of longitudinal and transverse sound. An optimized growth rate (between 5 and 10μm/s) was found to yield single crystals about

half of the time. Slower rates led to polygonization (such as twinning), while faster growth rates produced “polycrystals” (the number of crystals was not described in detail). Just eight out of 239 samples investigated were grown from the superfluid phase. Both rapid pressurization and controlled growth were attempted. Although samples were optically clear during growth, or recrystallized within seconds upon completion to become so, no x-ray patterns were visible. Based on all earlier scattering measurements [**Keesom 1938**],[**Schuch 1962**],[**Minkiewicz 1968**],[**Henshaw 1958**], it is unclear why no x-ray signal was detected.

Sound anisotropy was also observed in the two birefringence studis. One study used CP growth from the normal fluid phase and reported a 50% success rate in producing single crystals [**Wanner 1970**]. No statistics were given in the study carried out on single crystals grown from the superfluid at CT. However, multiple crystals from the entire range of possible orientations were produced, indicating that the “unknown” samples from earlier optical measurements [**Heybey 1967**] were likely single crystals. The above studies [**Greywall 1971**],[**Crepeau 1971**],[**Wanner 1970**] have been used to determine the orientation of crystals in almost all sound velocity experiments on solid ^{4}He since the 1970s.

2.3.2.3 Dislocation Lines

There are various ways to quantify the quality of ^{4}He crystals. For example, the radial smearing of x-ray diffraction spots was observed upon expansion of a sample during irradiation [**Fain 1970b**]. One cannot talk about strain in a crystal without

mentioning dislocation lines. While high and low density regions of dislocations were observed in a recent study using x-ray topography [**Iwasa 2003**], in the future individual dislocations may be identified and monitored. It will be useful to compare these results with the many ultrasound experiments that have studied dislocated ^{4}He crystals.

Dislocation lines form an entangled web throughout each crystal, and can vary in density by more than five orders of magnitude ($<10^5 cm^{-2}$ to $10^{10} cm^{-2}$) in solid helium samples grown above 1K using different methods. The actual line density deduced from sound measurements [**Wanner 1976**] depends very sensitively (varying by four orders of magnitude) on the exact growth conditions of crystals [**Wanner 1976**],[**Tsuruoka 1979**]. For instance, CP growth was used in Ref. [**Wanner 1976**] to achieve densities $\sim 10^5 cm^{-2}$, while an awkward mix of CP and BC growth was used in Ref. [**Tsuruoka 1979**] and resulted in $\sim 10^9 cm^{-2}$. It can also vary by at least one order of magnitude from sample cell to sample cell, despite nearly identical growth procedures [**Wanner 1976**], [**Iwasa 1979**].

Lastly, trace amounts of ^{3}He are found to produce significant changes in the sound velocity and elastic constants measured in solid ^{4}He. These results indicate that ^{3}He impurities condense onto dislocation lines [**Suzuki 1980**].

2.3.3 Key Points on Solid ^{4}He Crystals

To summarize, the literature states that single crystals are easily and reliably (and can even be quickly) grown from the superfluid phase at a constant temperature. At higher pressures, the preferred method of growth is at a constant pressure.

When samples are grown with the blocked capillary method, the resulting solid is can be polycrystalline (although it is rare to achieve a collection of many randomly oriented crystallites). However, different conditions will lead to average grain sizes of anywhere from ~0.1mm to ~1cm, depending on the cell dimensions, temperature gradients, and growth rate. Annealing can lead to recrystallization and grain coarsening, which appears to be most effective in low pressure solids. To my knowledge, there is no evidence of extremely fine-grained (~1μm) polycrystalline samples having ever been grown.

However, the quality of single crystals and of individual crystallites within polycrystalline samples can vary by many orders of magnitude. Thus, both very lousy single crystals, and first-rate polycrystals, can be grown.

Chapter 3

Experimental Details

3.1 Torsional Matters

The torsional oscillator (TO) technique has already been described in too many theses. The reader is encouraged to view Dr. E. Kim's thesis [**Kim 2004a**] in particular, since it pertains to supersolid ^{4}He. In an effort to save some trees, I will not go into detail here.

The TO consists of a sample cell and torsion rod. The resonant period (τ) of the oscillator is therefore given in terms of the torsion constant (K) of the rod and moment of inertia (I) of the cell.

$$\tau = \sqrt{\frac{I}{K}} \qquad \text{Eq. 3.1}$$

When hydrogen or helium is introduced into the cell, the resonant period lengthens in accordance with the mass loading. Since the additional mass is small,

$$\delta\tau_{loading} = \frac{\tau}{2}\frac{\delta I_{loading}}{I} \qquad \text{Eq. 3.2}$$

Further changes in τ are, in the simplest cases, associated with changes in the sample mass that rotates with the container. In other words, changes can be proportional to the superfluid fraction (ρ_S/ρ).

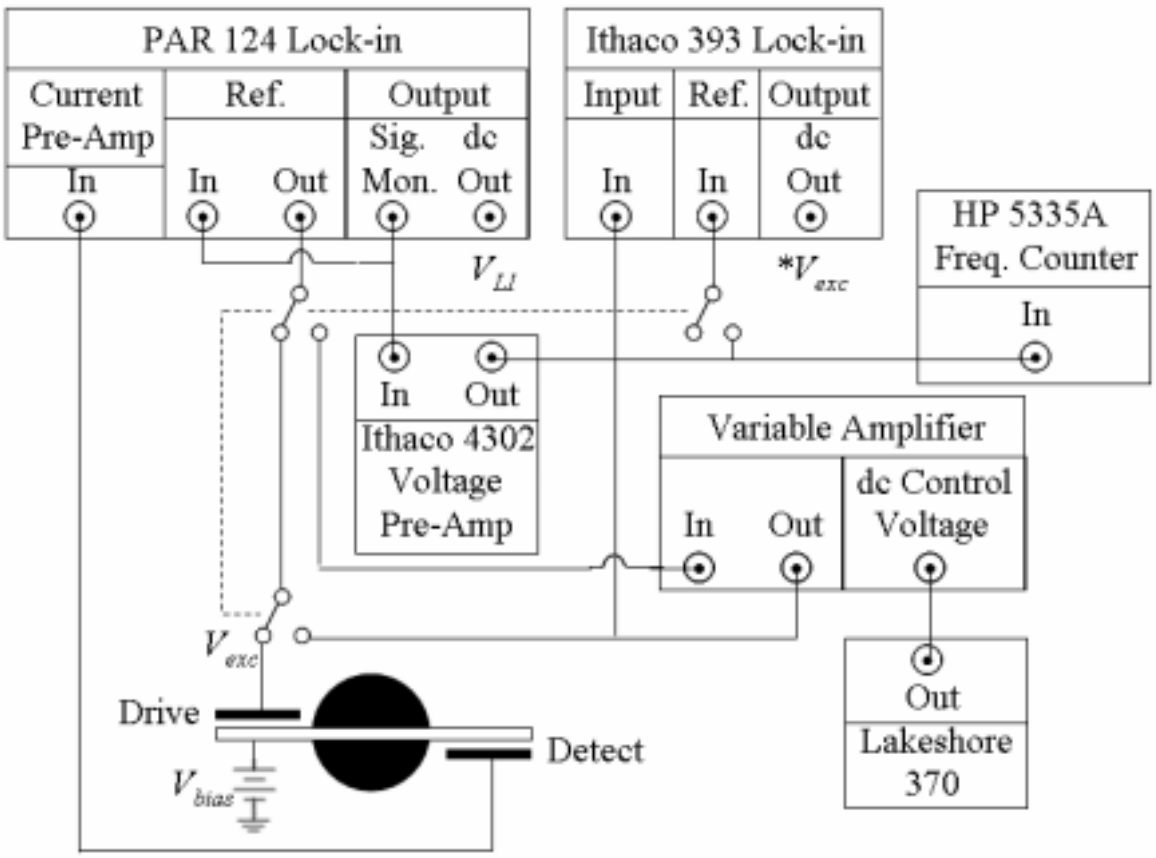

Fig. **3-1**: Block diagram of the circuits used in the solid H_2 and ^{4}He studies. The present switch settings correspond to constant drive mode. Constant velocity mode was only used in the ^{4}He experiments.

$$\frac{\rho_S}{\rho} = \frac{\delta I_{decoupling}}{\delta I_{loading}} = \frac{\tau_{decoupling}}{\delta\tau_{loading}} \qquad \text{Eq. 3.3}$$

Throughout this thesis I use the term NCRIF in place of ρ_S/ρ, as that is the currently accepted term in the literature.

3.1.1 Electronics

The block diagram of the usual circuit used in Chan's laboratory is shown in Fig. 3-1. The current switch settings in the figure correspond to the operation normally used, where the TO is driven on resonance by the ac output voltage of the primary lock-in amplifier (PAR 124). The excitation is varied at one of two electrodes that are capacitively coupled to a fin (or pair of fins) attached to the torsion bob. Currently depicted in the figure is the so-called "constant drive mode," for which the rms amplitude of the excitation voltage is kept constant. The ensuing motion is detected by the second electrode. The induced current is amplified and fed back into the lock-in. The "signal monitor" of the PAR is connected to the lock-in's own external reference port, so that the drive voltage remains on resonance.

For many of the measurements on solid ^{4}He, I was interested in how the maximum rim speed (v_{MAX}) of the TO affected the measured NCRIF. In lieu of the dissipation peak [**Kim 2004a**], during which v_{MAX} can decrease by as much as 40%, I incorporated a variable gain amplifier into the circuit [**Zassenhaus 1999**]. The design is shown in Fig. 3-2. The variable amplifier is adjusted as to maintain a constant lock-in output voltage (V_{LI}), enabling what is called "constant velocity mode." The amplifier used in the helium experiment had a maximum gain of 4X. This can easily be increased by an order of magnitude by switching out the 100Ω resistor with a larger value. The gain is set by a DC voltage. I used one of the variable analog outputs of a Lakeshore 370 resistance bridge, which could be continually updated by LabVIEW code that I wrote. Computer control is provided by the "PID" loop written into the code (actually, just

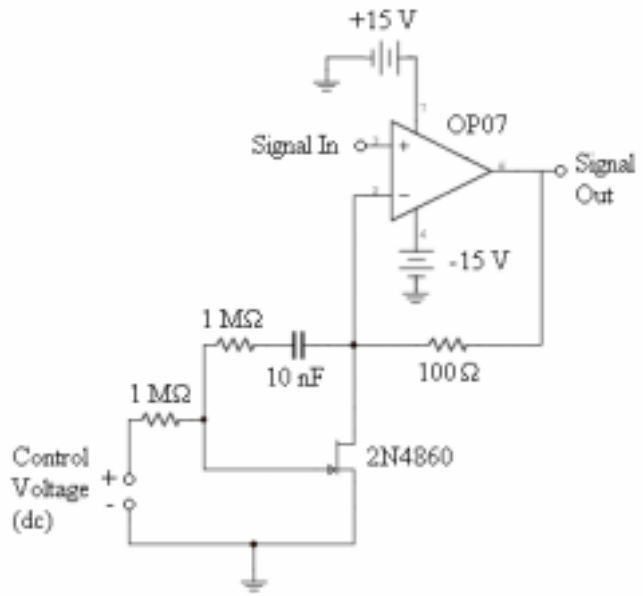

Fig. **3-2**: Circuit design of the variable amplifier that enables the constant velocity mode of oscillation.

Proportional and Integral – no Derivative), yielding an oscillation speed stability of ~1%. Further tinkering revealed that the primary bottleneck to improvement was the slowed response of the computer when multiple programs were running. In the future, a post-1995 pc will solve the problem. Also, at low excitations a second lock-in (Ithaco 393) is required to reliably measure the drive voltage [see Fig. **3-1**]. Using a standardvoltmeter results in highly noisy dissipation data, which is proportional to V_{exc} [see Eq. **3.5**].

The maximum amplitude (d_{MAX}) and maximum rim speed can be calculated in the same fashion for either circuit. The derivation in Ref. [**Kim 2004a**] yields the following expression.

$$v_{MAX} = \frac{2\pi}{\tau} d_{MAX} = \frac{\sqrt{2} V_{LI} A \varepsilon_0}{G_{LI} G_{PA} V_{bias} C^2} \qquad \text{Eq. } \mathbf{3.4}$$

The area (A) and capacitance (C) correspond to the detection electrode. The gain of the lock-in (G_{LI}) and current pre-amplifier (G_{PA}) are typically (1 to 100mV)/(10V full scale) and 10^8 V/A, respectively. The bias voltage (V_{bias}) used in this experiment was 220V.

The internal dissipation is proportional to the inverse quality factor (Q^{-1}) of the oscillator,

$$Q^{-1} \propto \frac{input}{output} = Q_0^{-1} \frac{V_{LI,0}}{V_{LI}} \frac{V_{exc}}{V_{exc,0}} \qquad \text{Eq. 3.5}$$

The specific values measured at 20mK of the quality factor (Q_0^{-1}), maximum lock-in output voltage ($V_{LI,0}$), and drive voltage ($V_{exc,0}$) are used as reference points. Any changes that occur in Q^{-1} are then simply reflected in either V_{LI} or V_{exc}, depending on whether it is constant drive mode or constant velocity mode.

3.1.2 Future Members of the "Oscillator Graveyard"

Most students in Chan's lab have the honor of building multiple oscillators, many of which leak, have a design flaw, or just end up being swept under the rug. Hence, we all get to start our own graveyard. In this chapter I only describe the oscillators that were of the most use. Brief descriptions and schematics are given in the next two sections. Table 3-1 lists relevant parameters for all of the TO's.

Table 3-1: Information on the Torsional Oscillators. The stated periods and quality factors were measured at ~20mK.

Label	Samples	Geometry	Volume [cc]	Period [ns]	*Q*
H2TO-1	H_2 (200ppm)	annulus	0.17	980,486	$5x10^5$
H2TO-2	HD, pure H_2	cylinder	0.38	560,395	$2x10^6$
H2TO-3	pure H_2, HD	annulus	0.394	709,693	$5.2x10^5$
H2TO-4	pure H_2	blocked annulus	0.38	703,943	$1.1x10^6$
H2TO-5	H_2 (200ppm)	blocked annulus	0.25	781,171	$8.9x10^5$
HeTO-1	^{4}He (1ppb)	cylinder	0.38	1,167,770	$6.5x10^5$
HeTO-2	^{4}He (1&300ppb)	cylinder	0.317	932,932	$4.7x10^5$

3.1.2.1 Hydrogen Torsional Oscillators

Above I mentioned the different solid hydrogen samples that have been investigated. They are "commercial purity" H_2, "HD-depleted" H_2, and HD. While several TO's were built along the way, eventually I took the systematic approach [**Clark 2006b**] and studied high purity H_2 and HD in an annular geometry, as well as H_2 in a blocked annulus of otherwise identical dimensions. Below I describe all of the TO's used in chronological order.

The original TO had its unpleasant end after a rapid warmup of the refrigerator. The quality factor was horrible (zero) following the dismemberment of the magnesium cover. While no data from this cell has been published, it served its purpose as a H_2 vessel during what became months of trouble shooting the OP conversion process. The H_2 space in this cell was an annulus. The internal dimensions are shown in Fig. **3-3**. The samples studied in this cell were grown from commercial purity H_2 gas.

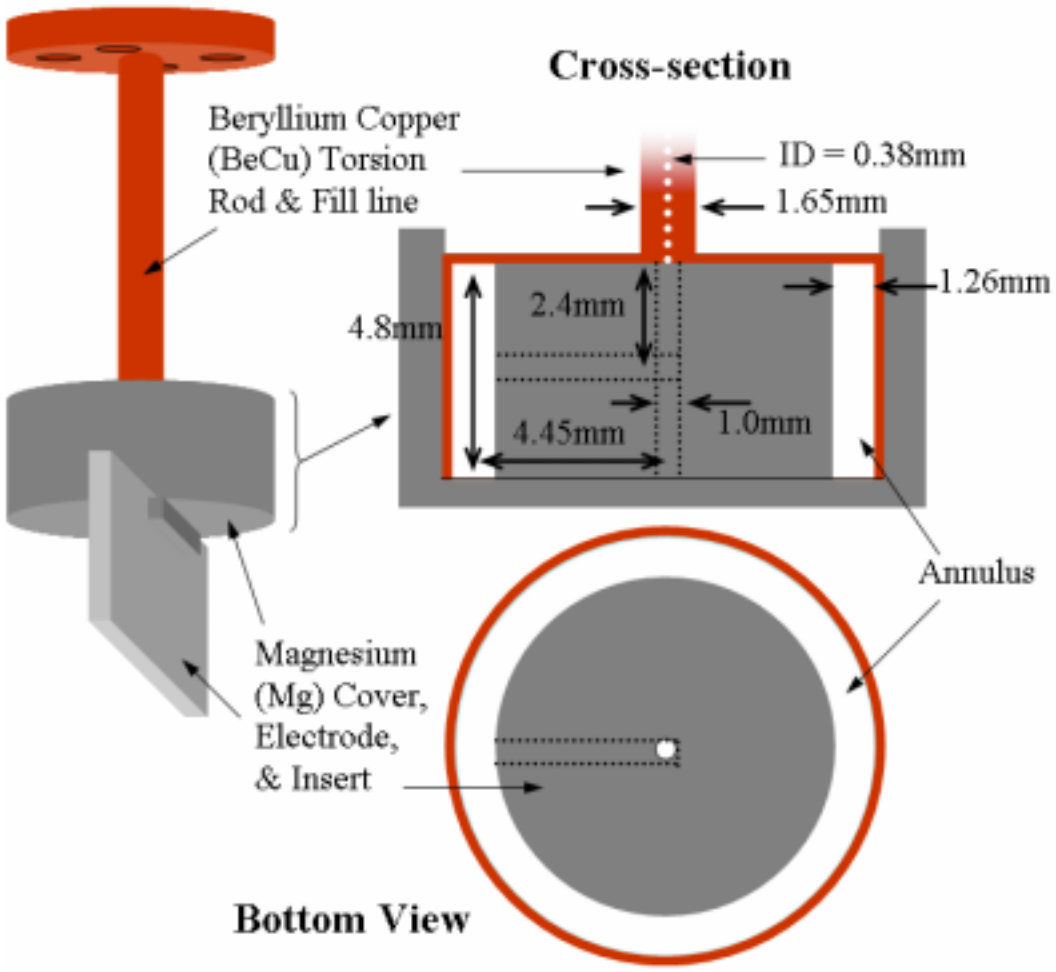

Fig. **3-3**: Schematic of the first TO used to study solid H_2.

In the next experiment I investigated solid HD as part of a control experiment. A new TO had to be built and, to increase the sensitivity, a cylindrical volume was used. The new torsion rod had an OD = 2.1mm and an ID = 0.38mm. The Mg electrode and cover from the first cell were actually re-used, since it was the thin bottom disc of BeCu that had previously failed under pressure. The lack of the Mg insert is therefore the only difference between the two torsion bobs. The radius of the open cylindrical geometry is 10.0mm.

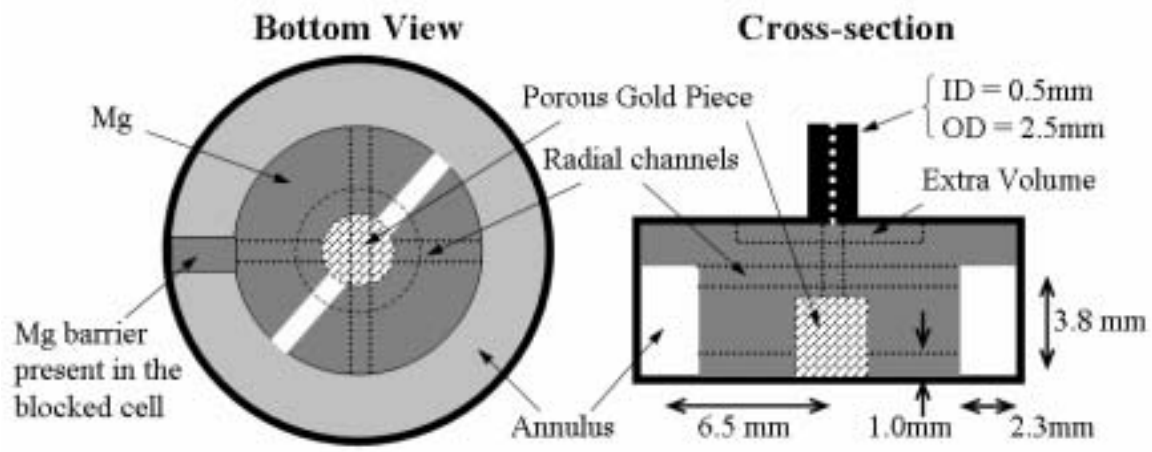

Fig. **3-4**: Internal geometry of the open and blocked annular cells used to study high purity solid H_2. The partially etched AgAu cylinder is 2.5mm in diameter and 3.3mm tall. The porous gold layer constitutes 2% of the total cell volume, and negligible inertia.

To avoid HD contamination in future experiments, the bulk of the gas handling system was either cleaned or replaced. One sample of "HD-depleted" H_2 was grown in the cylindrical cell mentioned above. However, in anticipation of the irrotational flow control experiment [**Kim 2004c**], I returned to the annular geometry for further H_2 studies. Two new TO's were constructed [see Fig. **3-4**]. With the exception of the barrier itself, the dimensions of the blocked cell are identical to the open annulus cell. Actual photographs of the two TO's are shown in Fig. **3-5**. The internal design is slightly complicated and requires some explanation. First, low pressure solids were desired since they are the most likely to exhibit supersolid properties. Since the cell is filled with relatively low pressure liquid (~1bar), there is opportunity for open spaces to form within the cell upon solidification. I therefore included some non-annular space within the TO that constitutes a greater fraction of the total volume (10%) than moment of inertia (3%). Second, based on preliminary measurements in the first cell I included a cylinder of

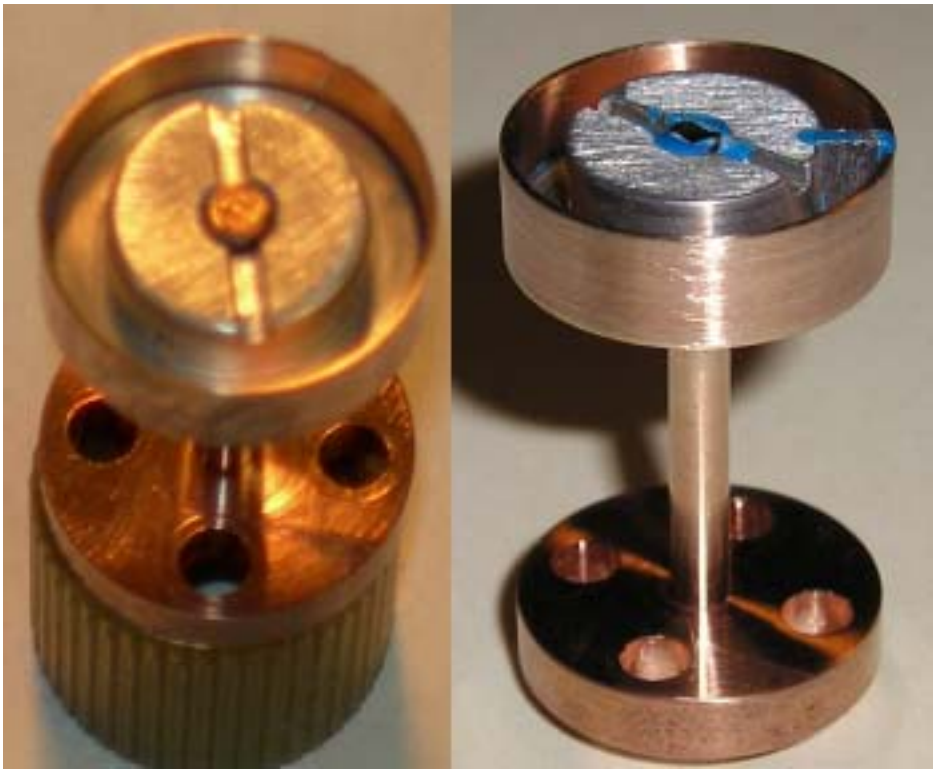

Fig. **3-5**: Photographs of the open and blocked annulus cells used to study HD-depleted hydrogen samples.

silver-gold alloy in the center of the cell. The outer surface of the cylindrical piece was etched in nitric acid to produce a layer of porous gold [**Yoon 1997**]. The piece was slightly oversized so that strong mechanical and thermal contact to the torsion bob could be made. The ~0.4m^2 of surface area lowers the thermal resistance between the cell walls and solid H_2, which was intended to counteract the internal heat leak generated by OP conversion. All but one of the solid samples grown in these TO's were done so using HD-depleted H_2. The one exception was a sample of HD that was studied in the repetition of the isotope control experiment.

Due to reasons addressed in Chapter 4, a second blocked cell was built and tested. With the addition of a barrier, the design is just as that in Fig. **3-3**. The average radius and

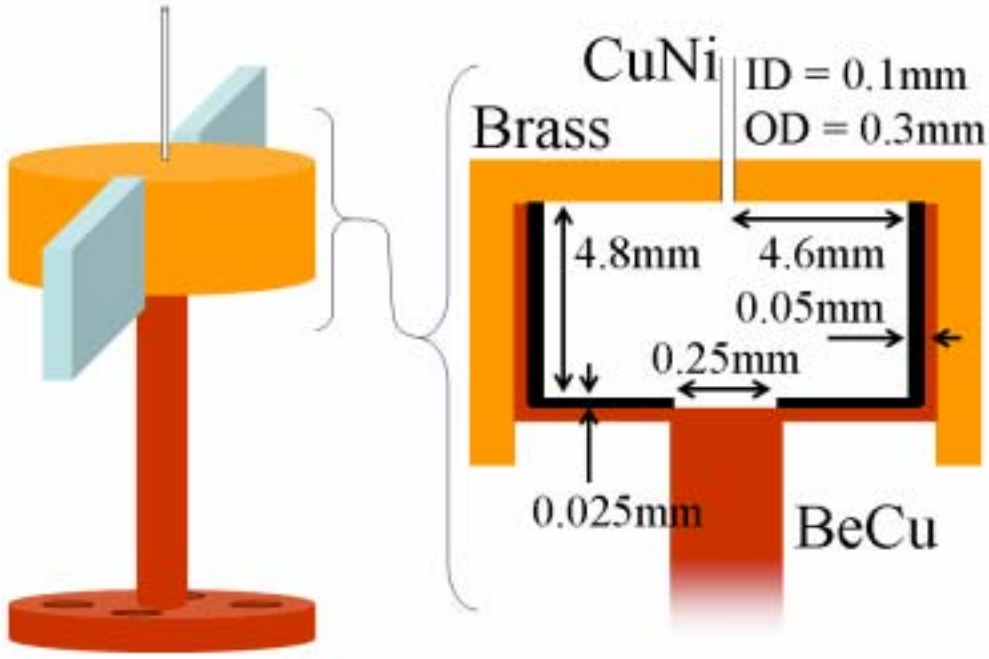

Fig. **3-6**: HeTO-2 was used to grow ^{4}He crystals at constant temperature and pressure.

width are 6.99 and 2.54mm, respectively. The torsion rod diameter is 2.5mm.

3.1.2.2 Helium Torsional Oscillators

The two torsional oscillators used these experiments are different from all of those in earlier TO studies of ^{4}He [**Kim 2004a**],[**Rittner 2006**],[**Rittner 2007**],[**Kondo 2007**],[**Penzev 2007**],[**Aoki 2007**] in that the filling line, which usually is drilled into the torsion rod, consisted of a capillary affixed to the cell at the opposite to the cooling source. Most of my work was carried out in HeTO-2, shown in Fig. **3-6**. The BeCu cup was filled with Stycast 1266 epoxy. The cured epoxy was machined down to leave a thin layer on the walls, with the exception of the bare BeCu cold spot at the bottom of the cell. A final of 1266 was applied to the machined surface to create a smooth finish. Within the

first cell, HeTO-1, no epoxy coating was present. Instead, a BeCu “nipple” was machined into the bottom of the cell with the purpose of seeding crystals. However, we found the thermally insulating layer to be crucial for reliable formation of single crystals.

The TO can be a very sensitive detector, so every attempt to optimize the *Q* is usually taken. In this regard there is a great deal of folklore “explaining” high and low *Q*-values of various oscillators. For this reason I was especially happy to see that the addition of the capillary did not significantly alter the *Q* [see Table **3-1**], which is typically 0.5 to 2 million. One note that should be made is that it is best to pull the capillary taught and affix the far end, on axis with the torsion rod, to some refrigerator stage. This is a precaution that is also normally taken with the bias voltage wire or thermometer leads [**Kim 2004a**].

The cover piece for TO’s is usually made from a low density metal to improve the mass sensitivity to helium in the torsion bob. However, in fear of a possible leak I used brass so that the small cupro-nickel capillary could be soft soldered to the cover. For this reason, any extra material that could be removed from the brass piece was machined away. However, from other ongoing experiments in the laboratory I have recently found that an epoxy seal is sufficient and does not affect the *Q*, so magnesium or aluminum covers should be used in the future.

3.2 Sample Growth

The growth conditions for hydrogen samples differed drastically from those of ^{4}He. At the time the hydrogen experiments were carried out we welcomed the idea of a

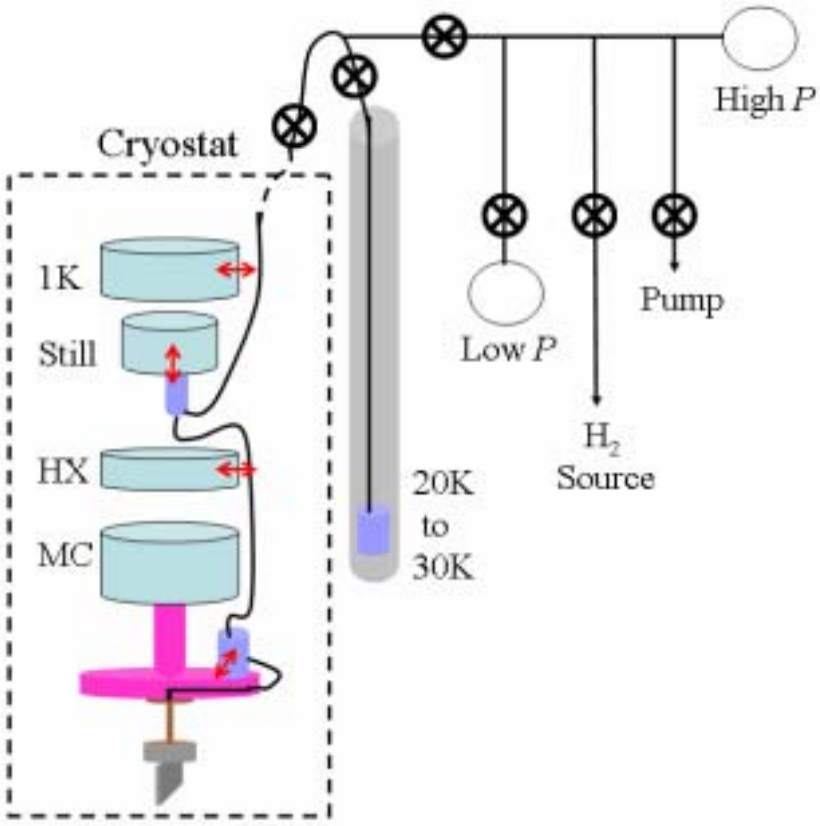

Fig. **3-7**: Original gas handling system that enabled the growth of H_2 with x ~0.01. The first stage of OP conversion is carried out at ~20K in a "column" separate from the dilution refrigerator. H_2 is condensed into the cell from the column. The lower conversion chambers in the capillary system are typically held around ~15K during sample growth. In later experiments the stage at the still, originally containing catalyst, was emptied in order to prevent unwanted para-to-ortho conversion. Also, a final conversion "filter" was placed at the entrance to the cell [see Fig. **3-8**].

disorder-induced supersolid phase, and took no special care in growing nice crystals. Ironically, the purpose of the ^{4}He experiment was exactly the opposite. Below I describe the particulars of each growth procedure, beginning with hydrogen.

3.2.1 Hydrogen Samples

Three different sources of hydrogen were used in these experiments. I collected gas samples from each source and, with the generous aid of Pratigya Polissar and Courtney Turich from the Penn State Geosciences Department, measured the isotopic composition by mass spectrometry. The first measurements were carried out on samples condensed from "commercial purity" H_2 gas purchased from GT&S, which is consistently found to contain 205± 5ppm of HD impurities. The bulk of measurements pertained to "HD- depleted" H_2 gas that was obtained from Cambridge Isotope Laboratories, Inc., and was claimed to have <10ppm of HD and D_2 impurities. The mass spectrometer readings on samples from this gas were between 55 and 65ppm. However, since the instrument is almost always used for samples with much higher HD concentrations the above numbers are considered as the background level even in the "clean limit," i.e. after one day of purging with ^4He or N_2 gas. The final gas investigated was HD, also from C.I.L., of <2% isotopic impurities.

3.2.1.1 Gas Handling of the Hydrogens

A schematic of the capillary system used to grow samples is shown in Fig. 3-7. Following some preliminary measurements slight modifications were made, as noted in the caption and in Fig. 3-8. The gas handling system included a gauge for both low (MKS 124) and high (Paroscientific digiquartz pressure transducer) pressure. The absolute accuracy of the MKS gauge had previously been tested in adsorption studies by comparing the measured and tabulated saturated vapor pressures of N_2 and ^4He. In

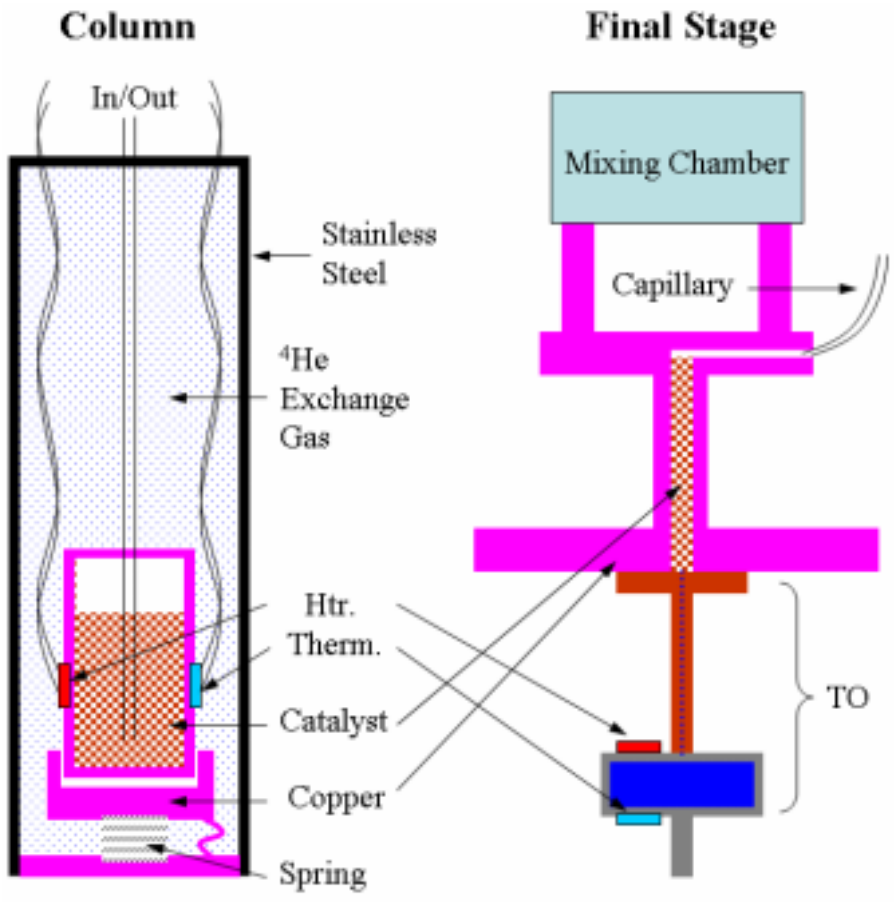

Fig. 3-8: Design of first and last stages of OP conversion in the gas handling system. The column was typically maintained at 20 to 25K during sample growth. The final ortho-H_2 "filter" always remained below 20K, typically at ~15K.

addition, the atmospheric pressure reading was cross-checked with that of the mercury manometer in Osmond Laboratory. The digiquartz and MKS gauges gave consistent readings between ~0.1 and 1.5bar. The high pressure gauge was also used in the helium experiments, and found to have an absolute accurate of ~1% at two fixed (triple) points on the ^{4}He phase diagram.

In order to generate low ortho-concentrations the H_2 was first condensed into a "column" that housed a 40cc chamber partially filled with FeO(OH), a magnetic catalyst

purchased from Sigma-Aldrich. The design of the column is shown in Fig. **3-8**. The entire column is immersed in a storage dewar of liquid ^{4}He. The space within the outer stainless shell can filled with trace amounts of exchange gas or pumped to vacuum. A spring was hard soldered to two copper pieces that were also connected by a flexible copper wire. Mechanical contact, via the spring, between the inner chamber and upper copper piece created a thermal link to the lower piece that was exposed to the ^{4}He liquid or vapor in the storage dewar. The thermal link was tuned in preliminary cooldowns so that the thermometer and heater could be used in a control loop to maintain the temperature. In many cases, however, the temperature stability at any fixed height above the surface of the liquid ^{4}He was found to be sufficient. Thus, upon adding exchange gas to the column, the temperature was adequately modulated by raising or lowering the entire column.

Prior to making samples the liquid in the column was held at ~15K for several hours or even overnight, at which temperature x_{eq} ~10^{-4}. To condense H_2 into the cell the temperature of the column was necessarily raised to between 20 and 25K, where the vapor pressure is >1bar and ~10^{-4} < x_{eq} < ~10^{-2}. The valve to the capillary system inside the refrigerator was then opened and condensation within the topmost chamber proceeded. Since there was difficulty in filling the lower stages with liquid, the upper chamber and capillary were often heated to ~40K. For this reason the upper conversion chamber in Fig. **3-7**, which originally contained a magnetic catalyst, was emptied. That is, I wanted to avoid as much re-conversion to ortho-H_2 as possible (which is much slower in the capillary than in any conversion chamber). The chamber remained in the system and was used as a H_2 source for later samples which were sometimes grown while keeping the internal components of the refrigerator isolated from the room temperature

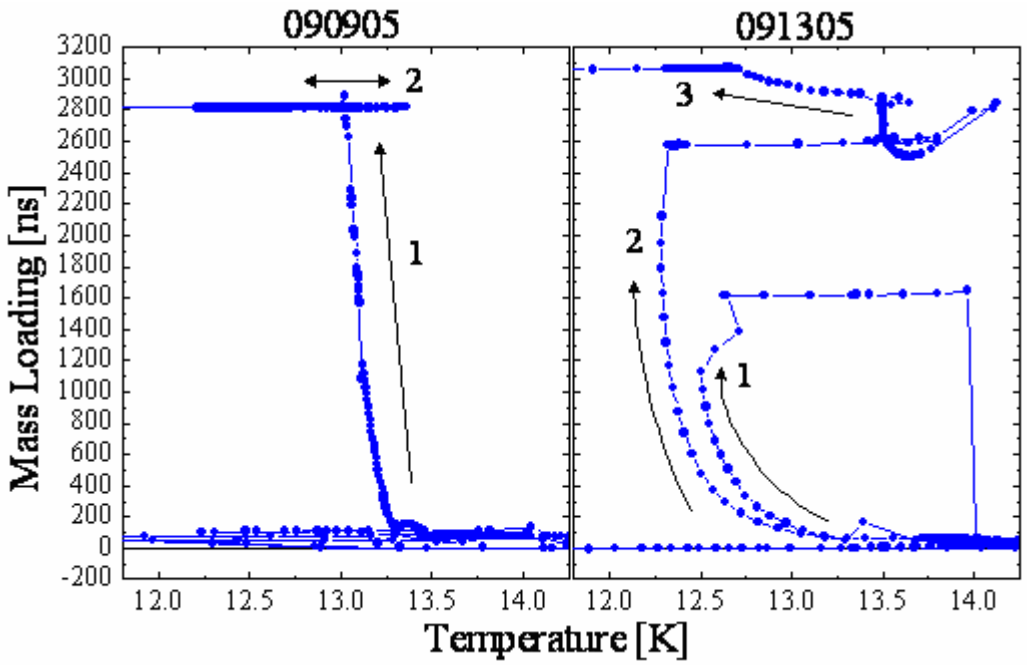

Fig. **3-9**: Two examples of hydrogen mass loading in H2TO-3. Sample 090905 has a mass loading of 2810ns and is ~92% full. Sample 091305 is ~100% full, i.e. 3036ns.

gas handling system.

The column was not used during the growth of HD samples, but rather the gas was directly condensed into the cell. The capillary system within the refrigerator was similar, such that the OP conversion of any remnant H_2 impurities should have taken place. Following the two separate HD studies (in H2TO-2 and H2TO-3), components of the capillary system were either replaced, or disassembled, rinsed with acetone, and dried by running N_2 gas through them for several days.

At the time of the experiment there was no incentive to grow high quality hydrogen crystals (based on the original idea that vacancies or other defects might induce supersolidity [**Andreev 1969**],[**Kim 2004b**]), some effort was necessary to fill the cell in the first place. The basic growth procedure was the same for all samples in every TO,

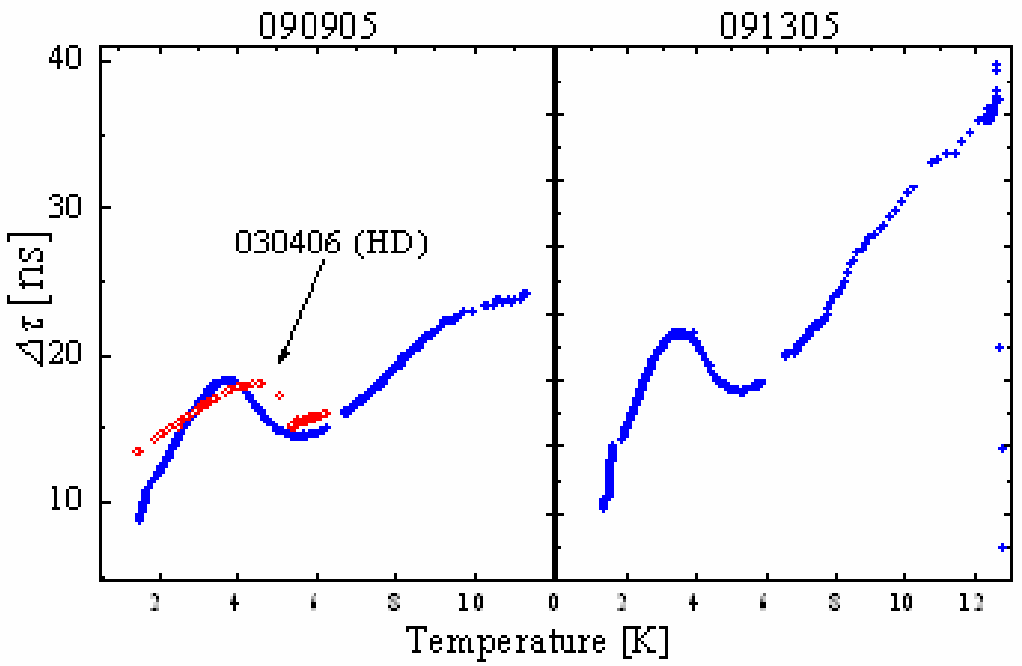

Fig. **3-10**: Anomalous feature observed upon cooling all samples in all TO's. The size varied slightly from sample to sample. The few HD samples that were also studied exhibited a similar bump (shown on left). The H_2 samples are the same as in Fig. **3-9**. The HD sample mass loading and filling factor are 4675ns and ~91%.

although slight changes to the capillary system were employed between several cooldowns. There was a thermometer and heater on each of the capillary heatsinks, which were located at the four primary stages labeled in Fig. **3-8**. The response of each thermometer made it evident whether hydrogen was being condensed into the lower conversion chamber and cell, or if there was a solid H_2 block in the capillary.

The triple points of H_2 and HD are 13.8K and 15.6K, respectively. The main problem with this is that traditional TO's have the fill line in the torsion rod (this was prior to the era of my HeTO's), so that the fairly massive copper stage connected to it also needs to be significantly warm. The first attempt to achieve this was with a liquid ^{3}He heat switch like the one used in an earlier TO study from our laboratory [**Kim 2006**].

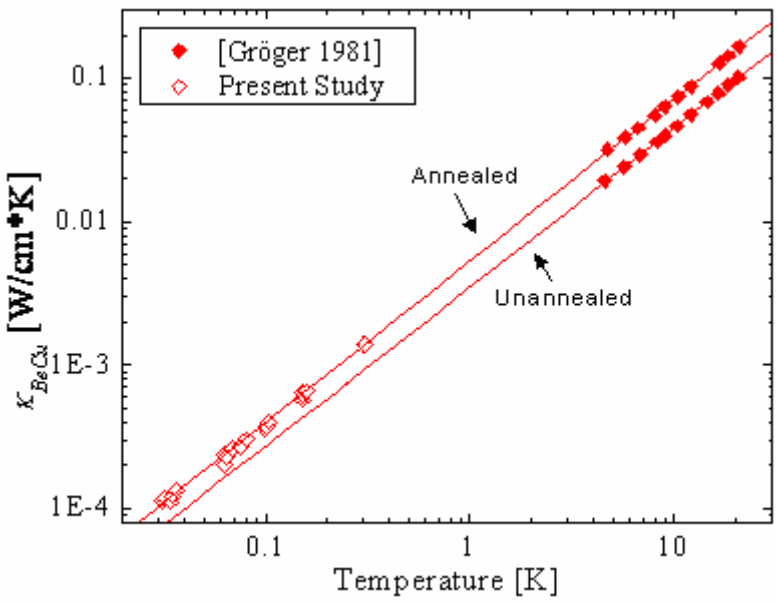

Fig. **3-11**: Measured thermal conductivity of BeCu. Data at high temperature is from Ref. [**Gröger 1981**].

The term "switch" means that the ^{3}He gas existing at high temperature does not efficiently conduct heat so that the stage can be thermally decoupled from the mixing chamber. However, at low temperature the liquid conducts heat about as well as brass and therefore sufficiently cools the stage. While this was fairly effective, the low temperature thermal conductivity was somewhat lacking. Thus, in the end I found that enough cooling power could be provided to solidify hydrogen when ^{3}He exchange gas was added to the inner vacuum chamber of the refrigerator. The typical pressure of the "vac can" measured at a room temperature where the line emerged from the cryostat was ~10^{-5}Torr, consistent with the several hundred micromoles of gas that were added to the 12L chamber at 4K. The exchange gas was sufficient to cause a slight temperature gradient between the torsion bob and the above stage where heat was input. As the heat was decreased the stage and cell drifted down in temperature through the freezing point, below which

hydrogen mass loading of the TO occurred. This process sometimes had to be repeated many times to adequately fill the cell, such as sample 091305, which is one of the samples shown in Fig. **3-9**. As can be seen in both samples, supercooling below the triple point was observed. Upon complete solidification, samples could be warmed up to ~13.8K before melting. Despite this stability, one strange feature was noticed upon cooling every sample (H_2 and HD). The bump in the period data is shown in Fig. **3-10**, and is of unknown origin. It occurs for samples in all H2TO's, #1 through #5. At first I thought this feature could possibly be from a mechanical coupling between the TO and small vibrations from the condensation of the refrigeration coolants. However, while it also occurred in HD samples, the jump was much sharper. In addition, it is reproducible upon repeated warming and cooling. In contrast, the temperature dependence of H_2 and HD samples are different below the bump. Thus, it appears to be of some interest. However, most of my investigations focused on the low temperature behavior where NCRI was considered possible.

3.2.1.2 Sample Composition

There were a great many samples formed in H2TO-1 that were never studied because the base temperature of the cryostat was limited to 150mK. This was prior to incorporating several stages of OP conversion.

After employing the OP conversion column, the average ortho-concentration for each sample in the torsion bob was determined by keeping the mixing chamber at 20mK and measuring the temperature difference across the torsion rod. Based on this

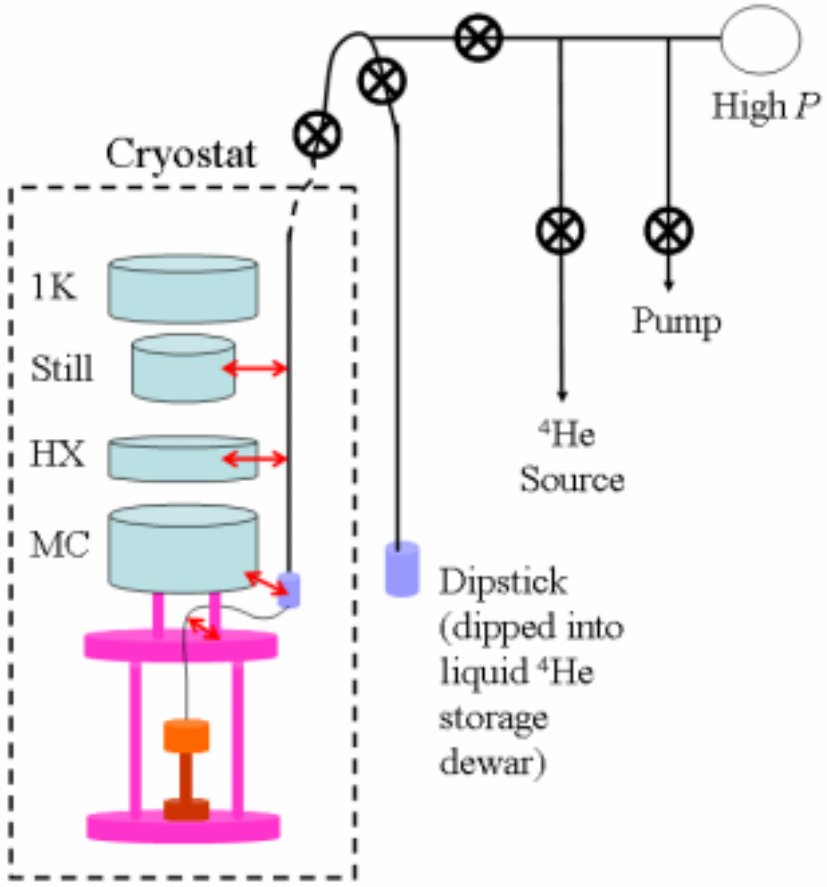

Fig. **3-12**: Gas handling system for ^{4}He. A chamber filled with silver sinter was weakly heatsunk (0.7cm stainless steel screw) to the cold stage below the mixing chamber. The capillary was also weakly heatsunk at one heat exchanger and at the still, but not at the 1K pot. This was to allow the continuous running of the 1K pot. The refrigerator was in normal circulation during CT and CP growth from the superfluid phase.

measurement and the thermal conductance of the Be-Cu torsion rod, we could infer the power being emitted during OP conversion, and hence x_0. Simply, I used

$$\dot{Q} = U\frac{kx_0^2}{(1+kx_0t)^2} = \frac{\kappa_{BeCu}A}{l}\left(T_{cell} - T_{stage}\right) \qquad \text{Eq. 3.6}$$

The smallest measurable temperature gradient of ~0.1mK corresponded to x = 0.005. To limit the uncertainty in the absolute value of x we measured the thermal conductivity of

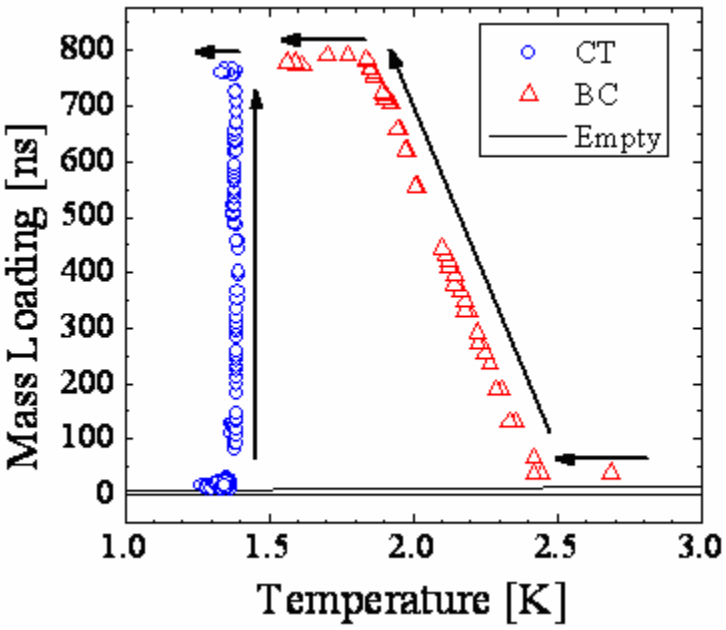

Fig. **3-13**: CT and BC growth in HeTO-2. For the BC sample the molar volume (V_M) of the solid during growth ranges from 19.3cc/mol at T = 2.45K and P = 55bar, to 20.7cc/mol at T = 1.8 K and P = 30.7bar. In contrast the sample grown at 1.38K from superfluid was subjected to temperature variations of about 20mK, which translate into a variation in V_M of 0.07\% (versus the 5% value for the BC sample).

our Be-Cu rod, finding very good agreement with the literature [**Gröger 1981**] upon extrapolation to T >1K. The data is shown in Fig. **3-11**.

3.2.2 Growth of Helium Samples

The gas handling system is shown in Fig. **3-12**. The TO design in Fig. **3-6** allowed me to seed a crystal at the cold spot and maintain an open filling line during freezing. This enabled the growth of crystals at CT and CP within a TO for the first time. Representative data showing the difference between CT and BC growth is shown in

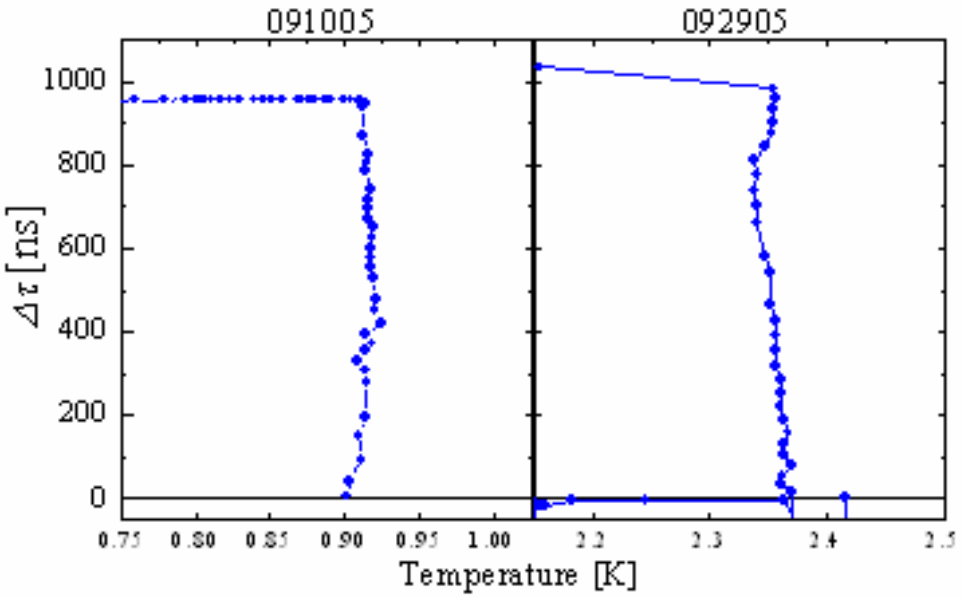

Fig. **3-14**: CT (091005) and CP (092905) growth in HeTO-1.

Fig. **3-13**. Having nearly replicated the exact conditions in Ref.'s [**Heybey 1967**],[**Lipschultz 1965**],[**Crepeau 1971**], most of the samples should be single crystals or at worst comprised of just a few large crystals.

In the preliminary study where HeTO-1 was used, I grew four samples at CT, two at CP, and two by BC. The CT samples were grown from the superfluid (~25bar) and the CP samples from the normal fluid. Also, one sample was grown by rapidly raising the pressure above the superfluid by 20bar. Mass loading data for two CT/CP samples is shown in Fig. **3-14**. The data for BC samples is similar to that in Fig. **3-13**.

In HeTO-2, eleven crystals were grown at CT, one at CP, thirteen by BC, and two by rapid pressurization (RP) from the superfluid. These samples were all of 1ppb purity. The duration of solidification for BC samples varied between several minutes to six hours. The time dependence of the mass loading and temperature for two samples is shown in Fig. **3-15**. Similarly, the growth rate was varied among the different CT

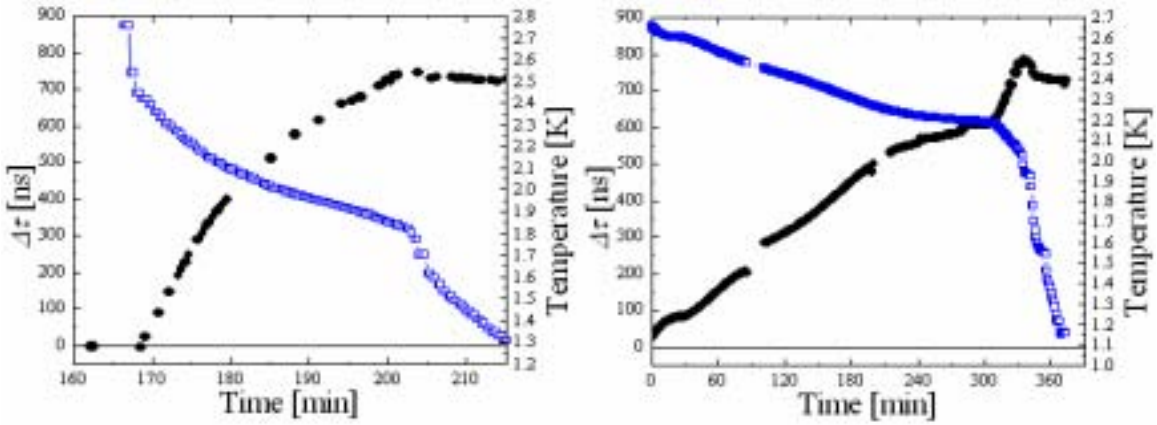

Fig. **3-15**: BC growth for two samples in HeTO-2. The cell temperature is also shown (open square).

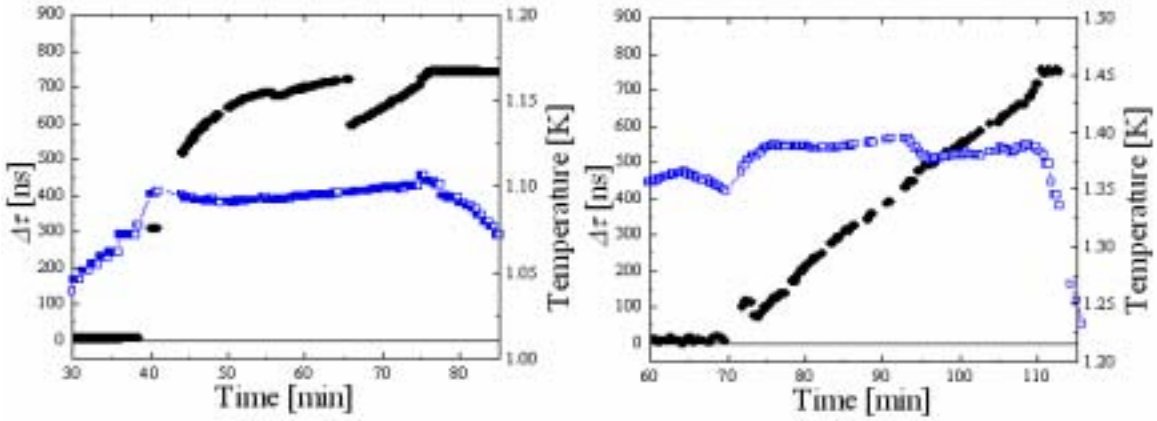

Fig. **3-16**: CT growth for two samples in HeTO-2.

samples, although ~1μm/s was common. In some cases, recrystallization was assumed to take place [see left-hand side of Fig. **3-16**]. Attempts were also made to "zone-refine" crystals during their growth. In this case, repeated melting and refreezing would be carried out by slightly lowering and raising the pressure. One such example is shown in Fig. **3-17**. Due to the flat melting curve at these temperatures, pressure swings (instigated by the room temperature gas handling system) of ~100mbar causes large temperature swings (but not density swings).

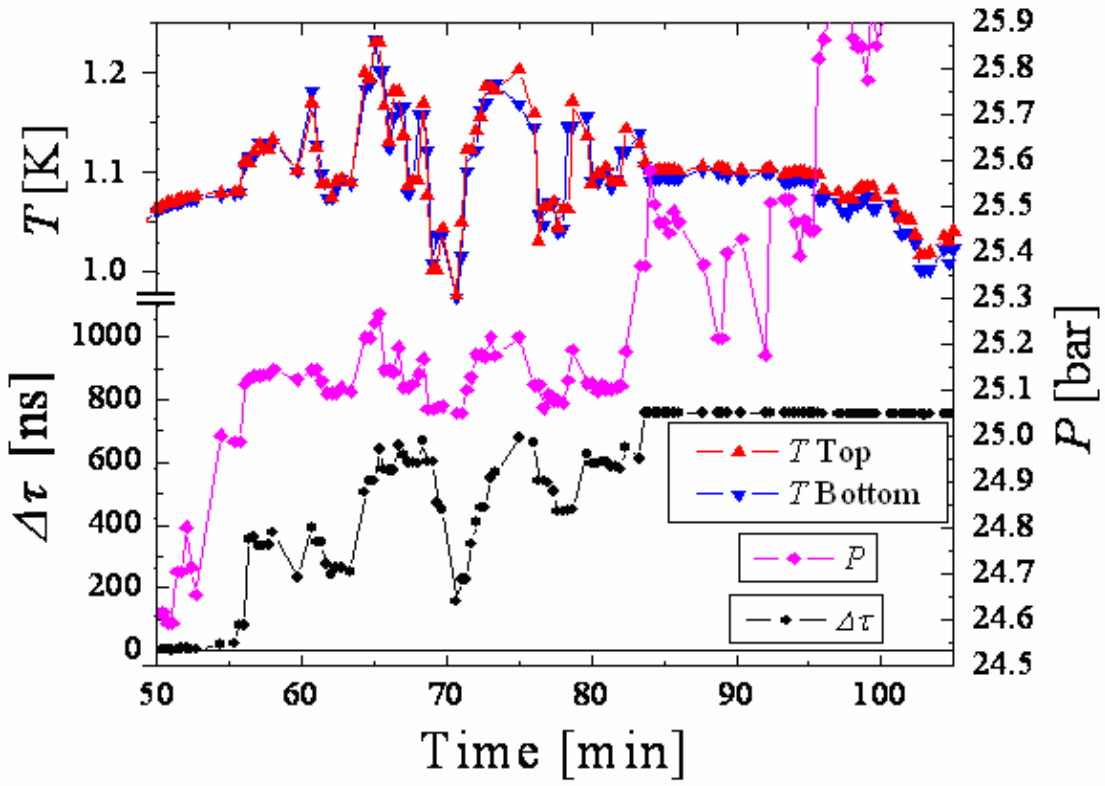

Fig. **3-17**: Loading, temperature, and pressure during zone-refining process.

There were a few instances of irregular growth that I have lumped into the BC category. In Fig. **3-18** it can be seen that in some cases a sample was grown by BC, and then upon reaching the upper triple point [see Fig. **2-4**] a rush of superfluid entered the cell, increasing the pressure and mass loading. After converting back to the normal phase, the capillary was again effectively blocked and BC growth continued.

Although an *in situ* pressure gauge in the form of a strain gauge resistor [**Kim 2004a**] was glued to both the HeTO-1 and HeTO-2 cells, the sensitivity was only ~1bar and therefore unable to detect any variations during the growth of CT/CP crystals. Therefore, the maximum pressure variations during growth were extracted from temperature fluctuations according to the solid-liquid coexistence curve [**Wilks 1967**].

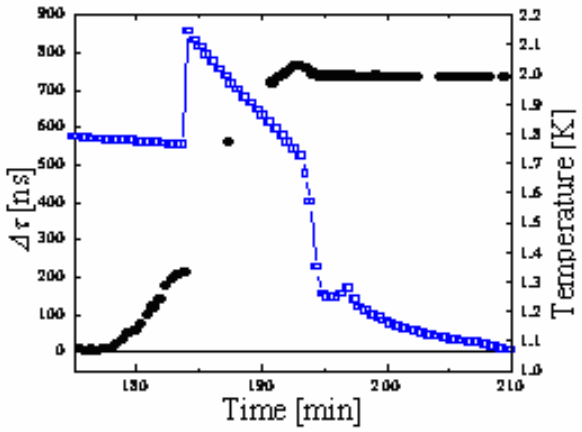

Fig. **3-18**: An instance of irregular growth.

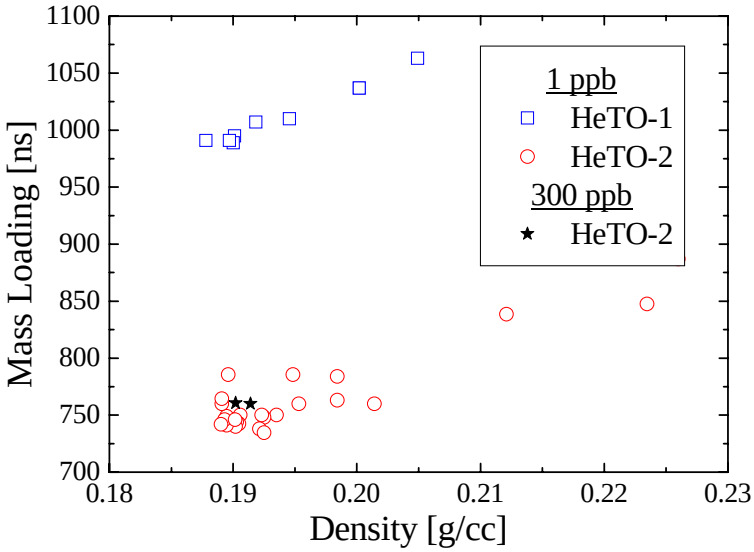

Fig. **3-19**: Mass loading of each oscillator. The period increases linearly with density.

In Fig. **3-19**, the mass loading of each TO is plotted versus the solid density, which was taken from the melting curve [**Wilks 1967**] at P_F for each sample. A summary of the important parameters for all of the samples is given in Chapter 5, since they are lumped together with NCRI fractions, etc. Lastly, data from two 300ppb samples are also

shown in Fig. **3-19**. One was grown from the superfluid at CT (at ~10μm/s). The other sample, grown by BC, was formed through the bcc phase.

Chapter 4

Solid Hydrogen

As Moses says, this was a bit of a detective story. I begin below with a brief description of the initial observation of NCRI-like phenomena in solid H_2 at low temperature. I then describe the systematic study that was carried out in the H2TO-3 and H2TO-4 cells that determined that the observed period shift was not due to supersolidity, but rather is related to ortho-H_2 motion within the solid.

4.1 First Glimpse

Several samples were grown in H2TO-1. However, the ortho-concentration was higher in the first several samples (x is not precisely known since there was no thermometer on the torsion bob in the earliest studies), so that sufficiently low temperatures were not reached until two months after the first sample was made. Since the H_2 contained in the capillary was re-used, over those months the continual conversion resulted in lower x-values in each successive sample. The final one studied is depicted in Fig. **4-1**.

The first observation at low temperature was that the resonant period reading took surprisingly long to come to equilibrium. However, it was clear that a definite shift in the resonant period occurred near 150mK, which corresponded to 0.035% of the H_2 mass loading. The possible NCRIF = 0.035% was about thirty times less than the only value

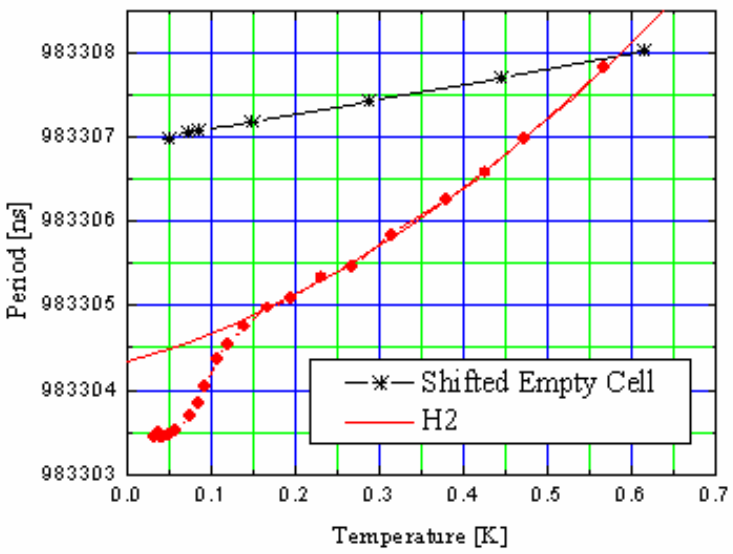

Fig. **4-1**: First clear indication of a period shift below several hundred millikelvin.

yet seen in solid ^{4}He at the time, i.e. ~1%. This was found reasonable, but the onset temperature was surprisingly high. Since ^{3}He impurities had been shown to enhance T_O in solid ^{4}He [**Kim 2004b**], I acquired a bottle of HD-depleted H_2 in order to explore the same possibility. Due to the small signal, one other complication was the strangely modified "high temperature background," which was not linear in *T* like the empty cell, but rather could be fit well with a quadratic function. Before spending any more time on H_2, which could have been considerable since OP conversion was still not terribly efficient, I instead proceeded to study HD to see if there was an isotope effect.

Excitement raced through the lab when I found the period shift to be absent in HD. After cleaning the gas handling system I investigated HD-depleted samples in the same cell, H2TO-2. The empty cell, HD, and H_2 data are shown in Fig. **4-2**.

The presence of either hydrogen isotope modifies the temperature dependence of the period from that of the empty cell. This effect was almost identical for 50mK < *T*

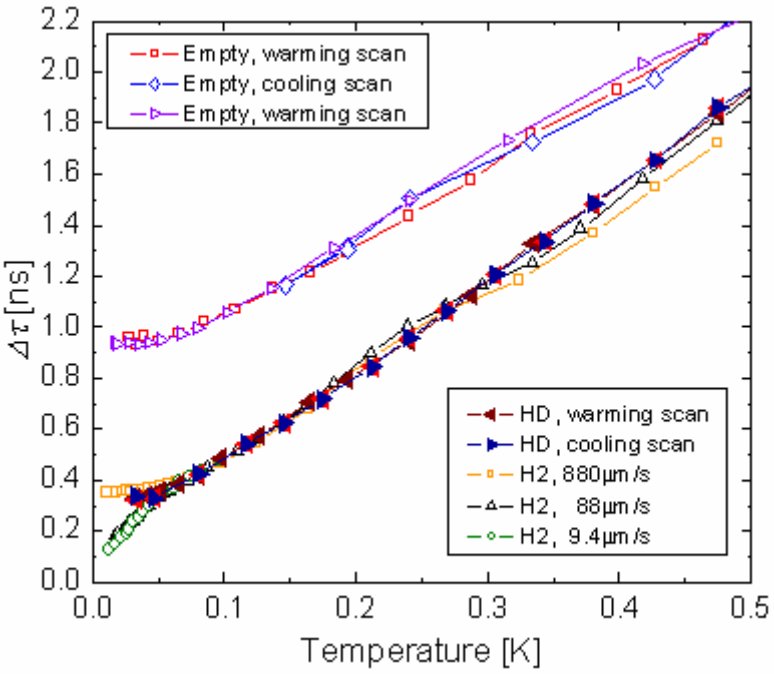

Fig. **4-2**: Hydrogen data in the cylindrical cell.

<700mK, and only at high oscillation speed was the low temperature behavior of H_2 the same as that of HD. These observations, as well as the lower T_O in the higher isotopic purity hydrogen, were all consistent with the traits of NCRI in solid helium [**Kim 2004a**]. Thus, it appeared that in high purity H_2 we could define T_O ~60mK, and NCRIF ~0.014%. From these experiments it became clear that the equilibration time of τ was longer for H_2 samples than for HD. Long times had also been observed with H2TO-1, and therefore were further investigated in the next series of experiments.

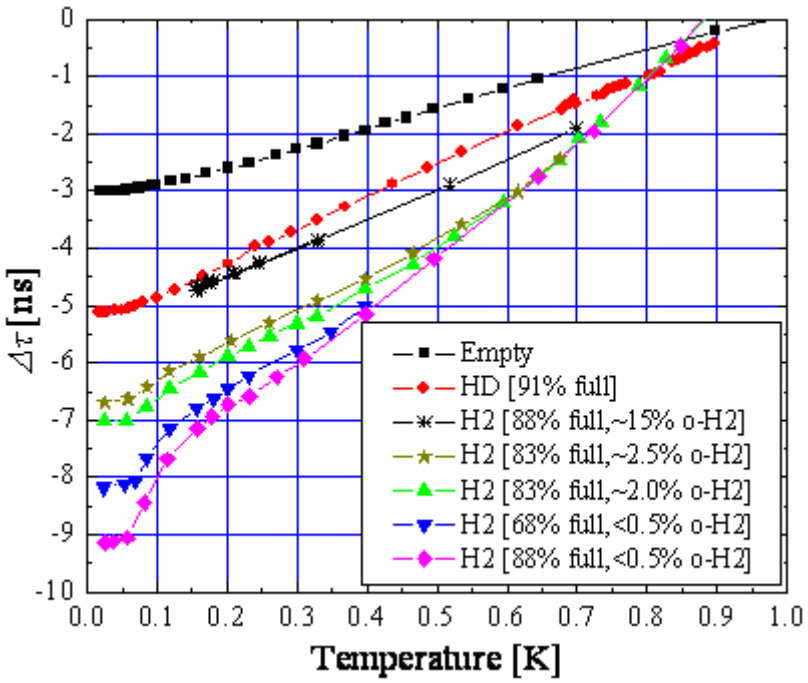

Fig. **4-3**: Temperature dependence of τ for H2TO-3. All datasets have been shifted vertically for easy comparison. The two scans with 83% filling correspond to one sample (the temperature scans were several weeks apart so that *x* had decreased).

4.2 Systematic Study in Relation to Supersolidity

Several datasets for hydrogen samples in the H2TO-3 cell are shown in Fig. **4-3**. The first observation is that there are still no interesting features in the HD data. The H_2 samples studied were of various *x*-values. One sample of very high concentration was unable to be cooled to below 150mK (the refrigerator cooled, but the torsion bob did not). Among the lower concentrations the period shift was largest for the most dilute, and just barely discernible in the $x = 2.5\%$ sample.

However, there were several peculiarities. For instance, the temperature dependence of τ in H_2 samples was much like that obtained with H2TO-1, with the

apparent onset of NCRI once again near 200mK. This contradicted the previous results of the HD-depleted sample in the cylindrical cell. Also, in an attempt to re-investigate the effects of oscillation speed, which had previously appeared consistent with Ref. [**Kim 2004c**], I realized that the difference between each temperature scan was influenced by the irreversible OP conversion that continually transpired. The ortho-concentration was not determined in the preliminary measurements using H2TO-1 and H2TO-2, so it was unclear if this could explain any discrepancies.

To ascertain whether the observed effect in solid H_2 was a signature of superfluidity, the blocked annulus control experiment was carried out. The purpose of the barrier in the annulus [see Fig. **3-4**] was to make the path of irrotational superflow much more tortuous, thus leading to a predictable decrement in NCRIF [**Fetter 1974**]. This control experiment provided a convincing case for the supersolid phase of ^{4}He [**Kim 2004c**]. It was found for ^{4}He that when the annulus was blocked, NCRIF was reduced by a factor of 70 from the open annulus value. This reduction is in agreement with what is expected for irrotational superflow in the geometry that was used [**Mueller 2004**].

The results from the control experiment for solid H_2 are plotted alongside the data of the open annulus cell in Fig. **4-4**. The period drop below 180mK was still present for H2TO-4. In fact, the magnitude was even found to be larger. One possible reason for this was that, while each sample had x <0.005, the exact ortho-concentrations of all three samples may have differed. Regardless, this result clearly indicated that the period shift in H_2 was not related to superfluidity. We note that, as in the open cell, long relaxation times were observed just above the saturation temperature of 60mK. Still, in the faint

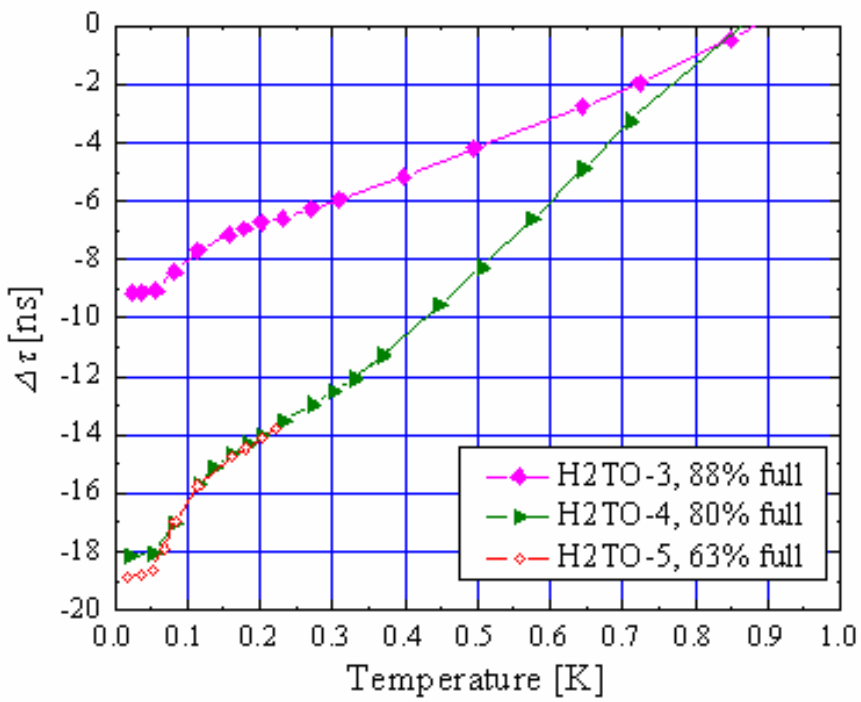

Fig. **4-4**: Comparison of open annulus and blocked annulus cells. For all samples shown, x <0.005.

hope (or just denial) that H2TO-4 provided some strange circulating path to allow NCRI, the second blocked cell of simple design was constructed and tested. As expected, the same result was obtained.

4.3 Ortho-Hydrogen Motion

In Chapter 2 I introduced the concept of ortho-H_2 clustering via resonant "hopping." While the motion of isolated singles and pairs has been monitored extensively with NMR, there are only a few other (eg., thermodynamic) investigations [**Meyer 1987**],[**Meyer 1998**], of which only one extends down to 100mK [**Li 1990**]. In all of these studies time constants were extracted from the data. For NMR, one looks at the

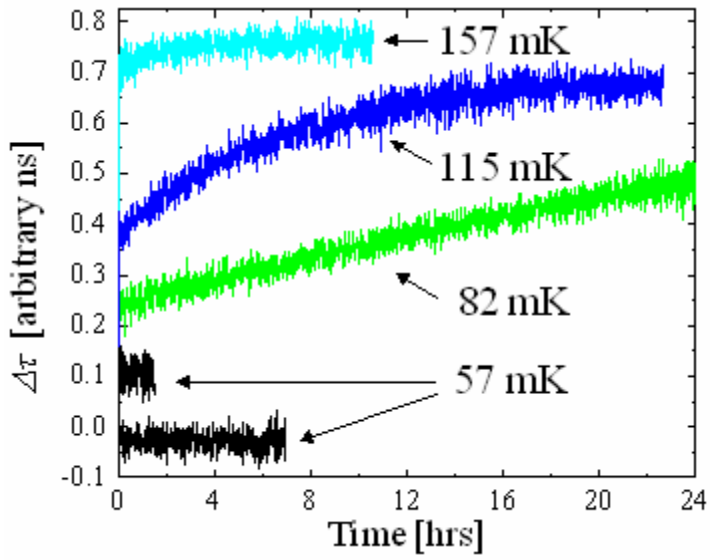

Fig. **4-5**: Time dependence of the period at different temperatures. The lower T = 57mK curve, from a previous sample, clearly demonstrates the time independence at low temperature. The curves are shifted vertically for clarity.

modulation in the peak amplitudes of the spectra associated with either isolated molecules or pairs of molecules. The growth and decay time constants of singles are directly related to their ability to propagate, i.e. they must move away or toward other impurities to alter the spectra. While similar ideas can be applied to pairs, their calculated mobility, even when including resonant OP conversion, is still small and even anisotropic [**Kranendonk 1980**]. Thermodynamic measurements probe the entire system and therefore typically yield longer time constants.

In order to compare the TO measurements with the literature, it was necessary to look at the time evolution of the period at different temperatures. However, while the data indicates that ortho-H_2 is responsible for the observed phenomena, it is still uncertain what "entity" or "variable" is actually measured by the TO. The first clear evidence of a temperature dependent relaxation time was the "brick wall" shown in Fig. **4-6**. After

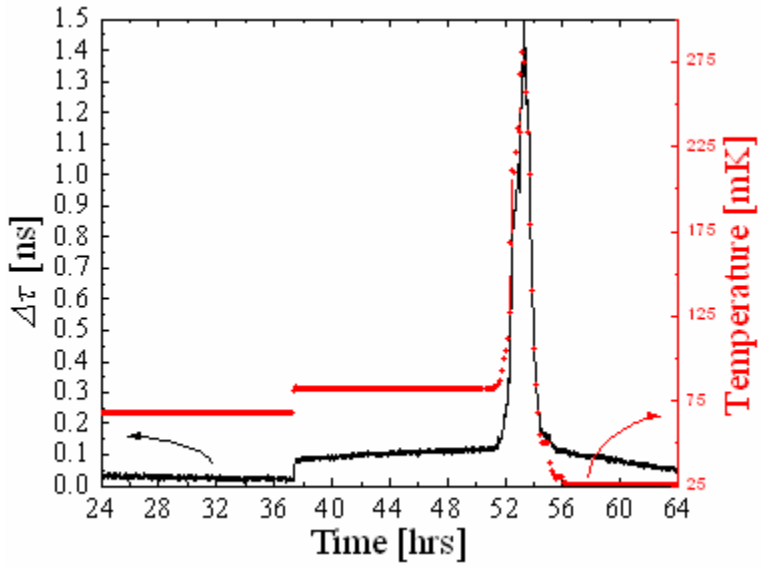

Fig. **4-6**: Time dependence of the period upon rapid warming and cooling. The system appears to remain in the "80mK state."

waiting several days at 20mK, I gradually warmed the TO by taking steps in temperature. Following each step the period would immediately change. However, near 80mK slow relaxation was observed following the abrupt temperature step. After realizing that equilibration would require several more days, I decided to rapidly warm the sample up to ~300mK. This was followed by an immediate reduction in temperature down to 20mK. I found that the period increased rapidly with temperature. However, upon cooling down through this region the period hit a brick wall at the same τ- reading where I had begun. It appeared as though the system remained in the "state" it had evolved into at 80mK.

From this point, TO data were obtained using the following protocol. Upon cooling H_2 samples to 20mK, one to two weeks were allowed for equilibration, during which time τ dropped smoothly until finally stabilizing to within a <0.05ns/day drift. It is known the rate of irreversible OP conversion is enhanced for T <200mK since local *x*-

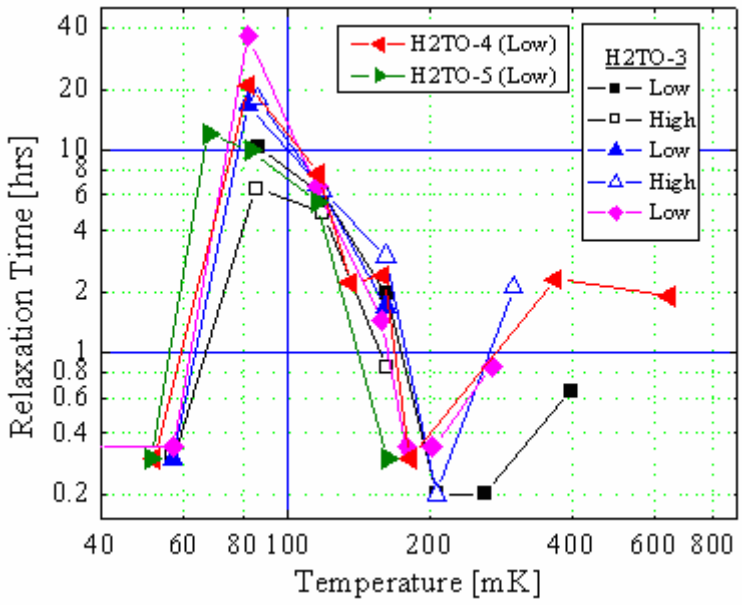

Fig. **4-7**: *T*-dependence of relaxation times (*t*) extracted from the time evolution of τ. The sharp increase in *t* coincides with the observed period shift. The largest values are observed near 80mK. "Low" and "High" refer to oscillation speeds of ~20μm/s and ~400μm/s.

values are higher in clustered regions [**Schweizer 1979a**]. A remnant drift at 20mK, which was barely discernible in some samples, is likely related to this process. This is also implied by the larger period shifts at low *x* presented in Fig. **4-3**. However, the drift was completely halted by raising the temperature to 40mK. After complete equilibration at 40mK or less the temperature was raised in successive steps, for each of which τ was measured as a function of time [see Fig. **4-5**]. When the temperature sweep was complete the system was returned to 20mK and allowed to re-equilibrate prior to a new scan.

The measured relaxation times for several samples are presented in Fig. **4-7**. The time dependence of the period was not exponential in many instances [see "82mK" in Fig. **4-5**] so the relaxation times in the figure were obtained "by hand," and are the e^{-1} values of period shift for each temperature. The overall behavior was the same for all

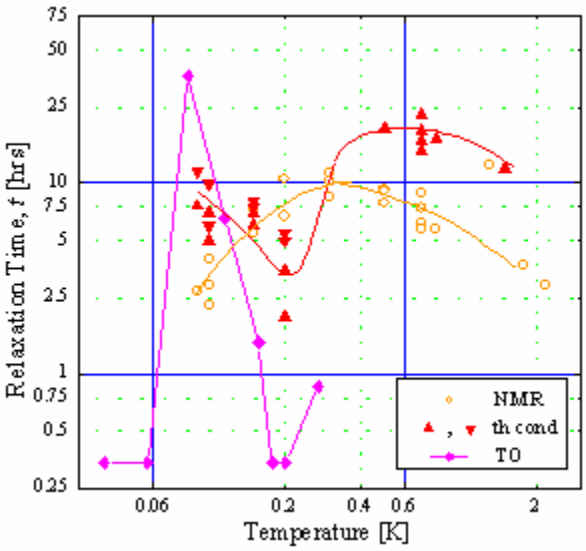

Fig. **4-8**: One dataset from Fig. **4-7** is re-plotted with the NMR and thermal conductivity data from Ref. [**Li 1990**]. The NMR data corresponds to growth (T <1K) and decay (T >1K) rates of singles. Below 300mK the qualitatively different time dependence of the conductivity is fit with two exponentials.

samples in the range studied ~0.5%< x <2.5%. Logarithmically speaking, the dependence on x is weak, varying by at most a factor of four near the peak. Two samples were also studied at high oscillation speed (a.k.a. large displacements). Although the first sample appeared to relax more slowly at high speed, the second was independent or perhaps oppositely affected. For all samples τ equilibrated quickly for any T <60mK. However, further increase in the temperature led to extremely slow relaxation. Near and above 180mK it was found that the time constant shortened to less than the thermal equilibration time.

The relaxation times are on the same order as those seen in other studies of dilute ortho-para mixtures. However, in this experiment clustering is allowed to ensue for up to two weeks at 20mK so that, according to decay times in the literature, no isolated ortho-H_2 singles [**Li 1990**] or pairs [**Washburn 1980**] should remain in our samples at the

beginning of each temperature sweep. Thus, the unclustering process is monitored upon gradual warming of the torsion cell. This is the opposite of the majority of measurements in the literature, which rapidly quench samples from some T >1K and monitor how clustering proceeds. For comparison I have plotted t-values from Ref. [**Li 1990**] (0.4%< x <3%) alongside one of the samples from the previous figure. It is interesting that the minimum near 200mK coincides with the transitional region observed in the thermal conductivity measurements. I should note that at T >500mK the relaxation once again began to noticeably increase, but I did not acquire data close enough to equilibrium to determine the e^{-1} time, which I estimate to be 5h or more.

4.4 Possible Explanations

It is clear from the data that the motion of ortho-H_2 impurities is affecting the resonant period. The moment of inertia and hence τ are extremely sensitive to the radial density profile of the sample. If changes in τ simply indicate the rearrangement of ortho-H_2 within the torsion cell, it is in such a way as to reduce or enhance the density at large radii. A possible explanation for the observed period shift below 180mK is the formation of large clusters of nearly pure ortho-H_2 in the center of the cell (fill line and radial channels), increasing the purity of para-H_2 in the annulus. Since the density of ortho-H_2 is 1.7% higher than that of para-H_2, clustering of ortho-H_2 toward the center can effectively reduce the moment of inertia. An extreme case is where all of the ortho-H_2 molecules cluster to the center of the torsion cell, which may take place below 60mK. If we take x = 0.01 as the upper limit, the reduction of τ is $1.7\text{x}10^{-4}$ of the total H_2 mass loading. This is

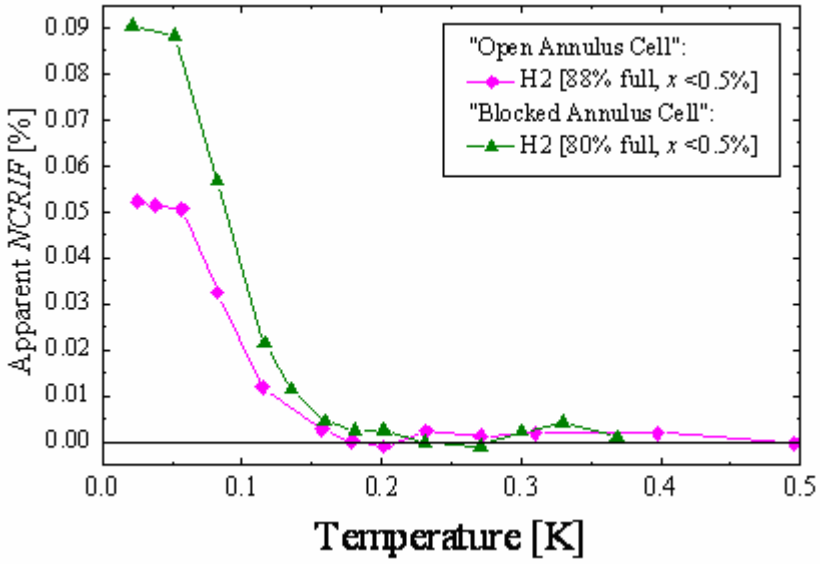

Fig. **4-9**: *T*-dependence of the period shift, normalized by the total H_2 mass loading. The dependence is similar to that observed in solid ^{4}He. However, the same effect is seen in the blocked cell.

on the same order of our observations [see Fig. **4-9**], i.e., 5.5×10^{-4} and 9.0×10^{-4} in the open and blocked cells, respectively.

However, the period shift is larger for smaller ortho-concentrations [see Fig. **4-3**]. One explanation for this could be that the mobility of ortho-H_2 molecules, and hence the phenomenon, is greater in the dilute mixtures. A similar effect has been observed [**Jarvis 1968**] in pressure measurements, although the crossover concentration was higher, i.e. enhanced mobility was found for $x < 0.07$.

It is known that solid H_2 does not wet many metal substrates [**Sohaili 2005**]. It is possible the contact angle of a sample (with a free surface within the annulus) is determined by the local ortho-para composition near the surface. During clustering either ortho-H_2 or para-H_2 can concentrate at the walls and possibly lead to an additional change in the moment of inertia. Along similar lines, the overall mechanical properties of the

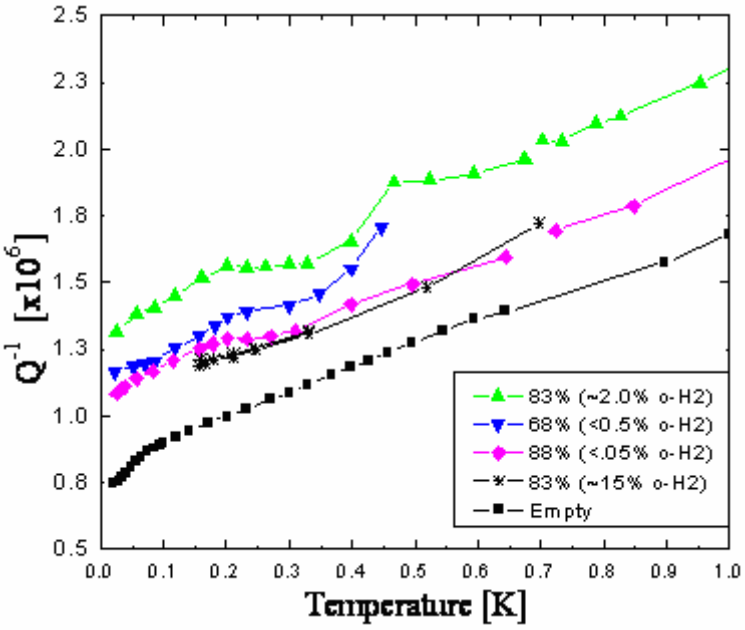

Fig. **4-10**: TO internal dissipation. Two peaks are observed, the larger being at higher temperature where no period shift occurs. The lower peak is barely discernible and is different from that of Ref. [**Kim 2004a**], in that it is not centered near the temperature where period changes most rapidly.

solid may be different in the clustered and unclustered configurations. However, it is difficult to predict the consequences this would have on the resonant period. Instead, one should measure the elastic constants and internal dissipation, the latter of which is possible and was done. In Fig. **4-10** we see that there is excess dissipation in the system at various temperatures. Interestingly, there are two peaks situated at 200 and 500mK. It is clear that these two temperatures are significant.

In Fig. **4-11** I have re-plotted the data alongside measured relaxation times. Since the samples I have studied are prepared in a clustered state, rather than a random configuration, the dissipation data taken warming up appears to mark two temperatures where unclustering occurs on a macroscopic scale.

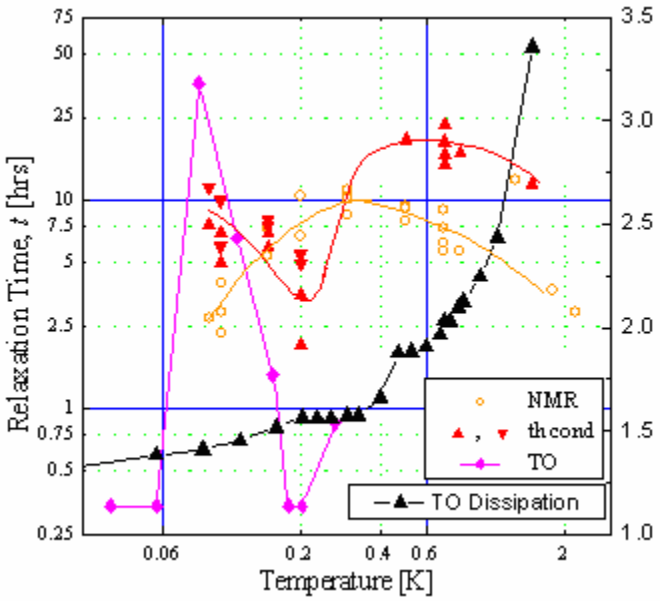

Fig. **4-11**: Comparison of the temperature dependence of relaxation times and dissipation.

Since the original incentive to study solid hydrogen was to search for supersolid behavior, further work on ortho-para mixtures has not been conducted in our laboratory. However, it is clear the torsional oscillator can serve as a sensitive probe of the dissipation in solid hydrogen and can therefore be used in future investigations.

Chapter 5

Solid Helium

The original purpose of this study was to determine whether a perfect crystal can exhibit supersolidity. Perfection is something that very few of *us* ever achieve. I still remember the day I managed to. As for ^{4}He, the highest quality crystals are grown in the limit of zero temperature. However, as noted in Chapter 2, single crystals can be grown without significant difficulty. I have studied the properties of such crystals and compared them with what are likely polycrystalline samples. General observations regarding the similarities and differences are presented first, followed by the very interesting and unexpected velocity dependencies that were found in all samples.

5.1 Temperature Dependence of NCRI

NCRI was observed in all 36 samples that were grown from 1ppb purity helium. The NCRIF in the low temperature limit is recorded in Tables **5-1**, Table **5-2**, and **5-3**. The 300ppb samples grown in HeTO-2 are also included, and are located at the bottom of Tables **5-2** and **5-3**. The results from HeTO-1 are presented first, followed by HeTO-2.

5.1.1 HeTO-1

The results from all samples grown in HeTO-1 are shown in Fig. **5-1**. As can be seen, NCRIF varies from 0.35% to 0.75%, and the onset from 95 to 120mK. It appeared

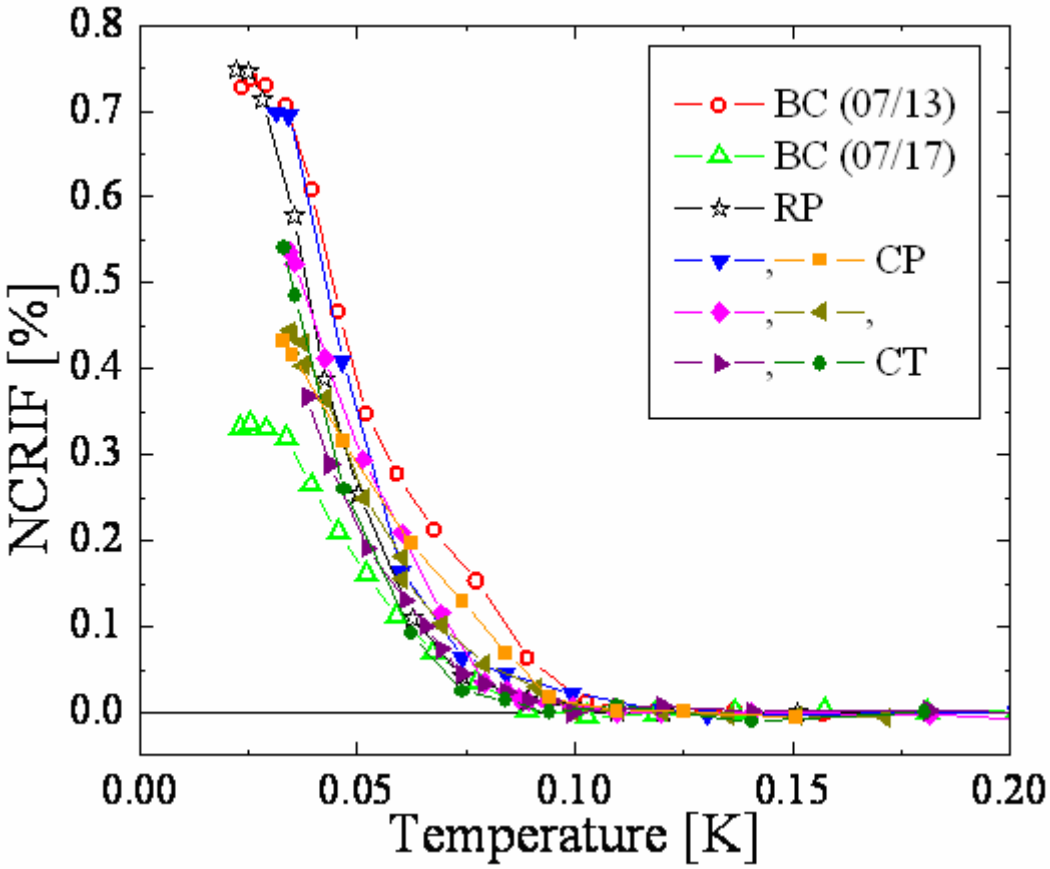

Fig. **5-1**: NCRIF versus *T* for the samples grown in HeTO-1. All scans were obtained at maximum rim speeds between 2 and 4μm/s.

strange that NCRIF could be so irreproducible in CT/CP samples, so I began to rethink the design of the cell. It was decided that the optimal conditions from the many references in Chapter 2 were not yet replicated. For example, Ackerman and Guyer found that polycrystalline samples easily formed in a copper cell, even at constant pressure [**Ackerman 1966**]. It was considered that the highly conducting walls led to multiple nucleation sites. Believing the metal walls also to be my problem, HeTO-2 was built and tested.

Table 5-1: Growth parameters, NCRIF, and T_O for all samples grown in HeTO-1. The uncertainty in NCRIF is ± 0.01%, and for T_O it is ± 5mK (except where noted). RP = rapid pressure increase of more than 5bar. *The first 87% of CP-09/24 was grown at CP (35.7bar), at which point the capillary blocked and caused the pressure and temperature to drop.

Growth-Date	V_M Range [cc/mol]	T_F Range [K]	P_F Range [bar]	Mass Loading [ns]	NCRIF [%]	T_O [mK]
BC-07/13	18-19.98	2.4-2.11	53-41.5	1037	0.73	120
BC-07/17	19.8-20.85	2.2-1.7 (bcc)	44.8-29.6	1007	0.33	95 ± 10
RP-07/20	19.98	2.11	41.5	1037	0.74	110
CP-09/29	19.46-19.52	2.37-2.34	51.8-50.5	1063	0.7	120
~CP-09/24*	20.29-20.56	1.96-1.85	35.7-32.2	1010	0.43	100
CT-09/03	21.05-21.04	1.4-1.43	25.81-25.97	995	0.45	99
CT-09/14	21.06-21.05	1.38-1.4	25.73-25.81	989	0.37	96
CT-09/19	21.13-21.085	1.25-1.34	25.32-25.58	991	0.54	94
CT-09/10	~21.3	0.9-0.925-0.91	~25	991	0.52	110

5.1.2 Blocked Capillary Growth in HeTO-2

The results from several samples are shown in Fig. 5-2. Again, a large variation in NCRIF was observed from sample to sample. However, this is not unexpected for BC samples since the quality and morphology cannot be carefully controlled.

The low temperature NCRIF varied from 0.25% to 2.0%. Most of the samples were grown over the same duration of time, 20 to 40min. However, the difference between the two samples in Fig. 5-2 with T_F =2.02K is that the one with a smaller NCRIF

Table 5-2: Growth parameters, NCRIF, and T_O for BC samples grown in HeTO-2. The uncertainty in NCRIF is ± 0.01%, and for T_O it is ± 5mK. *Irregular growth referred to in Chapter 3.

Growth-Date	V_M Range [cc/mol]	T_F Range [K]	P_F Range [bar]	Mass Loading [ns]	NCRIF [%]	T_O [mK]
BC-03/21	~16.8-17.7	~4.38-3.58	~150-107	887	0.61	100
BC-03/26	~17.91-18.86	~3.4-2.71	~98-66.3	838.5	0.95	100
BC-12/10*	20.71-19.4-19.86	1.786-2.4-2.17	30.5-53-43.5	760	1.38	135
BC-02/23	18.94-20.16	2.66-2.02	64-37.8	763	0.632	86
BC-01/30	18.99-20.16	2.63-2.016	63-37.6	784	2-1.86	93
BC-01/03*	20.23-20.75-20.48	1.986-1.7686-1.88	36.6-29.75-33	760	1.2	98
BC-03/23	19.2-20.53	2.5-1.86	57-32.55	785.5	1.2	85
BC-01/25	19.3-20.67	2.45-1.8	55-30.7	750	1.3	89
BC-11/29*	19.75-20.78	2.226-1.749	45.6-29.95 (bcc)	748	0.99-1.1	275
BC-01/23	19.6-20.8	2.296-1.738	48.8-29.8 (bcc)	750	0.96	100
BC-02/05	19.77-20.82	2.2-1.72	45-29.6 (bcc)	738	0.68	78
BC-03/12	20.1-20.78	2.05-1.679	39-29 (bcc)	734.5	0.246	90
BC-01/24*	20-21.05-20.99	2.1-1.4-1.53	41-25.81-26.6 (bcc)	750	0.46	95
RP-03/14	~17.9	~3.45	~100	847.5	~0.5	140
RP-01/19	20?	1.52?	26.5 (bcc)?	742.5	0.55	90
BC-04/18 (300ppb)	20.65-20.9	1.81-1.63	31-28.3 (bcc)	760	0.96	160 ± 10

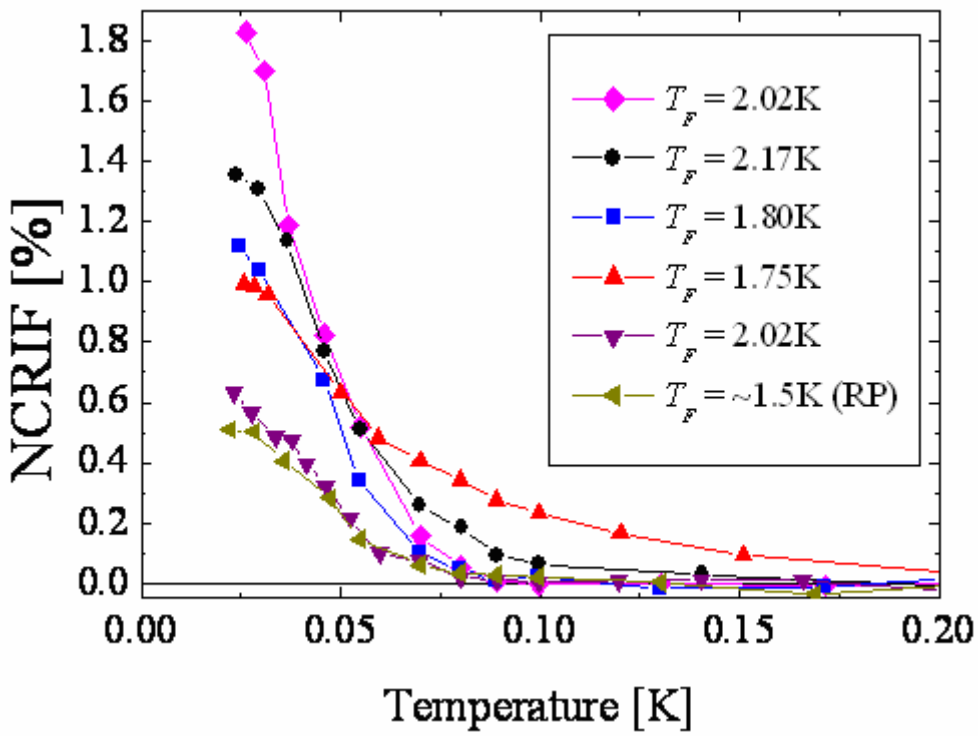

Fig. **5-2**: NCRIF versus *T* for several BC samples grown in HeTO-2. All scans were obtained at maximum rim speeds of <3μm/s. One RP sample is shown for comparison.

was grown over a 6h duration. It appears, on the basis of Ref. [**Rittner 2006**], that when a sample is grown slowly enough considerable annealing will take place before solidification is complete. Even so, the smallest NCRIF is much greater than other recent measurements of solid ^{4}He samples grown by BC within an open cylindrical geometry [**Rittner 2007**],[**Aoki 2007**], where it was found that 0.03%< NCRIF <0.15%. Rather, the NCRIF here is closer to that obtained in a 0.6mm wide annulus [**Kim 2004c**],[**Kim 2006**]. The rapid pressurization yielded a smaller NCRIF than the samples grown by BC. This was even true for one sample listed in Table **5-2** that was accidentally pressurized to 100bar after having completely grown from the superfluid at ~1K.

Table 5-3: Growth parameters, NCRIF, and T_O for CP/CT samples grown in HeTO-2. The uncertainty in NCRIF is ± 0.02%, and for T_O it is ± 5mK. ZR = zone refined. *Purposefully grown quickly. **Explained in text.

Growth – Date	V_M Range [cc/mol]	T_F Range [K]	P_F Range [bar]	Mass Loading [ns]	NCRIF [%]	T_O [mK]
~CP-11/21	21.15-21.035	1.45-1.18	26.18-25.3	746	0.33	77
CT-11/08*	21.026-21.02	1.48-1.495	26.33-26.43	744	0.5	76
CT-01/17	21.03	0.9?-1.447	26.07	740	0.5	73
CT-01/05	21.08-21.05	1.375-1.395	25.7-25.79	746	0.378	80
CT-02/06**	21.165-21.15-21.07	1.035-1.2-1.367	25.07-25.22-25.68	746	0.45	165
CT-02/08 (ZR)	21.157-21.096	1.128-1.324	25.14-25.52	785.5	0.31	80
CT-03/02 (ZR)	21.155-21.11	1.146-1.297	25.17-25.42	749	0.276	80
CT-11/16*	21.134-21.11	1.07-1.29	25.09-25.41	741	~0.49	90
CT-01/18	21.16-21.13	1.069-1.24	25.09-25.3	746	0.385	88
CT-03/31	21.162-21.155	1.078-1.147	25.095-25.162	760	0.26	79
CT-02/15 (ZR)	21.137-21.172-21.155	1.234-0.9726-1.139	25.29-25.04-25.153	764.5	0.333	74
CT-11/01	21.165-21.162	1.045-1.08	25.035-25.055	742	0.3	73
~CT-04/13 (300ppb)	21.14-21.03	1.21-1.46	25.24-26.15	760	0.6	150

The onset temperature was taken as the point where NCRI first becomes resolvable from the noise, which varied in the BC samples of this study from 78mK all the way up to 275mK. For the most part T_O <150mK, with the lowest values being

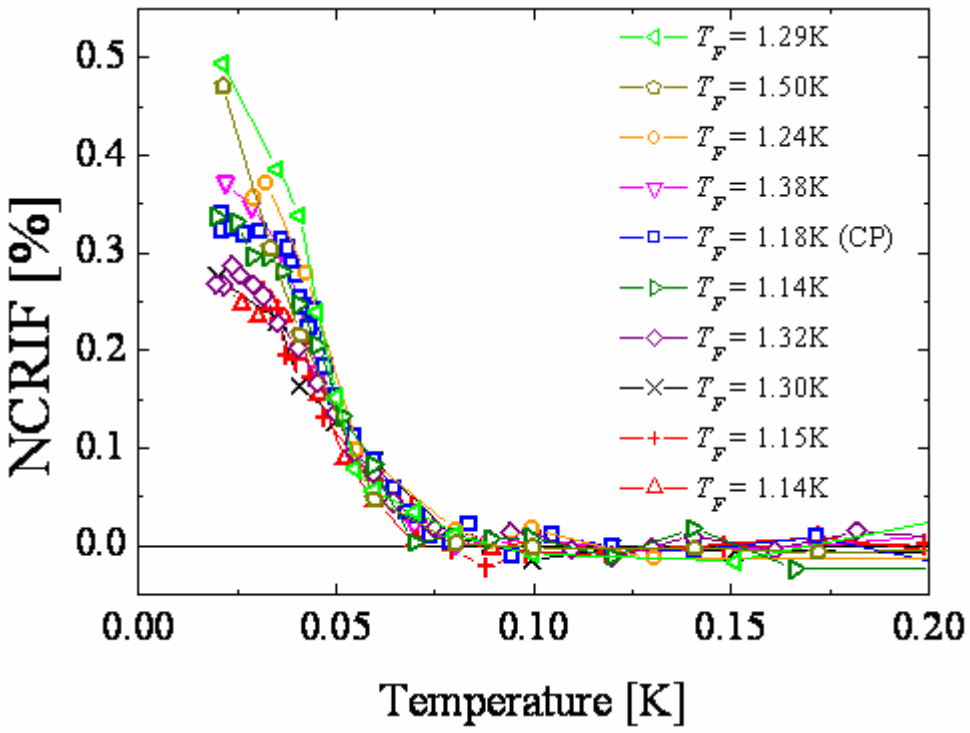

Fig. **5-3**: NCRIF versus T for most CT/CP crystals grown in HeTO-2. All scans were obtained at maximum rim speeds of <3μm/s.

consistent with the only other measurement of 1ppb purity helium (~85mK) [**Kim 2007**]. The variation in T_O for different samples demonstrates that ^{3}He impurities alone do not determine the onset, although they obviously play a major role.

5.1.3 Constant Temperature and Pressure Growth in HeTO-2

In Fig. **5-3** I have plotted the NCRIF for the majority of crystals grown at CT/CP. The magnitude of NCRIF is still on the same order, a few tenths of a percent, however the obvious difference from BC samples is the much more reproducible temperature dependence. In fact, the data from all samples very nearly collapse onto a single curve between 40 and 80mK. Moreover, of the two samples with the largest NCRIF, one was

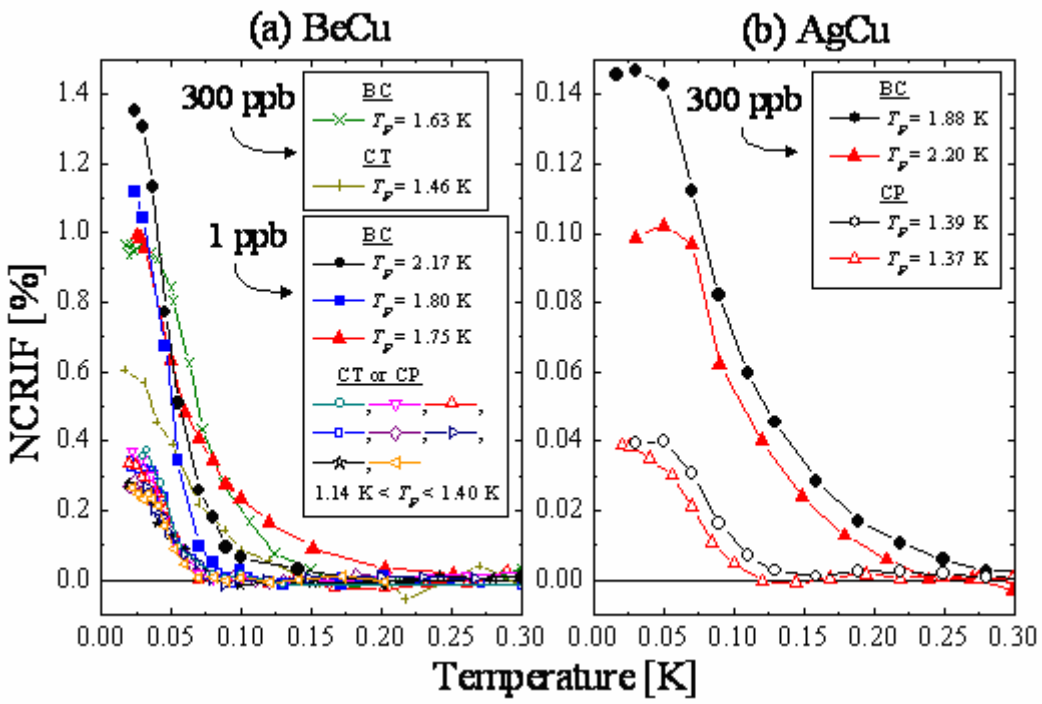

Fig. **5-4**: Comparison of BC and CT/CP samples grown in two different TO's [**Clark 2007**]. Single crystals exhibit a sharper and more reproducible temperature dependence. The magnitude of the NCRIF is highly cell dependent. The ^{3}He concentration in HeTO-2, labeled (a), was later increased to 300 ppb, verifying that this was not due to isotopic impurities.

purposely grown within 4min (versus ~40min) and cooled down rapidly. The other was grown carefully, but just within the hcp/bcc phase boundary. Thus, the one exception** to the consistency in Table **5-3** (not shown in Fig. **5-3**) is a sample that was zone refined, but accidentally warmed through the freezing point after solidification was complete. This undoubtedly strained the crystal severely since no actually melting occurred, but rather additional mass loading from ^{4}He flowing into the cell.

The repeatability of the NCRIF versus *T* curve in each sample suggests that single crystals are reliably grown within the TO. If this is the case it also indicates that the low temperature NCRIF is very sensitive to remnant defects within the crystal, much more so

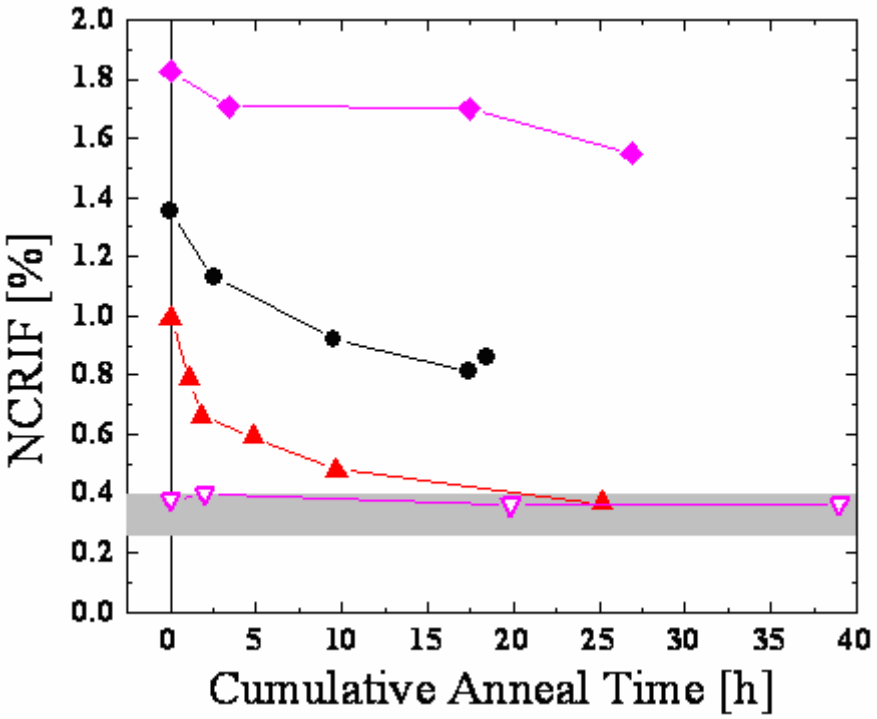

Fig. **5-5**: Change in NCRIF upon annealing. The most dramatic decrement occurs for a low pressure, disordered sample. The grey band denotes the range of NCRIF in which all but two CT/CP samples lay. The CT sample is unchanged.

than near T_O. Although the samples consist of one or a few large crystals, the magnitude of NCRIF is still greater than that in some BC samples [**Rittner 2007**],[**Aoki 2007**], including measurements from our own laboratory [**Clark 2007**]. The fact that the difference among (very likely) single crystal samples between two different TO's is just as substantial as in BC samples [see Fig. **5-4**], supports the notion that grain boundaries are not responsible for the disparity. Rather, the relevant defects appear to be very sensitive to the exact internal geometry, construction materials, and thermal properties of the cells. However, it appears that the presence of grain boundaries influences the onset temperature.

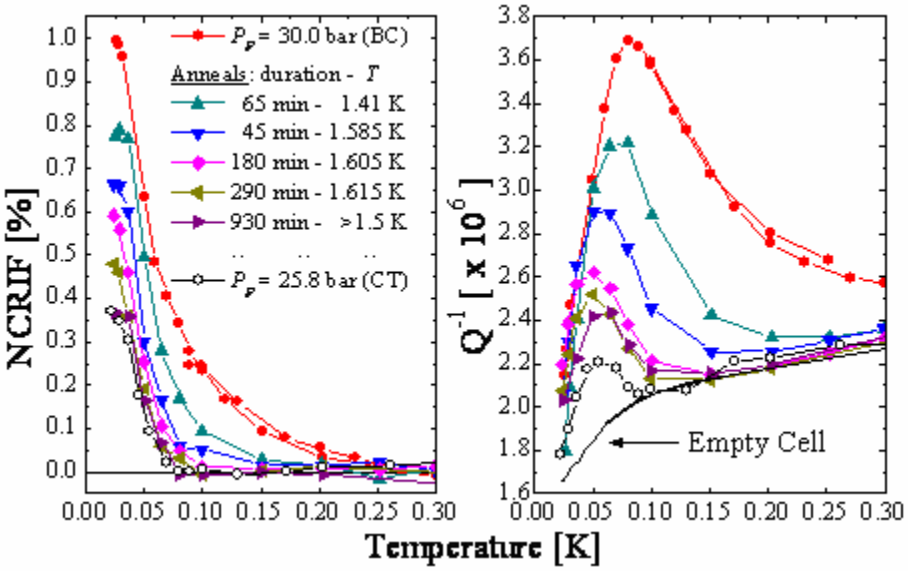

Fig. **5-6**: NCRIF after each sequential anneal for a BC sample. A CT crystal grown from the superfluid is potted for comparison. (b) Asymmetric reduction in Q^{-1} following each anneal. All data was obtained at maximum rim speeds of ~2μm/s.

5.1.4 Annealing of Samples

Several annealing studies were performed to further investigate the defects in the crystals grown. Previous studies have found annealing to both reduce [**Rittner 2006**] and amplify [**Penzev 2007**] NCRIF. As in earlier attempts from our laboratory [**Kim 2006**],[**Kim 2007**], the NCRIF was found to increase, decrease, and in some cases remain the same [**Clark 2007**]. The measured NCRIF at several stages of annealing is shown in Fig. **5-5** for four different samples. The symbol for each sample is repeated from those depicted earlier in either Fig. **5-2** or **5-3**. Modest to significant decrements in NCRIF occur for a variety of BC samples, while no change is observed for a CT sample. The most dramatic reduction occurs in BC-11/29. The NCRIF and Q^{-1} data for this sample are

displayed in Fig. **5-6**. The sizeable tail of NCRIF present in the sample is such that T_O =275mK. This is dramatically reduced following the first anneal at relatively low temperature. In fact, after 25 cumulative hours of annealing the entire temperature dependence of NCRIF asymptotically approaches that found in CT/CP samples. A CT crystal showing no deviation in NCRIF after 40h of annealing is also plotted in the figure for comparison. Annealing the BC sample also leads to a dramatic reduction in the dissipation, which accompanies NCRI in the form of a peak [**Kim 2004c**]. Repeated heat treatments reduce the width of the peak, such that its position remains close to the temperature where the NCRIF changes most rapidly. The fully annealed dissipation peak, just as the NCRIF, approaches that found in CT/CP samples.

A phenomenological model associates the dissipation with a temperature dependent coupling between the superfluid and normal components of the solid, and predicts $(\Delta\tau/\tau)/(\Delta Q^{-1})$ ~1 for a homogeneous sample (>1 indicates inhomogeneity) [**Huse 2007**]. The ratio I observe throughout the annealing of this BC sample evolves non-monotonically from 9.5 to 12 to 10.5. It is perhaps surprising that this ratio, if related to homogeneity, would not reflect improvement with each anneal. One can look at the relationship between the dissipation and period shift in the same way as is done in dynamical treatments of the Kosterlitz-Thouless transition in thin superfluid films [**Ambegaokar 1978**]. As seen in Fig. **5-7**, there is a change in the overall shape of the curve of ΔQ^{-1} versus $2\Delta\tau/\tau$ upon annealing. This is connected to the excessive NCRI tail that initially is present in the sample. Upon the disappearance of the high temperature tail the curves in Fig. **5-7** become almost symmetric.

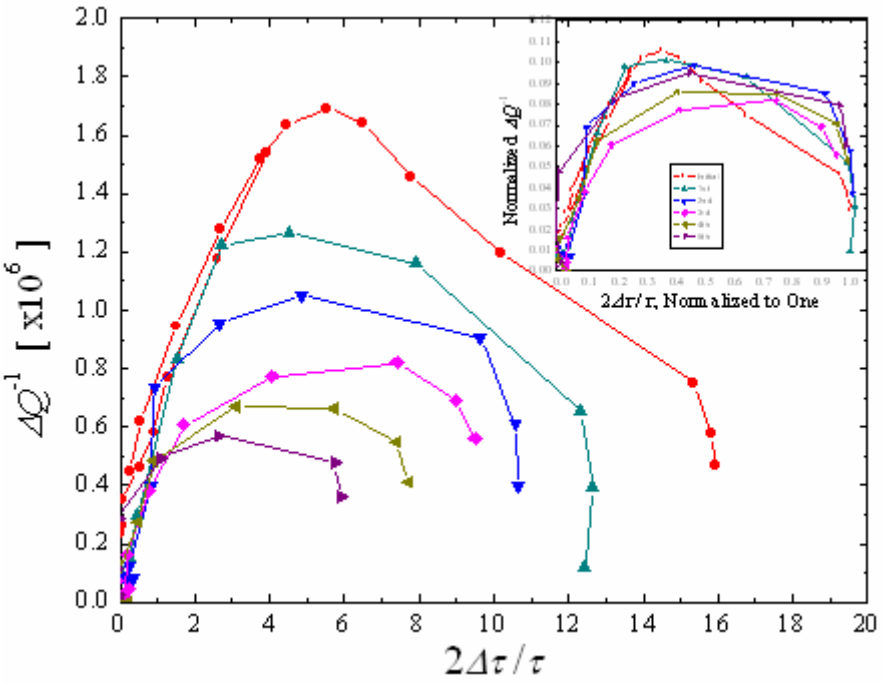

Fig. **5-7**: AHNS treatment of the data [**Ambegaokar 1978**]. Inset: the period data has been normalized to one, and the dissipation has been scaled by the same factor.

A rather different result was obtained for BC-12/10. Although the NCRIF did not drop as dramatically as that in BC-11/29 [see Fig. **5-5**], there was a clear change in the dissipation. The ΔQ^{-1} versus $2\Delta\tau/\tau$ plot is shown in Fig. **5-8**. This sample did not exhibit a true peak in the dissipation until after some annealing. Originally, the dissipation continued to increase as the temperature was lowered. This behavior is highly dependent on the rim speed, and so is further discussed later on in this chapter.

The above figures demonstrate how certain types of defects grown into the solid are more easily annealed away than others. Or in other terms, the NCRI below the onset observed in single crystals (79mK) is much more robust than that included in the high temperature tail. I will return to this latter point when discussing the effects of rim speed.

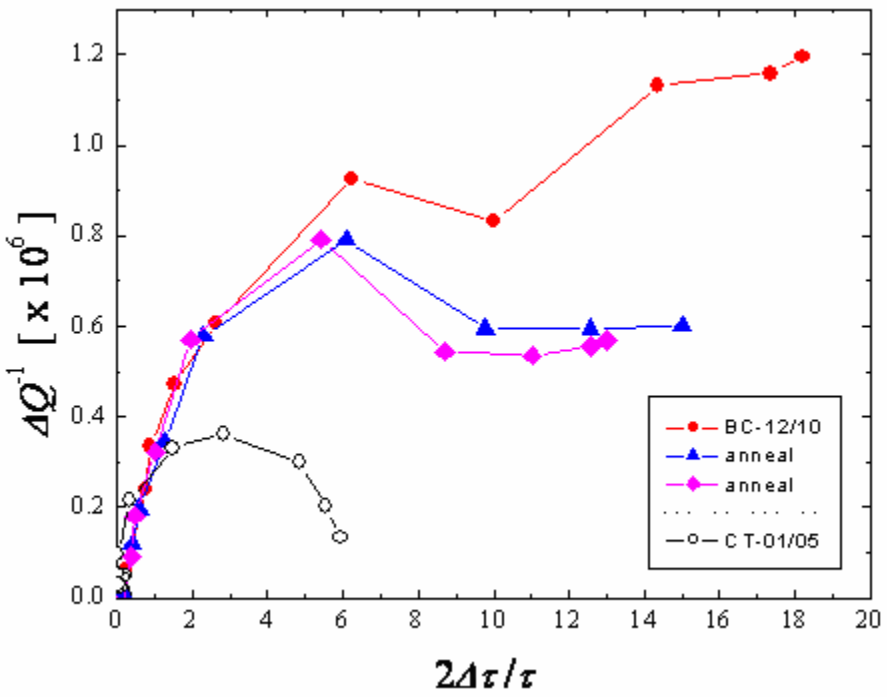

Fig. **5-8**: The pre- and post-annealing datasets are very different. Prior to any annealing there is no dissipation peak, but rather a step. For comparison, a CT sample is included. All data was taken at ~2μm/s.

5.1.5 Implications of the Temperature Dependence

Grain boundaries cannot account for the absolute magnitude of NCRIF, which varies by three orders of magnitude. When the results of the present set of measurements are considered together with the myriad of data from earlier studies [**Kim 2004a**],[**Kim 2007**],[**Rittner 2006**],[**Rittner 2007**],[**Penzev 2007**],[**Aoki 2007**], dislocations emerge as one of the important types of defects. Dislocation densities can vary by more than five orders of magnitude in solid helium samples grown above 1K using different methods [see Chapter 2]. The large range of line densities and their sensitivity to sample growth

and containment can conceivably explain the very different NCRI fractions observed, even for single crystals. It is also known that only some types of dislocations can be annealed away, which may explain the unreliable effectiveness of annealing on the reduction of NCRIF. However, recrystallization is also a factor since polycrystalline samples exhibit a broader transition.

The quantum mechanical motion of a single dislocation has recently been considered [**de Gennes 2006**], but a meaningful comparison with experiments requires a thorough analysis of complex dislocation networks. Recent simulations from another group have shown that the core of some dislocations may support superflow [**Boninsegni 2007**]. However, as in the grain boundary model, the total number of ^{4}He atoms in the vicinity of dislocation lines is much too small to account for experimental NCRI fractions. In addition, the predicted T_O, when the entire dislocation network is taken into account, goes as the square root of NCRIF. We find the onset of NCRI is constant to within ten percent among all CT/CP samples, while NCRIF varies by a factor of two, from 0.26% to 0.5%.

In addition to the magnitude of NCRIF, the high temperature tail and thus T_O are correlated with the way samples are originally prepared [see Fig. **5-4**]. Several points can be drawn from the data in the Fig. **5-9**, which is scaled by the low temperature NCRIF. First, the high temperature tail of NCRIF varies greatly in BC samples, which are presumably polycrystalline. Second, the behavior in CT/CP samples is distinct, in that the temperature dependence is much sharper and the NCRI possesses a well-defined onset temperature. This is most apparent in crystals of 1ppb purity [**Clark 2007**]. The

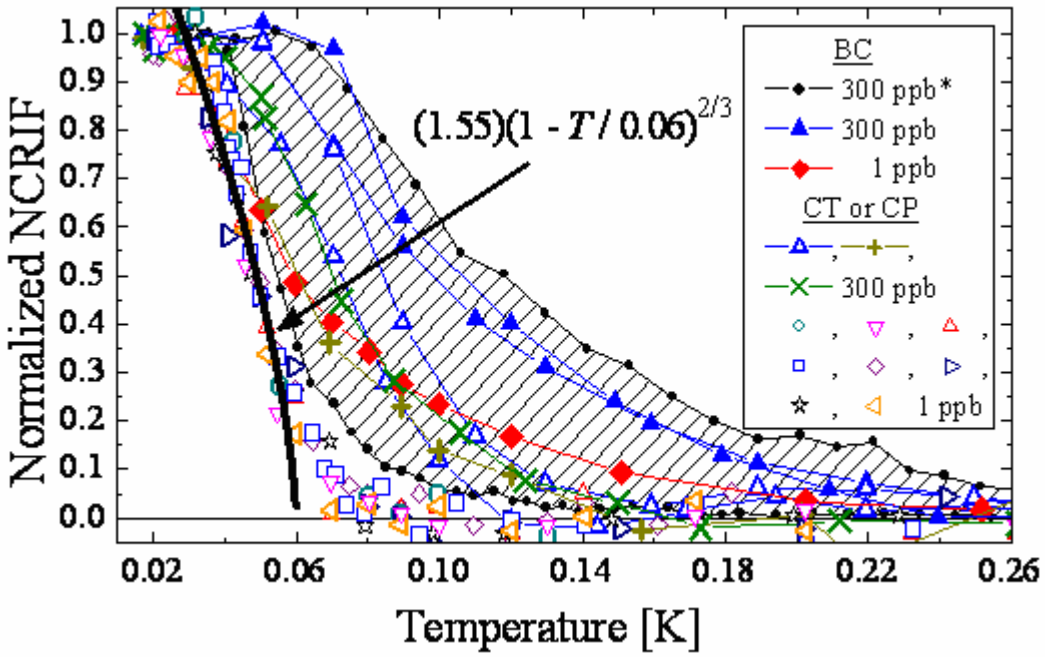

Fig. **5-9**: Normalized NCRIF in various samples [**Clark 2007**]. *There is a wide spread in the data from the original KC experiment [**Kim 2004c**]. The BC samples possess a high temperature tail of NCRI. The CT samples have a considerably sharper onset. A two-thirds power law is plotted for comparison.

addition of ^{3}He slightly broadens the transition and pushes the onset of NCRI to higher temperature. The sensitivity to impurities in this study confirms the general trends observed for a great number of BC samples that were studied over a wide range of ^{3}He concentrations [**Kim 2007**].

A broad heat capacity peak near 75mK was recently observed in solid ^{4}He [**Lin 2007**]. This finding supports the notion that the appearance of NCRI is a genuine signature of the transition in ^{4}He between the normal and supersolid phases. It is then natural to wonder if it falls into the same universality class as that of superfluid ^{4}He, i.e., the 3D XY model. The gradual onset of NCRI previously observed is not consistent with this expectation. On the other hand, the sharp onset present in CT/CP crystals,

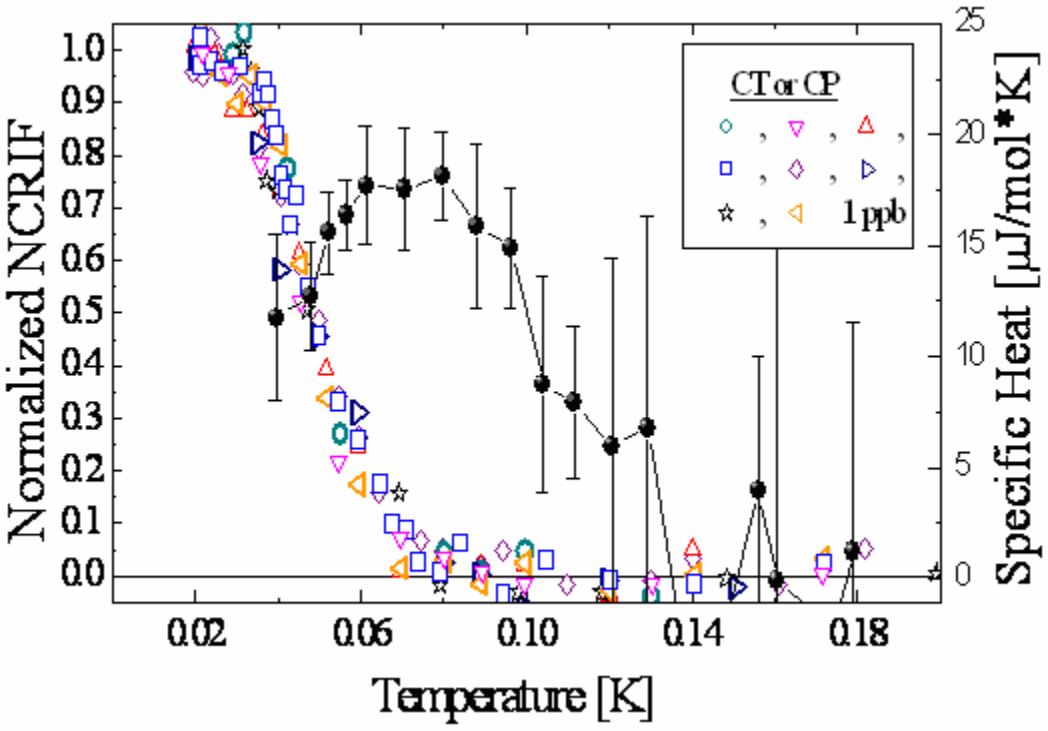

Fig. **5-10**: Comparison of torsional oscillator and specific heat capacity data.

particularly those of 1ppb purity, is intriguing. We noted above that the temperature dependence of the NCRIF near onset in all CT/CP samples collapses onto a single curve. It is interesting that the NCRIF data of these crystals between 30mK and 57mK, as shown in Fig. **5-9**, can be qualitatively represented by the two-thirds power law expected for the 3D XY model, with a critical temperature T_C ~60mK. If this highly speculative "fit" is applicable then the tail between 60mK and 80mK is attributable to the finite measurement frequency [**Aoki 2007**], residual (1ppb) ^{3}He impurities [**Kim 2007**], and crystalline defects. Measurements at a much lower frequency may reveal if there is any validity to this speculation. However, the ^{3}He-independent specific heat peak that coincides with NCRI in 1ppb crystals is very suggestive [see Fig. **5-10**].

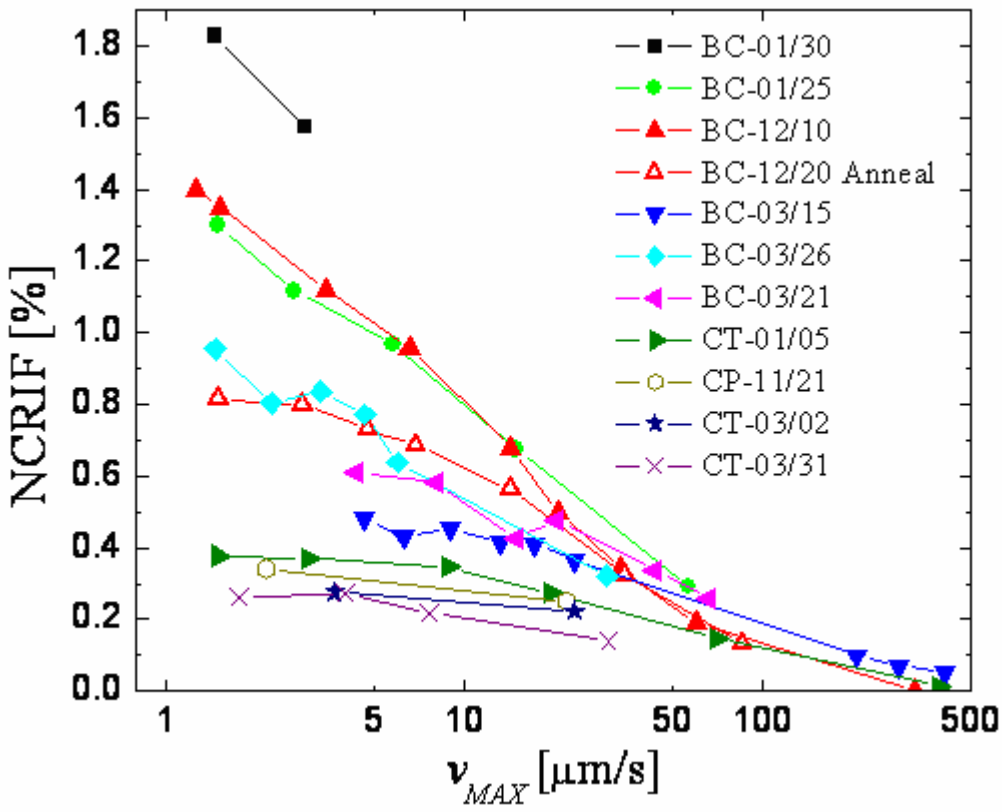

Fig. **5-11**: Effect of oscillation speed on the low temperature limiting value of NCRIF.

5.2 Velocity Dependence

All of the data in Fig. **5-9** were obtained at similar measurement frequencies (~1kHz). I mentioned in Chapter 1 that a recent TO measurement on the same 300ppb sample at two different frequencies found T_O =220 mK at 1173Hz and T_O =150mK at 496Hz. They also reported irreversible changes in NCRIF below ~40mK upon variation of the oscillation speed. This result, as well as previously observed critical velocities on the order of one quantum of circulation [**Kim 2004c**],[**Kim 2006**], suggest that the excitations in the system are vortices. In the present study I have observed new

phenomena that are largely in support of this idea.

5.2.1 Maximum Rim Speed and the Low Temperature Limit

All of the data presented thus far were obtained with relatively low maximum rim speeds. Following the lead of Ref. [**Kim 2004a**], I also made measurements at higher speeds with the original intent of determining the "critical velocity" in single crystals of 1ppb helium. I was surprised to find that in some samples the low temperature limit of NCRIF does not saturate in magnitude even down to 1μm/s [Fig. **5-11**]. This is most apparent in two samples where NCRIF actually doubles when v_{MAX} is decreased from 10 down to 1μm/s. Also included in the figure are data from BC-12/10 following 17h of cumulative annealing. The velocity dependence is only modified at small v_{MAX} upon annealing. In fact this is a general trend for all samples, i.e. the velocity dependence only fans out at low speeds.

5.2.2 Maximum Rim Speed and the Temperature Dependence of NCRI

Changes in the temperature dependence of NCRIF for different velocities also reveals information. The effects of velocity on NCRIF are shown in Fig. **5-12** for a BC sample, annealed BC sample, and CT sample. At first glance there is no new information from that obtained in Ref. [**Kim 2006**]. However, I have closely inspected the similarities and differences of these three (anneal counted as one) samples.

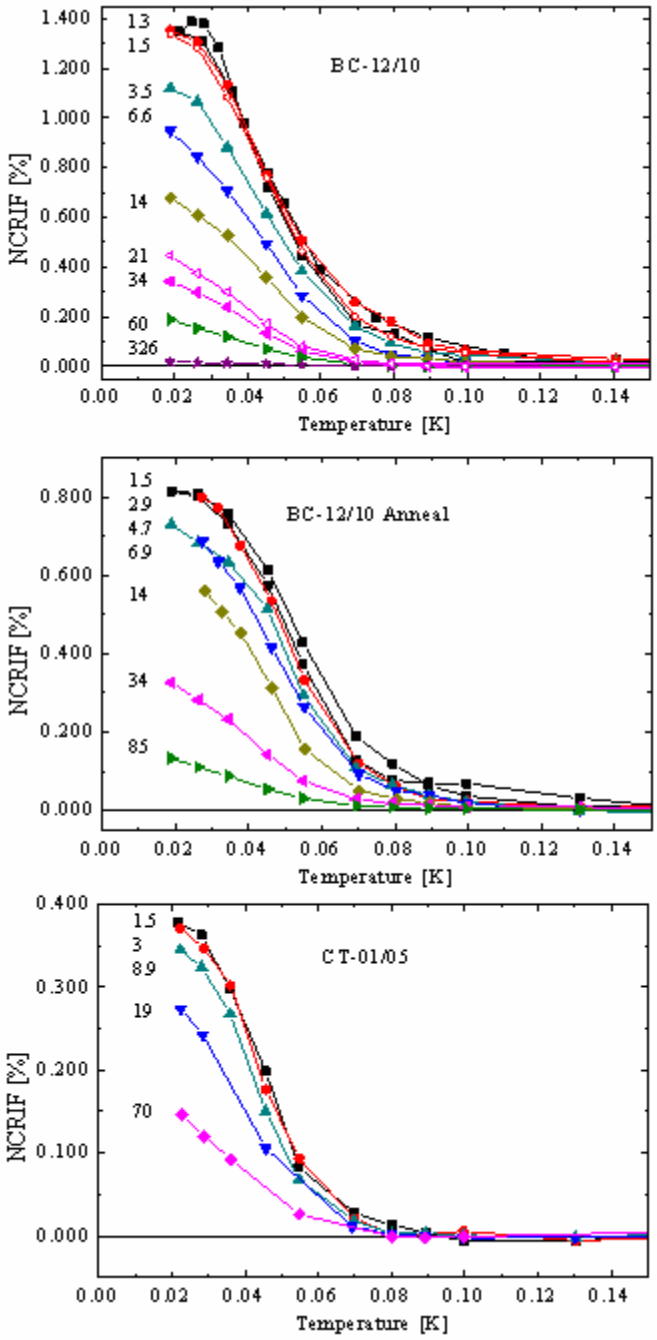

Fig. **5-12**: Velocity dependence of NCRIF versus *T* for a BC and CT sample. Rim speeds are listed to the left of each curve.

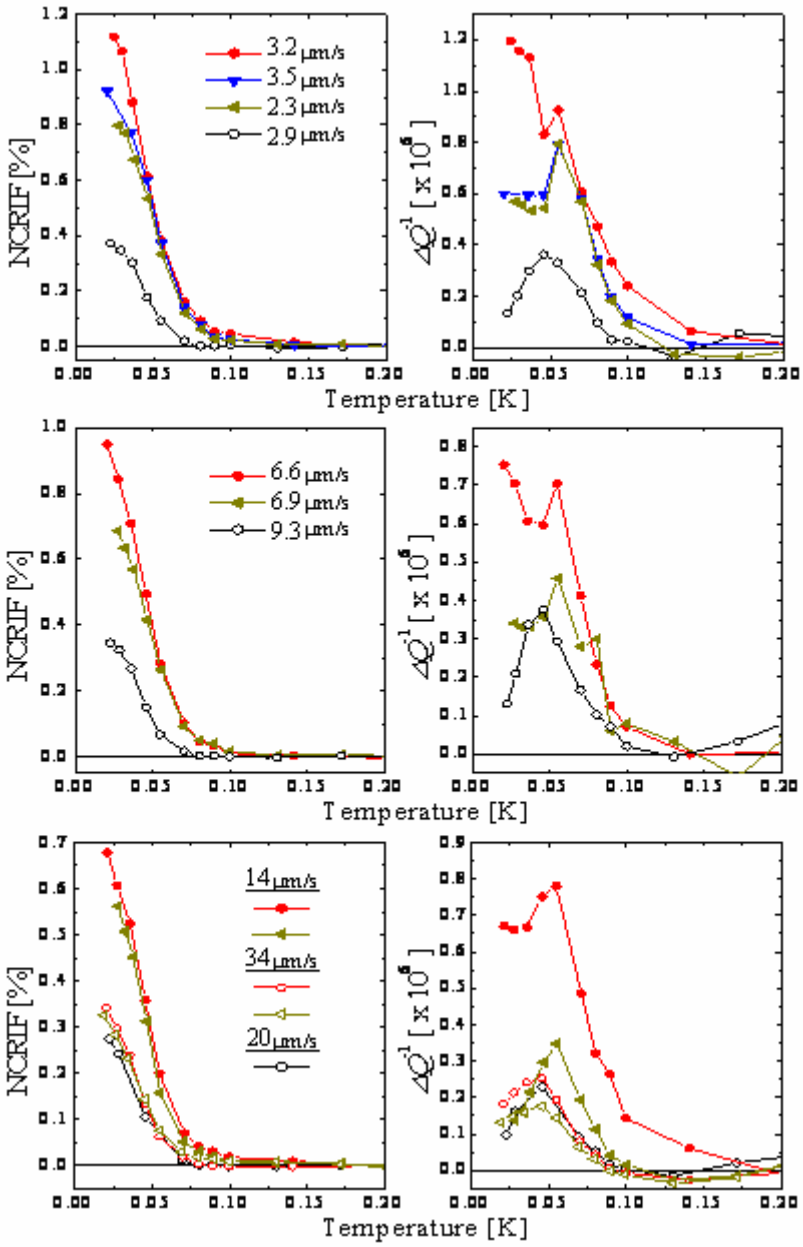

Fig. **5-13**: Comparison of CT-0105 and BC-12/10 at different stages of annealing. At higher velocity the BC sample coincides with the CT sample. At low temperature there is still significant dissipation in the BC sample, such that Q^{-1} is less of a peak and more of a step. Both higher rim speeds and annealing appear to have the same effect, in that they reduce the observed dissipation.

In Fig. **5-13** is plotted the NCRI and ΔQ^{-1} of the three samples at different stages of annealing. The first observation is that, unlike in Fig. **5-6**, annealing primarily reduces NCRIF and ΔQ^{-1} at low temperature. However, the much less significant high temperature tail of NCRI and dissipation make is difficult to say what the effects really are above 80mK. Second, ΔQ^{-1} at 20mK is still quite significant in the BC sample. Annealing reduces the dissipation to some extent, however not to the value of the CT sample. Third, at velocities >30μm/s the data from each sample is very nearly the same over the entire temperature range, as one might expect after viewing Fig. **5-11**. Interestingly, by driving the system at larger rim speeds the response in any given sample is made to look like that of a higher quality sample. As an extreme example, it is worthwhile to check this aspect in what is arguably my "worst" sample, BC-11/29. In Fig. **5-14** the similar effects from annealing and high oscillation speed are demonstrated. By driving the system at 19μm/s part of the high temperature NCRI tail and dissipation are removed. Further, at 223μm/s there is no sign of anything above 79mK. Below this point however there is a sizeable fraction. This demonstrates the robust nature of the onset temperature that we have observed in single crystals, as well as the almost "counterfeit" nature of the high temperature tail. One last point about Fig. **5-14** is that the small shoulder in the 19μm/s scan suggests that the data might be the summation of two dissipation peaks. This has not yet been investigated further.

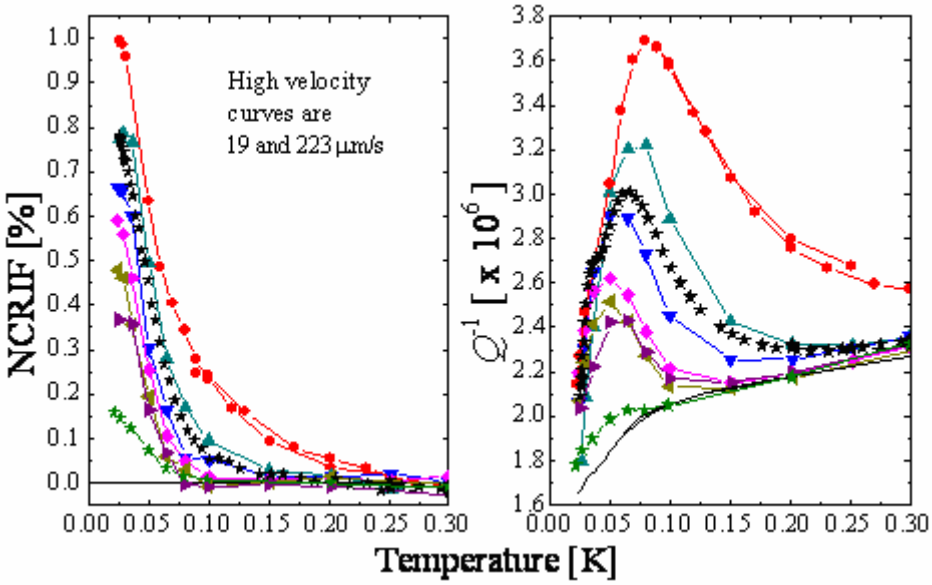

Fig. **5-14**: The effect of annealing and oscillation speed on NCRIF and Q^{-1}. The black and green stars correspond to the medium and high velocity scans of the unannealed sample.

5.2.3 Thermally History, NCRI Metastability, and Anderson's Model

A recent model [**Anderson 2007**] capturing several aspects of the experiments equates NCRI to the rotational susceptibility of a vortex liquid phase. The high temperature tail of NCRI is said to reflect the finite response time of vortices within the sample, which are further slowed by ^{3}He atoms dragged along with them. However, the low temperature behavior of NCRIF that I present below, in addition to that reported in Ref. [**Aoki 2007**], indicate that at least a portion of the vortices are pinned.

All of data shown up to now were compiled from cooling temperature scans that began well above the onset temperature. With this procedure it was found that the NCRIF was diminished at higher velocities for all $T < T_O$ in a reproducible manner. However,

modulation of the oscillation speed below the transition region in many instances resulted in irreversible changes in NCRIF. In the context of superconductivity or magnetism (or superfluidity), the system is prepared differently if (velocity) field-cooling or zero field-cooling are employed. Careful examination of how the oscillation speed affects NCRIF reveals metastability at the lowest temperatures [see Fig. **5-15**]. Using the following protocol, the thermal history of NCRIF was investigated in crystals grown under different conditions. First, the temperature dependence of NCRIF was measured while cooling in the low velocity limit. At T ~20mK, the velocity was slowly increased by approximately a factor of ten. Then, multiple thermal cycles were performed in succession, indicated by the arrows in Fig. **5-15**. Complete equilibration was purposely avoided while cycling between 30mK and 60mK in order to observe multiple metastable states. The measurement culminated with a high velocity cooling trace that began well above the onset temperature.

Fig. **5-15** demonstrates the existence of several metastable states between the low and high field-cooled NCRIF curves. However, the initial velocity-induced decay of NCRIF (or lack of it) at low temperature varies from sample to sample. The measured NCRIF of a highly strained crystal (BC-12/10) immediately drops by about 40% of its magnitude following the increase in v_{MAX}. In contrast there is no change in the NCRIF of CT-11/21, which is perhaps exhibiting a Meissner-like effect [**Aoki 2007**]. This appears to indicate that NCRIF in either a polycrystalline or highly strained crystal is less metastable. However, the opposite is true if we instead define the metastability in terms of the overall difference between the largest NCRIF and the “equilibrium” value obtained from cooling.

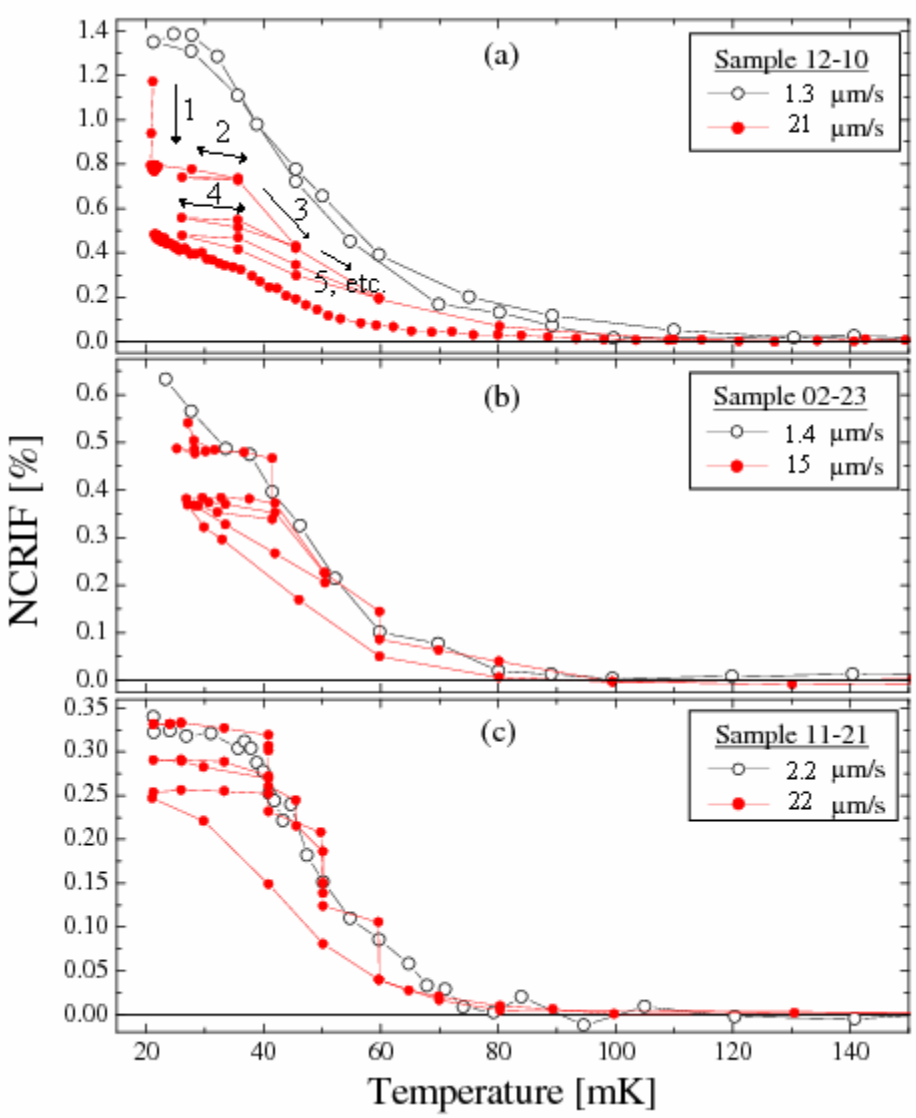

Fig. **5-15**: Thermal history of NCRIF for several samples following an increase in rim speed at the lowest temperature.

Once in a metastable state, NCRIF is very robust at 20mK in that no decay is observed on a time scale of days, as in Ref. [**Aoki 2007**]. This stability is drastically lowered as the temperature is raised. NCRIF for CT-11/21 is re-plotted in Fig. **5-16**, and fragments of the raw data from the "2nd" and "3rd" scans are displayed in Fig. **5-17**. It is clear that the NCRIF decay does not always adhere to one simple mathematical formula, and depends

highly on the initial conditions. For example, consider the points A and B in Fig. **5-17**(a). When the temperature is raised to 40mK, decay begins immediately, but slows down abruptly after only 1h. It then continues to decay at a lesser rate. This anomaly occurs right as the NCRIF measured at high rim speed meets the low speed cooling curve. In contrast, in Fig. **5-17**(b) we see in the 3rd scan that the decay rate of NCRIF slowly increases at 40mK. This is due to the NCRIF already being below the low field curve. This is even more apparent at 50mK. The slope of the NCRIF versus time curves again changes dramatically upon crossing the low field trace, at points B and E in the 2nd and 3rd scans. This is the most obvious in the 3rd scan since the sample was deliberately warmed rapidly to 50mK to result in a larger initial NCRIF at that temperature. The very different decay rates in regions above and below the low field scan demonstrate the physical significance of the data obtained at low speeds. On the other hand, the decay following point I on the 3rd scan could be fit with a simple exponential decay formula, with a time constant of 2.0 ± 0.3h. This implies that there is "different physics" above 60mK. This temperature is in agreement with the observations of Aoki *et al.*, as well as the estimated T_C in Fig. **5-9**. One other interesting point is that upon cooling from F in the 2nd scan the NCRIF increases quickly and sharply. This also happened again following the next cooling step.

I was unable to observe similar kinks in the time dependence of NCRIF for BC samples because the decay rates (by which I simply mean the time rate of change in NCRIF) are five to ten times higher in severely strained samples. As a result, it was difficult to warm up quickly enough and achieve NCRIF much greater than those obtained at low velocities.

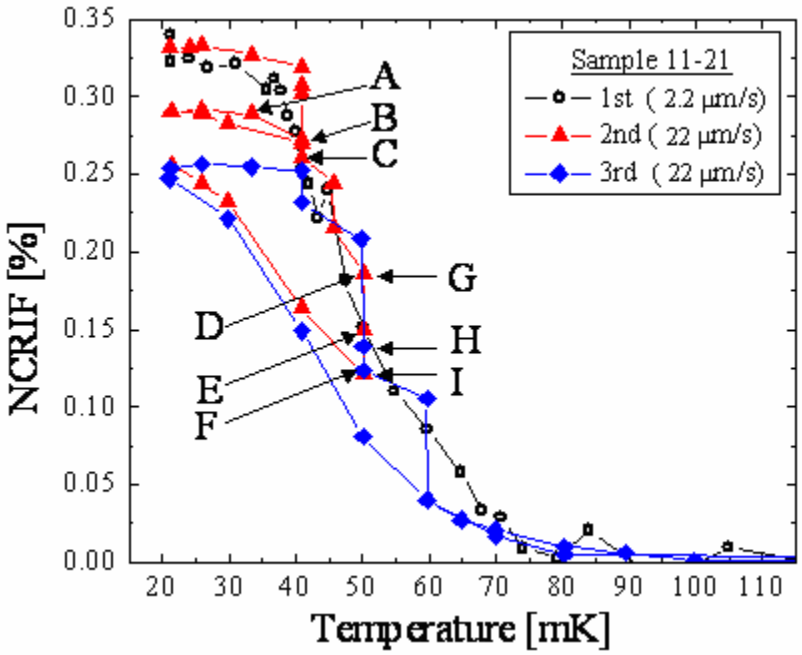

Fig. **5-16**: Magnification of the data shown in the previous figure for CT-11/21.

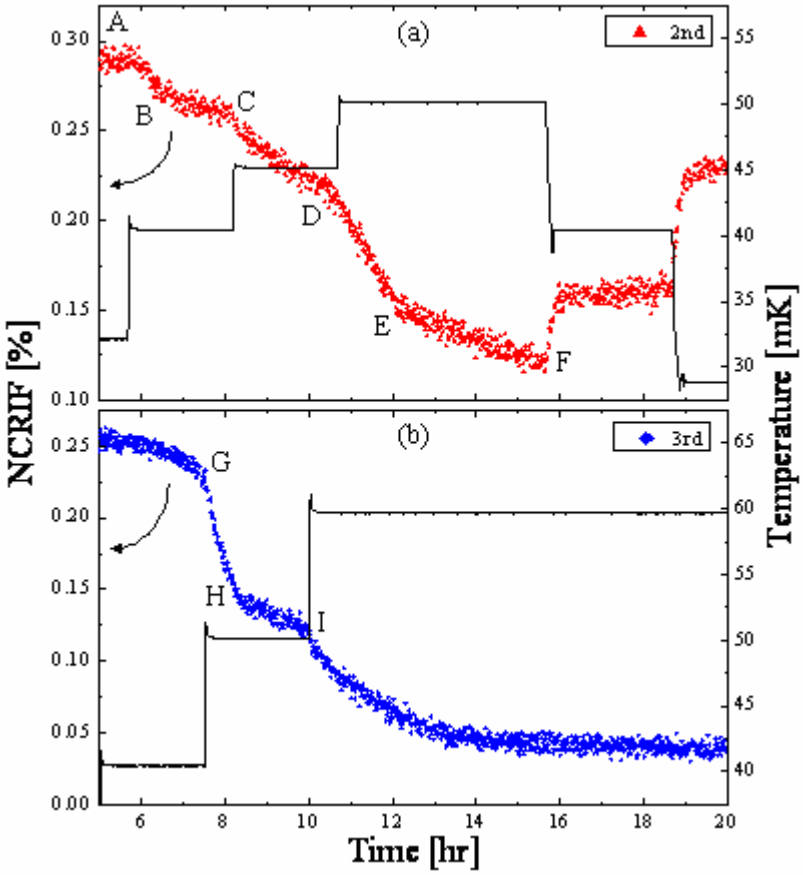

Fig. **5-17**: Raw data depicting irregular decay of NCRIF for CT-11/21.

Another intriguing result is the nearly equal spacing between each metastable NCRIF value portrayed in Fig. **5-15**. Persistent current measurements have demonstrated the quantization of circulation in superfluid liquid ^{4}He [**London 1938**]. In this dc type of experiment there are many possible values of the circulation, which can be determined by measuring the angular momentum of the supercurrent. In an ac experiment such as ours, sinusoidal acceleration will lead to continual changes in the sign, the number, and the configuration of vortices. The NCRIF is then inversely related to the number of vortices that are able to respond to the velocity changes taking place on the time scale of the resonant period of oscillation. Assuming a particular number of thermal vortices exist at any finite temperature, the discrete number of vortices that are effectively pinned within the bulk of the crystal should lead to a quantization of NCRIF. In this case the true supersolid fraction should be identical for every crystal (at least at one V_M), and the difference between each measured NCRIF would then simply reflect the variation in the number of pinning sites. Thus, the minimum quantum of NCRI should also be the same in every sample. To test this idea, I compared separations between each metastable NCRIF among the three samples, and obtained a consistent (albeit arbitrary) step size F_0 = 0.0413% [see Fig. **5-18**]. This is on the order of the minimum NCRIF that has been measured, as well as that calculated from the specific heat anomaly [**Lin 2007**]. The four states of sample BC-12/10 are NCRIF = 19F_0, 18F_0, 14F_0, and 12F_0. For sample BC-02/23, NCRIF = 12F_0 and 9F_0. Lastly, sample CT-11/21 possesses NCRIF = 8F_0, 7F_0, and 6F_0. The quantization is upheld very closely for all but one metastable state of sample BC-12/10, which is roughly in error of F_0/2 ~0.02\%.

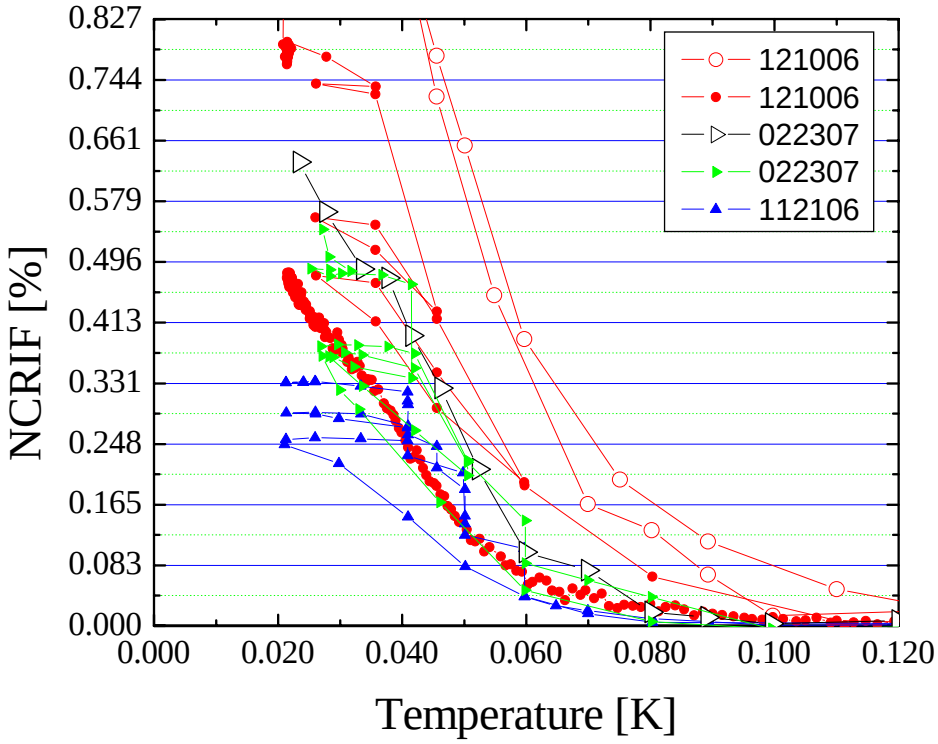

Fig. **5-18**: Discrete nature of NCRIF for three samples.

The slow decay between each metastable NCRIF suggests that there are actually many interlaying states. However, the gradual unpinning of a quantized vortex line in superfluid ^{4}He has been shown to result in a continuous, rather than discrete, change in circulation [**Karn 1980**]. While this coincidence is intriguing, it is only meant as interesting observation. In any case, to strictly test the condition of quantization the experimental precision needs to be improved.

5.2.3.1 "Microscopic Thoughts"

The velocity and thermal history effects presented above highly support the idea of vortex-like excitations in the solid. Vortices can enter the solid as the torsion bob rotates back and forth, the total number of which should increase with v_{MAX}. According to Anderson's model, perhaps more importantly there can also be thermally activated vortices regardless of the oscillation speed [**Anderson 2007**]. Their motion, caused by interactions with the imposed velocity field, can cause damping and effectively reduce NCRIF.

The dependence of T_O on the sample growth and ^{3}He concentration indicates that the combination of the structural defects and impurity atoms are relevant to vortex pinning. Now it is necessary to consider what appears attractive to a vortex line. The normal core of a vortex line in liquid ^{4}He has been shown to cling to non-superfluid elements in the system. This can be the container wall, impurity atoms or charges, permeating wires, etc. Since the microscopic basis of supersolidity is unknown, the fermion isotope, ^{3}He, is the one entity within a solid ^{4}He sample that can be said with certainty to attract vortices. However, there is new evidence that ^{3}He atoms are very mobile within the solid [**Lin 2007**], and therefore it may be difficult for them to be captured by vortices (or vice versa). Since impurities atoms can be immobilized by condensing onto dislocation lines or at grain boundaries, the sample growth procedure can indirectly influence the onset of the transition.

The unbinding of a vortex line from a dislocation line decorated by ^{3}He will be the result of the transfer of energy to either the vortex or the defects. It is known that ^{3}He

can be freed by enhanced vibrations of dislocations when an oscillating stress field is imposed on the lattice [**Suzuki 1980**]. However, this field is extremely small in TO experiments (~10^{-5}dyne/cm^2 for v_{MAX} ~1μm/s) since it stems purely from acceleration and deceleration of the helium in the torsion bob during each cycle of oscillation. In contrast, an estimate of the Magnus force per unit length acting on a vortex line fixed in relation to this flow field is greater by many orders of magnitude. The force per length, ~10^{-8}dyne/cm, results in large forces if the vortex line is completely pinned. However, ^{3}He separations along the dislocation lines is on the order of ~0.1μm. The force acting on segments of this length is ~10^{-13}dyne, versus ~10^{-16}dyne from the acceleration discussed above. For comparison, the binding force between dislocations and ^{3}He atoms is ~10^{-8}dyne, according to the observed stress amplitude of sound pulses (~1000dyne/cm^2) required to unbind them at 200mK from lines that are typically microns in length. Thus, it is more likely the interaction between pinned vortices and the velocity field that will cause breakaway.

I lastly want to return to the annealing studies and velocity dependence. In the vortex picture, one can understand the removal of dislocations and grain boundaries through annealing as a way to lower the overall number and strength of effective pinning sites. It is therefore reasonable to see a decrement in one of or both NCRIF and T_O. This is obviously different than many of the theories proposed to date, which usually associate the defective regions within the solid as superfluid-like. In fact, this may not be the case, which in some way is reasonable since these highly disordered regions and grain boundaries are where most of the ^{3}He impurities reside.

In the same manner as annealing, high rim speeds of oscillation can alter the observed NCRIF and T_O. High velocities inflict larger Magnus forces and can cause the unpinning of vortices, such that the curves in Fig. **5-11** reflect the distribution of pinning strength at sites throughout the sample. In a highly strained crystal, NCRIF is very sensitive to low speeds because there are many weak pinning sites that are beginning to take affect. In the CT/CP-samples there are less of these and therefore NCRIF saturates at higher speeds. There is little difference between any samples at large rim speeds since only the strongest pinning sites with the crystal remain. As a result, there is a plethora of free vortices that limit the size of NCRIF.

5.2.3.2 Supersolidity

Anderson's original suggestion that the real T_C has not yet been observed in experiments is under question. It is evident from the present work that not all vortices are truly free, at least on the time scale of the oscillator, due to pinning sites within the sample. The lack of a frequency dependence on NCRIF [**Aoki 2007**] and pinning [see Fig. **5-15**] below ~40mK, the Meissner-like effect (see Fig. **5-16** and [**Aoki 2007**]), the robust onset temperature [see Fig. **5-3**], and specific heat capacity peak near T_O (see Fig. **5-10** and [**Lin 2007**]), all point toward there being a real phase transition.

Still, the nature of this possible transition is unclear. If NCRI is mainly due to the pinning of thermally activated vortices, which normally screen supercurrents, then it seems NCRIF should scale with the number of pinning sites and T_O should reflect the strength of the sites. This would imply that the two *observed* quantities are independent

of one another. As can be seen from Fig. **5-4**, NCRIF does not scale with T_O. In single crystals of 1ppb helium the onset is 79mK, regardless of NCRIF. In BC samples both numbers vary dramatically, but not proportionally. Still, near T_O there is very little pinning, and therefore the possible glimpse of critical behavior presented in this study may be clearly demonstrated in the future.

Chapter 6

Conclusions

6.1 Solid Hydrogen

A resonant period shift in a torsional oscillator containing solid H_2 was observed. While the phenomenon shares some features with the supersolid transition in ^{4}He, there are several dissimilarities. Most notable is the presence of the period drop in both the open and blocked cells, ruling out superfluidity. The abrupt rise in the period, accompanied by a sudden increase in the relaxation time near 60mK, is consistent with a transition from an, at least, partially phase-separated configuration to one that is unclustered at high temperature. The unclustering process influences the mechanical properties of the solid, as indicated by the excess internal dissipation that is observed.

6.2 Solid Helium

For the first time solid ^{4}He has been grown within a torsional oscillator at a fixed point on the melting curve. The vastly improved reproducibility in the experimental results obtained from these samples is consistent with the expected single crystal morphology. The onset of non-classical rotational inertia is much sharper than previously observed, and occurs at ~80mK. The coincidence of this reliable onset temperature and the recent specific heat capacity signature measured by our laboratory, suggests that a real transition between normal and supersolid phases of ^{4}He occurs. In addition, the

presence of multiple metastable values of NCRIF available to the solid system at any given temperature below 35mK suggests that vortex-like excitations are present in the solid and become pinned at low temperature.

Bibliography

Ackerman, C.C. *et al.*, Phys. Rev. Lett. **16**, 789 (1966); Ackerman, C.C. and Guyer, R.A., Ann. Phys. **50**, 128 (1968).

Adams, M.A. *et al.*, Phys. Rev. Lett. **98**, 085301 (2007); Diallo, S.O. *et al.*, arXiv:cond-mat/0702347v1 (2007); Blackburn, E. *et al.*, arXiv:cond-mat/0702537v1 (2007).

Ambegaokar, V. *et al.*, Phys. Rev. Lett. **40**, 783 (1978); Phys. Rev. B **21**, 1806 (1980).

Amstutz, L.I. *et al.*, Phys. Rev. Lett. **21**, 1175 (1968).

Anderson, P.W., Nature Physics **3**, 160 (2007).

Andreev, A.F. and Lifshitz, I.M., Sov. Phys. JETP **29**, 1107 (1969).

Aoki, Y. *et al.*, Phys. Rev. Lett. **99**, 015301 (2007).

Arms, D.A. *et al.*, Phys. Rev. B **67**, 094303 (2003).

Armstrong, G.A. *et al.*, Phys. Rev. B **20**, 1061 (1979). Balatsky, A.V. *et al*., Phys. Rev. B **75**, 094201 (2007).

Balibar, S. *et al.*, Rev. Mod. Phys. **77**, 317 (2005).

Balibar, S., Bull. Am. Phys. Soc. **52**, 817 (2007).

Berman R. *et al.*, J. Phys. C: Solid State Phys. C **6**, 2119 (1973).

Boninsegni, M. *et al*., Phys. Rev. Lett. **97**, 080401 (2006).

Boninsegni, N. *et al*., Phys. Rev. Lett. **96**, 105301 (2006).

Boninsegni, M. *et al*., arXiv:0705.2967v1 (2007).

Burns, C.A. and Isaacs, D.E., Phys. Rev. B **55**, 5767 (1997).

Burovski, E. *et al*., Phys. Rev. Lett. **94**, 165301 (2005).

Cazorla, C. and Boronat, J., Phys. Rev. B **73**, 224515 (2006).

Ceperley, D.M., Rev. Mod. Phys. **67**, 279 (1995).

Ceperley, D.M. and Bernu, B., Phys. Rev. Lett. **93**, 155303 (2004).

Chester, G.V., Phys. Rev. A **2**, 256 (1970).

Clark, A.C. and Chan, M.H.W., J. Low Temp. Phys. **138**, 853 (2005).

Clark, B.K. and Ceperley, D.M., Phys. Rev. Lett. **96**, 105302 (2006).

Clark, A.C. *et al.*, Phys. Rev. Lett. **97**, 245301 (2006).

Clark, A.C. *et al.*, accepted for publication in Phys. Rev. Lett. (2007). arXiv:0706.0906v2 (2007).

Crepeau, R.H. *et al.*, Phys. Rev. A **3**, 1162 (1971).

Dash, J.G. and Wettlaufer, J.S., Phys. Rev. Lett. **94**, 235301 (2005).

Day, J. and Beamish, J., Phys. Rev. Lett. **96**, 105304 (2006).

de Boer, J., Physica (Amsterdam) **14**, 139 (1948).

de Gennes, P.-G., C. R. Physique **7**, 561 (2006).

Fain, Jr., S.C. and Lazarus, D., Phys. Rev. A **1**, 1460 (1970).

Fain, Jr., S.C. and Lazarus, D., J. Appl. Phys. **41**, 1451 (1970).

Fetter, A.L., J. Low Temp. Phys. **16**, 533 (1974).

Fox, J.N. *et al.*, Phys. Rev. Lett. **28**, 16 (1972).

Fraass, B.A. *et al.*, Phys. Rev. B **39**, 124 (1989).

Galli, D.E. *et al.*, Phys. Rev. B **71**, 140506(R) (2005).

Galli, D.E. and Reatto, L., Phys. Rev. Lett. **96**, 165301 (2006).

Greywall, D.S., Phys. Rev. A **3**, 2106 (1971).

Grigor'ev, V.N. *et al.*, arXiv:cond-mat/0702133v2 (2007).

Gröger, V. and Strangler, F., Z. Mettalkd. **72**, 487 (1981).

Harris, A.B. *et al.*, Phys. Rev. **175**, 603 (1968).

Henshaw, D.G., Phys. Rev. **109**, 328 (1958).

Hess, G.B. and Fairbank, W.M., Phys. Rev. Lett. **19**, 216 (1967).

Heybey, O.W. and Lee, D.M., Phys. Rev. Lett. **19**, 106 (1967).

Hogan, E.M. *et al.*, Phys. Rev. **185**, 356 (1969).

Hohenberg, P.C., Phys. Rev. **158**, 383 (1967).

Huse, D.A. and Khandker, Z.U., Phys. Rev. B **75**, 212504 (2007).

Iwasa, I. *et al.*, J. Phys. Soc. Jpn. **46**, 1119 (1979).Iwasa, I., Phys. Rev. B **66**, 14411 (2003).

Jarvis, J.F. *et al.*, Phys. Rev. **178**, 1461 (1968).

Kapitza, P., Nature **141**, 74 (1938); Allen, J.F. and Misener, A.D., *ibid*. **141**, 75 (1938).

Karn, P.W. *et al.*, Phys. Rev. B **21**, 1797 (1980). Keesom, W.H. and Taconis, K.W., Physica **5**, 161 (1938).

Keesom, W.H., *Helium*, Amsterdam, Elsevier (1942).

Kim, E., "Supersolid Transition of ^{4}He," PhD. Dissertation, The Pennsylvania State University, University Park, PA (2004).

Kim, E. and Chan, M.H.W., Nature (London) **427**, 225 (2004).

Kim, E. and Chan, M.H.W., Science **305**, 1941 (2004).

Kim, E. and Chan, M.H.W., J. Low Temp. Phys. **138**, 859 (2005).

Kim, E. and Chan, M.H.W., Phys. Rev. Lett. **97**, 115302 (2006).

Kim, E. *et al.*, in preparation (2007).

Kohn, W. and Sherrington, D., Rev. Mod. Phys. **42**, 1 (1970).

Kondo, M. *et al.*, J. Low Temp. Phys. **148**, 695 (2007).

Kosterlitz, J.M. and Thouless, D.J., J. Phys. C: Solid State Phys. **6**, 1181 (1977).

Kranendonk, J. Van, J. Low Temp. Phys. 39, 689 (1980).

Leggett, A.J., Phys. Rev. Lett. **25**, 1543 (1970).

Li, X. *et al.*, J. Low Temp. Phys. **78**, 335 (1990).

Lin, X. *et al.*, under review for Nature (London) (2007).

Lipschultz, F.P. and Lee, D.M., Phys. Rev. Lett. **14**, 1017 (1965).

London, F., Nature (London) **141**, 643 (1938); Phys. Rev. **54**, 947 (1938).

London, F., *Superfluids, Vol. I1*. Dover Publications, Inc., New York (1954).

Mahan, G.D. and Shin, H., Phys. Rev. B **74**, 214502 (2006).

Manousakis, E., Europhys. Lett. **78**, 36002 (2007).

Matthews, M.R. *et al*., Phys. Rev. Lett. **83**, 2498 (1999).

McFarland, T. *et al.*, Phys. Rev. B **50**, 13577 (1994).

Meisel, M.W., Physica B **178**, 121 (1992).

Meyer, H., Phys. Rev. **187**, 1173 (1969).

Meyer, H., Can. J. Phys. **65**, 1453 (1987).

Meyer, H., Low Temp. Phys. **24**, 381 (1998).

Meyerovich, A.E. *et al*., Physica B **194**, 925 (1994).

Mezhov-Deglin, L.P., Sov. Phys. JETP **22**, 47 (1965).

Minkiewicz, V.J. *et al.*, Phys. Rev. **174**, 267 (1968).

Mueller, E.J., private communication (2004).

Mukharsky, Yu. *et al.*, J. Low Temp. Phys **148**, 689, (2007).

Nielsen, M., Phys. Rev. B **7**, 1626 (1973).

Onnes, H. Kamerlingh, Proc. Roy. Acad. Amsterdam **13**, 1903 (1911).

Osheroff, D.D. *et al*., Phys. Rev. Lett. **28**, 885 (1972).

Oyarzun, R. and Van Kranendonk, J., Phys. Rev. Lett. **26**, 646 (1971).

Packard, R.E. and Sanders, Jr., T.M., Phys. Rev. A **6**, 799 (1972).

Penzev, A. *et al.*, J. Low Temp. Phys. **148**, 667 (2007).

Pollet, L. *et al.*, Phys. Rev. Lett. **98**, 135301 (2007).

Prokof'ev, N.V. and Svistunov, B.V., Phys. Rev. Lett. **94**, 155302 (2005).

Prokof’ev, N.V., Adv. Phys. **56**, 381 (2007).

Reatto, L., Phys. Rev. **183**, 334 (1969).

Rittner, A.S.C. and Reppy, J.D., Phys. Rev. Lett. **97**, 165301 (2006).

Rittner, A.S.C. and Reppy, J.D., Phys. Rev. Lett. **98**, 175302 (2007).

Sasaki, S. *et al*., Science **313**, 1098 (2006); J. Low Temp. Phys. **148**, 665 (2007).

Saslow, W.M. and Jolad, S., Phys. Rev. B **73**, 092505 (2006).

Schuch, A.F. and Mills, R.F., Phys. Rev. Lett. **8**, 469 (1962).

Schweizer, R. *et al*., J. Low Temp. Phys. **37**, 289 (1979).

Schweizer, R. *et al*., J. Low Temp. Phys. **37**, 309 (1979).

Shaln'kov, A.I., Sov. Phys. JETP **14**, 753 (1962).

Shi, Y., Phys. Rev. B **72**, 014533 (2005); *ibid.* **74**, 029901(E) (2006).

Silvera, I.F., Rev. Mod. Phys.**52**, 393 (1980).

Sohaili M. *et al.*, J. Phys. Condens. Matter **17**, S415 (2005).

Son, D.T., Phys. Rev. Lett. **94**, 175301 (2005); Dorsey, A.T. *et al*., *ibid*. **96**, 055301 (2006); Ye, J., *ibid.* **97**, 125302 (2006).

Suzuki H. and Iwasa, I., J. Phys. Soc. Jpn. **49**, 1722 (1980); Paalanen, M.A. *et al.*, Phys. Rev. Lett. **46**, 664 (1981).

Tilley, D.R. and Tilley, J., *Superfluidity and Superconductivity*, 3rd ed., Institute of Physics Publishing, Bristol and Philadelphia (1990).

Todoshchenko, I.A. *et al.*, Phys. Rev. Lett. **97**, 165302 (2006); JETP Lett. **85**, 555 (2007).

Tsuruoka, F. and Hiki, Y., Phys. Rev. B **20**, 2702 (1979).

Vignos, J.H. and Fairbank, H.A., Phys. Rev. **147**, 185 (1966).

Vitiello, S.A. and Schmidt, K.E., Phys. Rev. B **60**, 12342 (1999).

Vos, J.E. *et al*., Physica **37**, 51 (1967).

Wanner, R. and Franck, J.P., Phys. Rev. Lett. **24**, 365 (1970).

Wanner, R. *et al.*, Solid State Commun. **18**, 853 (1976).

Washburn, S. *et al.*, J. Low Temp. Phys. **40**, 187 (1980).

Webb, F.J. and Wilks, J., Phil. Mag. **44**, 664 (1953).

P.A., Whitlock *et al.*, Phys. Rev. B **19**, 5598 (1979).

Wilks, J., *The Properties of Liquid and Solid Helium*, Clarendon Press, Oxford (1967).

Wolfke, M., Ann. Acad. Sci. techn. Varsovie **6**, 14 (1939).

Yang, C.N., Rev. Mod. Phys. **34**, 694 (1962).

Yoon, J., "Superfluid Transition of ^{4}He in Porous Gold," PhD. Dissertation, The Pennsylvania State University, University Park, PA (1997).

Zassenhaus, G.M., "A High Resolution Specific Heat Measurement Near Superflow Onset in the Helium-4/Vycor System," Ph.D. Dissertation, Cornell University, Ithaca, NY (1999).

Zhai, H. and Wu, Y.-S., J. Stat. Mech. P07003 (2005).

VITA

Anthony Constine Clark

Anthony was born in Johnson City, NY on May 28th, 1979 at around two o'clock in the morning. He was raised by his parents, Richard and Candice, on the South side of Binghamton. During this time he refused to play with physics or chemistry sets, but instead enjoyed playing street football, stickball, ping pong, frisbee, or anything else mildly amusing. In fact, he should have patented a number of games that he created just to fill free time.

He attended McArthur Elementary, where he quickly elevated to playboy status by the first grade. His allure continued to grow until puberty hit. At this time he also lost his knack for impressions, such as Johnny Carson or Garth (from Wayne's World), due to the change in pitch of his voice.

Upon reaching Binghamton High, he distinctly remembers his brother telling him that older kids at school would beat on him if he insisted on being such a smart ass. Perhaps it was this conversation that motivated him to achieve a black belt in Tae kwon do, since it is clear that he is still rather "smart."

He attended Binghamton University (SUNY), majoring in physics and working in Cotts' Lab. It was there that he met Carolyn. Nearing graduation he realized that it would be difficult to find a job with a B.S. in physics, and therefore applied to graduate school.

Upon arriving in State College he was quickly absorbed into Chan's Lab, and the rest is history. For those living under a rock, Anthony became the greatest student in the entire history of Penn State.